Quantum Classical Hybrid Algorithms for Accurate Quantum Chemistry Calculations with Resource-Limited Quantum Computers

Luca Klaus Erhart

September, 2024

Quantum Classical Hybrid Algorithms for Accurate Quantum Chemistry Calculations with Resource-Limited Quantum Computers

A dissertation submitted to
THE GRADUATE SCHOOL OF ENGINEERING SCIENCE
OSAKA UNIVERSITY
in partial fulfillment of the requirements for the degree of
DOCTOR OF PHILOSOPHY IN SCIENCE

BY

LUCA KLAUS ERHART

SEPTEMBER, 2024

Abstract

Quantum computing offers new possibilities in quantum chemistry for calculating the electronic structure of a molecule. Quantum computers, which utilize quantum mechanical principles for their computations, are generally considered to be better suited for this task than classical hardware. On the other hand, quantum computers are severely limited by their number of qubits and the number of operations they can perform. This limits the number of degrees of freedom (i.e., orbitals) that can be considered in an electronic structure calculation for a molecule on a quantum computer. For the foreseeable future, quantum computers alone are unlikely to be able to handle problems involving molecules of realistic size. Practical problems in quantum chemistry require quantum-classical hybrid algorithms that combine a quantum computer with a classical computer.

In this thesis, we address the issue of the limitation of orbital numbers for calculating the electronic structure of a molecule using quantum computing in different ways. One way we effectively increase the number of orbitals that can be considered is by using a divide-and-conquer method. One particular algorithm that uses this method is the so-called deep Variational Quantum Eigensolver (deep VQE). It is well-known that this kind of method misses some correlation energies when recombining the divided systems. We examined multiple methods to recombine the divided systems and compared them regarding accuracy and computational requirements. Using our newly proposed strategies, the deep VQE algorithm can significantly reduce the number of qubits required to calculate the electronic structure of a molecule. We were even able to showcase this advantage by calculating the ground state energy of retinal, a molecule that plays an important role in the human retina.

Our second approach involves compensating for degrees of freedom that cannot be handled by the quantum computer using classical post-processing techniques. A common strategy is to reduce the computational cost of an electronic structure calculation of a molecule by using the active space approximation. In the active space approximation method, only a molecule's most relevant orbitals and electrons are considered for the calculation. However, such an approach can produce inaccurate results due to the missing electron correlation from ignored orbitals and electrons. We improved the active space approximation using a post-process correction method. We calculate the active space accurately on a quantum computer and take into account the missing electron correlation in a

follow-up tailored coupled cluster calculation on a classical computer. We show that we successfully reintroduce the missing electron correlation on multiple, different molecules and use it to predict the activation energy of a chemical reaction.

The third approach we explore involves developing an ansatz (wave function representation) that can be used interchangeably between quantum and classical computers. Coupled Cluster (CC) theory is a highly effective framework in computational chemistry to calculate electronic structures. The CC method is not variational, and it can fail to predict the electronic structures of molecules with strongly correlated electrons. A variational variant of the CC methods (VCC) prevents this failure. However, on a classical computer, VCC requires an exponential computational cost, making it virtually impossible for most molecules to calculate. We propose a method for applying an approximated version of the VCC that scales polynomials in system size on a quantum computer and allows us to represent an approximation of the VCC wave function. The parameters can be optimized in a quantum-classical hybrid approach. The relationship between VCC and CC allows for a classical approximation of the VCC parameters, resulting in fast convergence on the quantum computer and, in addition, the efficient extraction of information about the quantum state. We show that the approximated version of the VCC on the quantum computer produces results that are in good agreement with the conventional VCC algorithm.

We show three different approaches to using quantum-classical hybrid algorithms with a resource-limited quantum computer for accurate quantum chemistry calculations. Our research related to the combination of quantum and classical computing allows us to improve the divide-and-conquer method and the active space approximation. Such a combination also allows us to develop an approximative VCC method that scales exponentially better than conventional VCC.

Contents

1 Introduction **3**
- 1.1 Motivation for Quantum Chemistry with Quantum Computing . . . 3
- 1.2 Challenge of Resource-Limited Quantum Computer . . . 4
- 1.3 Goal of this Thesis . . . 4
- 1.4 Overview of this Thesis . . . 6

2 Preliminaries **9**
- 2.1 Mathematical Background . . . 9
  - 2.1.1 Hilbert Space . . . 9
  - 2.1.2 Different Types of Matrices . . . 10
  - 2.1.3 Commutators/Anti-Commutators . . . 10
  - 2.1.4 Chebyshev Expansion . . . 11
- 2.2 Quantum Chemistry . . . 12
  - 2.2.1 Electronic Structure Theory . . . 12
  - 2.2.2 Second Quantized Hamiltonian . . . 13
  - 2.2.3 Basis Sets . . . 14
  - 2.2.4 Hartree-Fock . . . 15
  - 2.2.5 Electronic Correlation . . . 16
  - 2.2.6 Configuration Interaction . . . 16
  - 2.2.7 Coupled Cluster . . . 17
- 2.3 Fundamentals of Quantum Computing . . . 19
  - 2.3.1 Qubits . . . 19
  - 2.3.2 Gates . . . 20
  - 2.3.3 Fermion to Qubit Mapping . . . 20
- 2.4 Quantum and Quantum-Classical Algorithms . . . 22
  - 2.4.1 Variational Quantum Eigensolver . . . 22
  - 2.4.2 Quantum Singular Value Transformation . . . 22

3 Local Bases of Deep Variational Quantum Eigensolver for Quantum Chemistry **25**
- 3.1 Introduction . . . 25
- 3.2 Theory . . . 27

3.2.1 Deep VQE . . . 27
3.2.2 Deep VQE for Fermionic System . . . 28
3.3 Method . . . 30
3.3.1 Basis Creation Strategies . . . 30
3.3.2 Remarks on Degenerate Eigenstates of Subsystems . . . 32
3.4 Numerical Simulation . . . 32
3.4.1 Setup . . . 32
3.4.2 Influence of Starting Vector for Degenerate Subsystems . . . 35
3.4.3 Different Basis Methods . . . 36
3.4.4 Interaction Based Deep VQE with Fixed Qubit Numbers 37
3.4.5 Retinal . . . 38
3.4.6 Performance Comparison . . . 39
3.5 Conclusion and Discussion . . . 41

4 Coupled Cluster Method Tailored with Quantum Computing 45
4.1 Introduction . . . 45
4.2 Theory . . . 47
4.2.1 Tailored Coupled Cluster . . . 47
4.2.2 Computational Basis Tomography . . . 48
4.2.3 QC-CBT-TCC . . . 50
4.2.4 Enhanced QC-CBT-TCC . . . 52
4.3 Results and Discussion . . . 52
4.3.1 Potential Energy Curves . . . 53
4.3.2 Number of Shot Dependency of QC-CBT-TCC . . . 56
4.3.3 Application to Cope Rearrangement . . . 58
4.4 Conclusion . . . 60

5 Variational Coupled Cluster Method for Quantum Computer 63
5.1 Introduction . . . 63
5.2 Methods . . . 65
5.2.1 Review of Variational Coupled Cluster . . . 65
5.2.2 Chebyshev Expansion of VCC towards Quantum Computing Applications . . . 66
5.2.3 The QSVT Implementation of HC^d-VCC Ansatz . . . 68
5.3 Computational Details . . . 68
5.4 Results and Discussion . . . 69
5.4.1 Chebyshev Approximation of VCCSD . . . 69
5.4.2 Robustness of *Trotterized* VCCSD . . . 69
5.4.3 Numerical Verification of HC^d-VCCSD . . . 70
5.5 Conclusions . . . 70

6 Conclusion 73

Bibliography 77

Appendix 93

Acknowledgments **97**

List of Publications **99**

Abbreviations

HF	Hartree-Fock
CC	Coupled Cluster
CCSD	Coupled Cluster with Single Double excitations
CCSD(T)	Coupled Cluster with Single Double, and a perturbative Triple excitations
VCC	Variational Coupled Cluster
VCCSD	Variational Coupled Cluster with Single Double excitations
C^d-VCC	Chebyshev expansion of VCC with degree d
HC^d-VCC	Hermitian-part Chebyshev approximation of VCC with degree d
UCC	Unitary Coupled Cluster
UCCSD	Unitary Coupled Cluster with Single Double excitations
MR-AQCC	Multi-Reference Averaged Quadratic Coupled-Cluster
CI	Configuration Interaction
FCI	Full Configuration Interaction
CASCI	Complete Active Space Configuration Interaction
CASSCF	Complete Active Space Self-Consistent Field
GTO	Gaussian-Type Orbital
STO	Slater-Type Orbital
RDMs	Reduced Density Matrices
NISQ	Noisy Intermediate-Scale Quantum
FTQC	Fault-Tolerant Quantum Computing
VQE	Variational Quantum Eigensolver
QPE	Quantum Phase Estimation
CBT	Computational Basis Tomography
QSVT	Quantum Singular Value Transformation
ITE	Imaginary Time Evolution
TCC	Tailored Coupled Cluster
PECs	Potential Energy Curves
QC-CBT-TCC	Quantum Classical Computational Basis Tomography Tailored Coupled Cluster Method
IQR	Inter-Quartile Range
JW	Jordan-Wigner transformation

Chapter 1

Introduction

1.1 Motivation for Quantum Chemistry with Quantum Computing

It has become clear that the achievements of humankind are founded on limited resources and are unsustainable for a growing human population. It is foreseeable that we will face multiple challenges in the near future. The climate and the energy crises or antibiotic-resistant bacteria are just the tip of the melting iceberg. Progress in quantum chemistry is desirable as it can be a part of finding solutions to these problems. Being able to make accurate predictions about the chemical properties of molecules would fundamentally change our development cycles and support the progress toward a sustainable interaction with the environment. At the heart of this task is the requirement to solve the Schrödinger equation, which describes the behavior of a quantum system. However, the Schrödinger equation is a partial differential equation for which there exists today no analytical method to solve. Numerical solutions with high accuracy are often not possible on classical computers since the computational cost even exceeds the capability of today's supercomputers. There is a remarkable effort from academia and industry to make quantum computing a helpful tool to support these numerical calculations.

Richard Feynman [1] proposed in 1982 that quantum computers have a distinct advantage in simulating quantum systems. Using a quantum device to represent a quantum system, it is more natural to simulate quantum effects than on its classical counterpart. A quantum computer only requires a polynomial growing number of qubits to represent a quantum state in comparison to the exponential growing memory requirement on a classical computer.

This favorable scaling on the system size gives quantum algorithms an advantage for certain problems over today's algorithms on classical hardware. Examples of such highly efficient algorithms are the Shor algorithm [2, 3], which factorizes large integers or the Harrow-Hassidim-Loyd algorithm [4], which solves linear systems of equations efficiently. In the quantum chemistry setting this

dependence on the system size suggests the promising potential of quantum computers to calculate the electronic structure of complex molecules efficiently. One of the algorithms to solve this problem is the Quantum Phase Estimation (QPE) [5–7]. The QPE algorithm samples a Hamiltonian's exact eigenvectors and eigenvalues, allowing the precise electronic structure of a molecule to be determined in a polynomial time with respect to the system size, in contrast to exponential scaling on classical hardware.

To successfully run such complex quantum algorithms, it is essential, due to the intrinsic noise of the qubits, to be in the fault-tolerant quantum computing (FTQC) era. This requires using quantum computers that are able to run quantum error correction codes.

1.2 Challenge of Resource-Limited Quantum Computer

To perform quantum chemistry computations on an error-corrected quantum computer, it is theorized that $\mathcal{O}(10^6)$ [8, 9] physical qubits are required. However, even when tremendous achievements in realizing quantum hardware have been made in the most recent years, we are still in what John Preskill [10] defined as the Noisy Intermediate-Scale Quantum (NISQ) era. This describes quantum hardware with a limited number of qubits of $\mathcal{O}(10)$ to $\mathcal{O}(100)$, with the qubits showing limited performance due to the intrinsic noise. Impressively, it has already been possible to demonstrate that NISQ quantum machines could be used for quantum chemistry calculations [11–13]. This is partly due to the promising method Variational Quantum Eigensolver (VQE) [14–16], which is able to run on NISQ devices. The VQE is a quantum-classical hybrid algorithm that approximates the ground state variationally. It uses an iterative process between a quantum and a classical computer that prevents errors from building up over time on the quantum device. However the performed calculations are currently still in reach of today's classical hardware due to the restrictions on the number of qubits in the NISQ era.

It is, therefore, clear that quantum computers will remain resource-limited in the NISQ era as well as far into the FTQC era. In the NISQ era, we will be limited by the intrinsic noise of the faulty qubits, whereas in the FTQC, we will be limited by the costly overhead of error correction codes. To consider how resource-limited quantum computers could be used successfully is, therefore, an essential undertaking.

1.3 Goal of this Thesis

The goal of this research is to perform accurate quantum chemistry calculations on a quantum computer even when they have limited resources. There are two main reasons why this is a challenging task.

- Quantum chemistry calculations are computationally expensive.

- Quantum computers have a limited number of qubits with low coherence time.

It has not yet been possible to use quantum computing for a calculation of an electronic structure of a molecule that is out of reach for classical hardware. This is due to the severe restrictions quantum computers, as of today and in the foreseeable future, have to face.

To perform quantum chemistry calculations with a quantum computer, it is essential to develop computational methods that work with limited resources. We tackle these issues by developing some quantum-classical hybrid algorithms. The basis of these algorithms originates from well-established methods in quantum chemistry performed on classical computers. Using such hybrid algorithms allows us to combine and utilize the favorable properties of both classical and quantum computers. This thesis is a step towards accurately predicting the electronic structures of bigger molecules.

There are multiple approaches [17–19] that allow the approximation of an electronic structure of a molecule where the orbitals exceed the number of available qubits on a quantum computer. One of these methods is the deep Variational Quantum Eigensolver (deep VQE) [20], which uses a divide-and-conquer approach to the molecule. Another approach is the so-called active space method, which regards only a subset of all orbitals and electrons most relevant in the electronic structure calculation. However, both of these methods are approximations. They neglect certain electronic correlations within the molecule, limiting the accuracy of the calculation. A goal of this thesis is to overcome these methodical errors. In the case of the deep VQE, we achieve this by improving the recombination of the divided subsystems by applying appropriate interactions. In the case of the active space approximation on a quantum computer, we reintroduce the missing electronic correlation using a post-process correction method. We calculate the active space accurately on a quantum computer and take into account the missing electron correlation in a follow-up Tailored Coupled Cluster (TCC) [21–26] calculation on a classical computer. We use Computational Basis Tomography (CBT) [27] to transfer the relevant Coupled Cluster (CC) [28, 29] coefficients onto the quantum computer. For quantum computing multiple methods [30–52] have been proposed to incorporate the missing electron correlation. However, they either suffer from tremendous measurement costs or require preexisting knowledge of the electronic correlation.

Even though CC is a potent method to calculate the electronic structure, it fails for strongly correlated systems [53]. A variational version of the CC method could fix this. It has been shown that the Variational Coupled Cluster (VCC) [53–63] method produces reasonable solutions for the electronic structure of a molecule [57, 61, 62]. However, the VCC scales exponentially on a classical computer. In addition, the VCC method can not be directly applied on quantum computers since they are limited to unitary operations. Our goal is to develop a quantum computing method that approximates the VCC state with polynomial computational cost. We achieve this by splitting the exponent of the VCC

ansatz into a Hermitian and anti-Hermitian part. The exponent of the anti-Hermitian part can be directly applied on the quantum computer since it is a unitary operation. We approximate the exponential of the remaining Hermitan part using a Chebychev approximation and apply it to the quantum computer using a Quantum Singular Value Transformation (QSVT) [64].

1.4 Overview of this Thesis

Chapter 2: Preliminaries
In Chapter 2, we discuss the background necessary to follow this thesis. We introduce the mathematical background as well as provide a quick introduction to quantum chemistry. We also discuss the fundamentals of quantum computing and show the relevant quantum or quantum-classical hybrid algorithms used in this thesis.

Chapter 3: Local bases of Deep Variational Quantum Eigensolver for Quantum Chemistry
In Chapter 3, we address the limited resource problem with a divide-and-conquer approach. In particular, we use deep VQE [20], which is a quantum-classical hybrid algorithm. Its goal is to determine the ground state of a quantum system that is too large to be mapped onto the quantum computer in full. We examine different subspace-forming methods and compare their accuracy and complexity on a 10 H-atom tree-like molecule as well as a 13 H-atom version. Additionally, we examined the performance on the naturally occurring retinal molecule. This Chapter is based on [Erhart, Mitarai, Mizukami, and Fujii, Phys. Rev. Applied 18, 064051].

Chapter 4: Coupled Cluster Method Tailored with Quantum Computing
In Chapter 4, we propose a method of using a quantum computer to solve an active space calculation and incorporate classical dynamic correlation. Our method is a CC split amplitude approach where we use a quantum computer to solve the static correlation and add the remaining dynamic correlation using a classical computer. The efficient state tomography CBT is used to transfer the relevant coefficients from the quantum computer onto the classical computer. This makes this approach feasible in the NISQ era as well as for FTQC. We show the performance of our method by predicting the potential energy curves (PECs) of LiH, H_2O, and N_2. Additionally, we examined the influence of the number of CBT measurements on the prediction uncertainty of our method. Furthermore, we predict the activation energy for the Cope rearrangement reaction of 1,5-hexadiene and compare it to established methods. This Chapter is based on [Erhart, Yoshida, Khinevich, and Mizukami, Phys. Rev. Research 6, 023230].

Chapter 5: Variational Coupled Cluster Method for Quantum Computer
In Chapter 5, we present a method to prepare the Variational Coupled Cluster with Single and Double excitations (VCCSD) state on a quantum computer approximately, making it available for the first time to be used in further algorithms such as QPE. We utilized the Chebyshev expansion to approximate the VCCSD ansatz as a polynomial and applied it using a QSVT. We demonstrate the accuracy of our method on highly correlated molecules such as linear H_4, H_6, and N_2, respectively. This Chapter is based on [Erhart, Yoshida, Khinevich, and Mizukami, arXiv:2406.07364].

Chapter 6: Conclusion
We summarize the thesis in Chapter 6 and show how the different approaches contributed to solving the current open questions. We also discuss some further possible research directions.

Chapter 2

Preliminaries

2.1 Mathematical Background

In this section, we discuss the mathematical background needed to follow this thesis.

2.1.1 Hilbert Space

In quantum mechanics, a quantum system's state can be described using a vector in a Hilbert space. A Hilbert space is a vector space with an inner product. The state vectors $|\phi\rangle$ are normalized under the inner product

$$\langle\phi|\phi\rangle = 1. \tag{2.1}$$

In this thesis, we are only concerned with finite-dimensional Hilbert spaces. Lets assume the dimension of the Hilbert space is N. Therefore, selecting a basis with N vectors is possible. It is often convenient to choose the computational basis set. The corresponding vectors can be written as

$$|0\rangle \equiv \begin{bmatrix} 1 \\ 0 \\ \vdots \\ 0 \end{bmatrix}, \cdots, |n-1\rangle \equiv \begin{bmatrix} 0 \\ \vdots \\ 0 \\ 1 \end{bmatrix}. \tag{2.2}$$

The computational basis set is orthogonal under the inner product

$$\langle i|j\rangle = \delta_{i,j}. \tag{2.3}$$

Since the Hilbert space is a vector space, the composition $\mathcal{H}_C$ of two systems Hilbert spaces $\mathcal{H}_1$ and $\mathcal{H}_2$ is a tensor product space

$$\mathcal{H}_C = \mathcal{H}_1 \otimes \mathcal{H}_2. \tag{2.4}$$

Consequently, the combined system's dimension is the product of the two subsystems

$$\dim(\mathcal{H}_C) = \dim(\mathcal{H}_1) \cdot \dim(\mathcal{H}_2). \tag{2.5}$$

2.1.2 Different Types of Matrices

This subchapter summarizes the different matrix types that play a role in this thesis. Most crucially, in this thesis, we deal with closed quantum systems. The multiplication of a unitary matrix onto the quantum state describes an operation on a closed quantum system. A unitary matrix is defined as follows:

Definition 1 (Unitary matrix)**.** A matrix U is called unitary when

$$U^{-1} = U^{\dagger}. \tag{2.6}$$

Unitary operations leave the inner product invariant. It consequently also conserves the normalization of quantum states.

Hermitian matrices play an important role in quantum mechanics. They represent the observable needed to perform a measurement.

Definition 2 (Hermitian matrices)**.** A matrix H is Hermitian if

$$H^{\dagger} = H. \tag{2.7}$$

Definition 3 (Anti-Hermitian matrices)**.** A matrix A is anti-Hermitian if

$$A^{\dagger} = -A. \tag{2.8}$$

It is possible to separate every matrix into a Hermitian and an anti-Hermitian part as follows:

$$M = \frac{1}{2}(M + M^{\dagger}) + \frac{1}{2}(M - M^{\dagger}). \tag{2.9}$$

As a side note, the anti-Hermitian matrices are the generators for unitary matrices, implying e^{M} is unitary when M is anti-Hermitian.

Definition 4 (Nilpotent matrices)**.** A matrix N is nilpotent if there exists an integer k such that

$$N^{k} = 0. \tag{2.10}$$

2.1.3 Commutators/Anti-Commutators

A commutator tests how the order of operators influences the product. A commutator is defined as follows:

$$[A, B] = AB - BA. \tag{2.11}$$

If the commutator is 0, the order does not play a role. In quantum mechanics, this is an important property. Since a measurement collapses the state to an eigenvector of the observable, measuring multiple observables with a single quantum state is often impossible. However, this is not the case when two observables commute. In such a case, the measurements don't interfere with one another and can be performed on a single-state vector.

Another important effect is when we consider the Baker–Campbell–Hausdorff formula

$$e^A e^B = e^Z, \tag{2.12}$$

with Z being

$$Z = A + B + \frac{1}{2}[A, B] + \frac{1}{12}[A, [A, B]] - \frac{1}{12}[B[A, B]] + \cdots . \tag{2.13}$$

If A and B commute, than $Z = A + B$. An anti-commutator is defined as follows:

$$\{A, B\} = AB + BA. \tag{2.14}$$

It is an important operation when we discuss the anti-symmetric properties of electrons or fermions in general.

2.1.4 Chebyshev Expansion

The Chebyshev expansion is often used to approximate a function with a polynomial. The Chebyshev polynomials of the first kind can be constructed using a recursive function

$$\begin{aligned} T_0(x) &= 1, \\ T_1(x) &= x, \\ T_{n+1}(x) &= 2xT_n(x) - T_{n-1}(x). \end{aligned} \tag{2.15}$$

They form an orthogonal basis and can be used to approximate a function $f(x) \in \mathbb{R}, -1 \leq x \leq 1$

$$f(x) = \sum_{n=0}^{\infty} a_n T_n(x). \tag{2.16}$$

The coefficients a_n are determined using an inner product

$$a_n = \frac{2 - \delta_{0,n}}{\pi} \int_{-1}^{1} \frac{T_n(x) f(x)}{\sqrt{1 - x^2}} dx. \tag{2.17}$$

For some functions such as $e^{ax}, |x| \leq 1$ there are analytical solutions

$$e^{ax} = I_0(a) + 2 \sum_{k=1}^{\infty} I_k(a) T_k(x), \tag{2.18}$$

where I_k are the modified Bessel functions

$$I_k(a) = \sum_{l=0}^{\infty} \frac{(-1)^l}{2^{2l+k} l!(k + l)!} (a)^{2l+k}. \tag{2.19}$$

This approximation is also valid when using functions of matrices.

2.2 Quantum Chemistry

Computational chemistry uses the principles of quantum mechanics in the sense that molecules and other chemical systems follow the laws of quantum mechanics. The time-dependent Schrödinger equation describes the evolution of a quantum system. In principle, we can predict the system's future development when we know the initial state. This would allow us to predict what happens during chemical reactions. However, this approach is rarely used in practice since the computational requirements are too high. To calculate the ground state of a system, we use the time-independent Schrödinger equation

$$\hat{H} \left|\phi\right\rangle = E \left|\phi\right\rangle , \tag{2.20}$$

with $|\phi\rangle$ being the wave function that describes the system.

2.2.1 Electronic Structure Theory

In this thesis, we are primarily concerned with solving the electronic structure problem, which is at the heart of molecular quantum chemistry. It describes how the electrons are distributed in the potential generated by the nuclei. In a mathematical sense, this boils down to finding the eigenvalue and eigenvector of a Hamiltonian as described in equation 2.20. A molecular Hamiltonian can be written as follows:

$$\begin{aligned}\hat{H} = &- \sum_i \frac{\hbar^2}{2m_i} \nabla_i^2 - \sum_A \frac{\hbar^2}{2M_A} \nabla_A^2 - \sum_{i,A} \frac{Z_A e^2}{4\pi\epsilon_0 |r_i - R_A|} + \sum_{i>j} \frac{e^2}{4\pi\epsilon_0 |r_i - r_j|} \\ &+ \sum_{A>B} \frac{Z_A Z_B e^2}{4\pi\epsilon_0 |R_A - R_B|},\end{aligned} \tag{2.21}$$

with $\hbar$ being the plank constant and ϵ_0 is the vacuum permittivity. The masses of the electron i and nuclei A are given by m_i, M_A. The electric charge of nuclei A is given by $Z_A e$, and the charge of an electron is indicated by e. The coordinates of the particle are given by $r_{i,j}$ for electrons and by $R_{A,B}$ for the nucleus. In this Hamiltonian, the first two terms describe the kinetic energy of the electrons and the nuclei. The following terms describe the interaction energy between nuclei and electrons. Because of their mass, nuclei change position much slower than electrons. Therefore, we can consider them static. This is the Born-Oppenheimer approximation. To solve the eigenvalue equation, we can separate the state of a quantum chemical system into two parts. One part describes the position of the electrons around the nuclei, and the other describes the position of the nuclei. The wave function can be written as

$$\left|\phi\right\rangle = \left|\phi(r, R)\right\rangle_{\text{elec}} \otimes \left|\phi(R)\right\rangle_{\text{nuc}} . \tag{2.22}$$

Since the nuclei do not change position, we can consider $\left|\phi(R)\right\rangle_{\text{nuc}}$ to be constant and only solve for the electronic part. This leaves us with the electronic

Schrödinger equation

$$\hat{H}_{\text{elec}} \left|\phi(r,R)\right\rangle_{\text{elec}} = E_{\text{elec}} \left|\phi(r,R)\right\rangle_{\text{elec}}, \tag{2.23}$$

where $\hat{H}_{\text{elec}}$ is given by

$$\hat{H}_{\text{elec}} = -\sum_i \frac{\hbar^2}{2m_i}\nabla_i^2 - \sum_{i,A} \frac{Z_A e^2}{4\pi\epsilon_0 |r_i - R_A|} + \sum_{i>j} \frac{e^2}{4\pi\epsilon_0 |r_i - r_j|}. \tag{2.24}$$

Throughout this thesis, we are mainly concerned with finding the eigenstate with the lowest eigenvalue of $\hat{H}_{\text{elec}}$. We call this state the ground state. In the following, we will refer to $\hat{H}_{\text{elec}}$ as $\hat{H}$.

2.2.2 Second Quantized Hamiltonian

Different formalisms exist to express a molecular system's Hamiltonian. The second quantization formalism with a basis set model is most commonly used. We utilized this model in this thesis and will explain it in detail here.

In a basis-set formalism, the Hamiltonian gets represented in the basis of N molecular spin orbitals $\{\chi_k(r_i,\omega)\}$. With r being the coordinates of the i-th electron and ω its spin. Combining the spacial coordinates r and the ω in a combined coordinate $\mathbf{x}$ is common. We introduce the basis sets used in this thesis in Sec. 2.2.3. The state of the electron system needs to be written in the same basis as the Hamiltonian. But the postulates of quantum mechanics demand that the state of composite electrons is anti-symmetric since they are $\frac{1}{2}$-spin particles.

We can accomplish this by writing the states in a basis created by the Slater determinant. A Slater determinant ϕ of N electrons is written as

$$\phi(\mathbf{x}_0,\ldots,\mathbf{x}_{N-1}) = \frac{1}{\sqrt{N!}} \begin{vmatrix} \chi_0(\mathbf{x}_0) & \chi_1(\mathbf{x}_0) & \cdots & \chi_{N-1}(\mathbf{x}_0) \\ \chi_0(\mathbf{x}_1) & \chi_1(\mathbf{x}_1) & \cdots & \chi_{N-1}(\mathbf{x}_1) \\ \vdots & \vdots & \ddots & \vdots \\ \chi_0(\mathbf{x}_{N-1}) & \chi_1(\mathbf{x}_{N-1}) & \cdots & \chi_{N-1}(\mathbf{x}_{N-1}) \end{vmatrix}. \tag{2.25}$$

The pre-factor $\frac{1}{\sqrt{N!}}$ is required since a state needs to be normalized. The Slater determinant has N electrons occupying N spin-orbitals χ_k. The rows indicate the electron, whereas the columns are labeled by the spin-orbitals. Interchanging the position of two electrons switches the order of the rows in the Slater determinant, which changes the sign. The Slater determinant, therefore, follows the anti-symmetric requirement from the quantum mechanic postulate. Having two electrons in the same spin-orbital results in two identical columns and a 0-determinate. Therefore, the Pauli exclusion principle is also directly met.

In the second quantization formalism, we write the Slater determinant as

$$\phi(\mathbf{x}_0,\mathbf{x}_1,\ldots,\mathbf{x}_{N-1}) \equiv \left|f_0 f_1 \cdots f_{N-1}\right\rangle, \tag{2.26}$$

where f_k is equal to 1 when the orbital χ_k is occupied by an electron and 0 otherwise. A general state can be written as a linear combination of Slater determinants like

$$|\phi\rangle = \sum_i c_i \left|f_0 f_1 \cdots f_{N-1}\right\rangle_i, \tag{2.27}$$

with c_i being the coefficients. The anti-symmetric property is accounted for by how operators act on these states. Electrons can be created and annihilated in an orbital i. The associated creation operator $\hat{a}_i^\dagger$ and the annihilation operator $\hat{a}_i$ act on a state in the following way:

$$\begin{aligned} \hat{a}_i^\dagger \left|f_0 f_1 \cdots f_{N-1}\right\rangle &= \delta_{i,0}(-1)^{\sum_{r=0}^{i-1} f_r} \left|f_0 f_1 \cdots f_i \oplus 1 \cdots f_{N-1}\right\rangle, \\ \hat{a}_i \left|f_0 f_1 \cdots f_{N-1}\right\rangle &= \delta_{i,1}(-1)^{\sum_{r=0}^{i-1} f_r} \left|f_0 f_1 \cdots f_i \ominus 1 \cdots f_{N-1}\right\rangle. \end{aligned} \tag{2.28}$$

The phase $(-1)^{\sum_{r=0}^{i-1} f_r}$ is needed to ensure the anti-symmetric property. This is required since the spin operators that act on an orbital do not follow the fermion anti-commutator relationship. We discuss how the creation and annihilation operators can be mapped to spin operators using the Jordan-Wigner (JW) [65] mapping in Chapter 2.3.3. The creation and annihilation operators follow the anti-commutator rules given by

$$\begin{aligned} \{\hat{a}_i^\dagger, \hat{a}_j^\dagger\} &= 0, \\ \{\hat{a}_i, \hat{a}_j\} &= 0, \\ \{\hat{a}_i, \hat{a}_j^\dagger\} &= \delta_{i,j}. \end{aligned} \tag{2.29}$$

Writing the Hamiltonian using these creation and annihilation operators takes the form

$$\hat{H} = \sum_{i,j} h_{ij} \hat{a}_i^\dagger \hat{a}_j + \frac{1}{2} \sum_{i,j,k,l} h_{ijkl} \hat{a}_i^\dagger \hat{a}_j^\dagger \hat{a}_k \hat{a}_l. \tag{2.30}$$

The single h_{ij} and double-electron integrals h_{ijkl} take the form

$$h_{ij} = \int \chi_i^*(\mathbf{x}) \left(-\frac{1}{2}\nabla^2 - \sum_A \frac{Z_A}{|\mathbf{r} - \mathbf{R}_A|} \right) \chi_j(\mathbf{r})\, d\mathbf{x}, \tag{2.31}$$

$$h_{ijkl} = \int \int \chi_i^*(\mathbf{x}_1) \chi_j^*(\mathbf{x}_2) \frac{1}{|\mathbf{r}_1 - \mathbf{r}_2|} \chi_k(\mathbf{x}_1) \chi_l(\mathbf{x}_2)\, d\mathbf{x}_1\, d\mathbf{x}_2. \tag{2.32}$$

2.2.3 Basis Sets

In the previous section, we described how the second quantized Hamiltonian is represented using a basis set of molecular orbitals. However, handling molecular

orbitals on a computer is computationally quite expansive. It is, therefore, common practice to approximate the molecular spin orbitals using easier functions

$$\chi_i(\mathbf{x}) = \sum_{j=0}^{n_{\text{basis}}} b_{i,j}\phi_j(\mathbf{x}). \tag{2.33}$$

In quantum chemistry, different types of basis sets $\{\phi_j(\mathbf{x})\}_{j=0}^{n_{\text{basis}}}$ are used to represent molecular spin orbitals. A common approach is to use a linear combination of atomic-type orbitals. Another approach is to use a plane wave representation, which is often utilized when describing solid-state systems.

For atomic-type orbitals, Slater-type orbitals (STOs) are physically well-motivated. However, they are computationally challenging for evaluating integrals, such as those in Eq. (2.32). To overcome this challenge, typically, an approximation of the STOs by a linear combination of Gaussian-type orbitals (GTOs) is used.

Various GTO-based basis sets have been developed and are available in databases [66]. In this thesis, we use the STO-nG basis set, in which each STO is approximated by n GTOs. Specifically, we used the basis set STO-3G [67]. Additionally, we use the 6-31G* [68] and the correlation-consistent polarized valence double-zeta basis set (cc-pVDZ) [69] basis sets. The 6-31G* basis set is a split-valence basis set that represents the core orbitals with 6 GTOs, while the valence orbitals are approximated with two STOs that are represented with 3, respectively, 1 GTO. The asterisk indicates that polarization functions are also included in the basis set. The cc-pVDZ is a widely used basis set for accurate quantum chemistry calculations. The cc-pVDZ basis set is a type of basis sets called cc-pVnZ, for which n indicates the number of zeta functions. Increasing the parameter n allows for a systematic convergence to the complete basis set limit.

2.2.4 Hartree-Fock

We need a method to optimize Eq. (2.33) to find the molecular orbitals. For this, it is common to use the Hartree-Fock (HF) method. The HF method is an efficient method to solve the electronic structure problem using a classical computer. However, the electronic structure can only be solved exactly for particular systems. The HF method simplifies the problem by treating each electron as moving independently in the mean-field created by the other electrons. This is achieved by approximating the Hamiltonian with the Fock operator. The Fock operator includes the contribution of the electron-electron repulsion only in a mean-field way. This treatment, however, ignores electron-electron correlation. The HF method approximates the system's ground state as a single Slater determinant. The method follows an iterative process. It begins with an initial guess for the molecular orbitals using one of the previously discussed basis sets. The Fock operator is represented within this basis. Using the solution of the Fock equation, the molecular orbitals' approximation is updated. This process of defining a Fock operator and updating the molecular orbitals is repeated

until convergence. The converged molecular orbitals and the energy are the final output of this method. However, because the HF method treats electron-electron interaction using only a mean field of electrons, it ignores electronic constellation. This neglect leads to the requirement to use post-HF methods to incorporate these correlations. The HF method is most effective for systems where a single Slater determinant dominates, and correlation plays a minor role.

2.2.5 Electronic Correlation

The HF theory is not exact since it considers the influence on the electrons from all the other electrons by a single mean field. The difference between the exact energy E_{exact} and the HF energy E_{HF} is called the correlation energy. The physical reason for this difference is that electrons are correlated. This means that the probability for one electron to be in one specific position depends on the positions of the other electrons. In quantum chemistry, we consider two different types of correlations. Firstly, the strong (or static) correlation is an effect that occurs when a single Slater determinant can not accurately describe the ground state of a system. This is most noticeable with systems with near-degenerate electronic states. It is also essential to describe the breaking of chemical bonds. As a bond breaks, the system transforms from a single molecule with a bond to two separate molecules; this requires multiple electronic configurations to be described accurately. The second type of correlation is called weak (or dynamic) correlation. It describes the correlation of electronic motion. It can even play a role when a single Slater determinant is sufficient to describe the ground state but when the electron-electron interaction is not accurately described. In many molecular systems, both correlations play a role simultaneously. In order to increase the accuracy of quantum chemical calculations, Post-Hartree-Fock methods are required to take this electronic correlation into account.

2.2.6 Configuration Interaction

Configuration Interaction (CI) is a Post-Hartree-Fock method used to describe the electronic correlation in a molecule. In contrast to HF, it approximates the eigenstates of a Hamiltonian as a linear combination of Slater determinants instead of a single Slater determinant. The Slater determinants are usually constructed by considering excitations from the HF state as the reference state. In the CI algorithm, the eigenstate of the Hamiltonian is approximated by variational optimization of the coefficients in the linear combination of the Slater determinants

$$|\Phi\rangle_{\text{CI}} = C_0 |\phi_0\rangle + \sum_{i,a} C_i^a |\phi\rangle_i^a + \sum_{i,j,a,b} C_{i,j}^{a,b} |\phi\rangle_{i,j}^{a,b} + \cdots . \tag{2.34}$$

Typically $|\phi_0\rangle$ is the HF state $|\phi\rangle_{\text{HF}}$. The other states are created by acting with excitation operators on the $|\phi_0\rangle$, $|\phi\rangle_i^a = \hat{a}_a^\dagger \hat{a}_i |\phi_0\rangle, |\phi\rangle_{i,j}^{a,b} = \hat{a}_a^\dagger \hat{a}_b^\dagger \hat{a}_i \hat{a}_j |\phi_0\rangle, \cdots$. The indices $a, b, \cdots$ indicate empty orbitals and $i, j, \cdots$ orbitals occupied with

electrons. Therefore, to consider all possible determinates, the sums in Eq. (2.34) need to continue until excitations that excite all possible electrons are also considered. This method is called Full Configuration Interaction (FCI) and is exact considering the basis set. However, since the number of different Slater determinants scales exponentially with the number of electrons and the number of basis functions, it is often necessary to reduce the computational cost by introducing approximations. One way to reduce the computational cost is to only consider a subset of all the electrons and orbitals in the molecule. This is a so-called active space. This method is called CASCI, which stands for Complete Active Space Configuration Interaction. Another approach to reduce the computational cost is only considering a subset of the excitations. It is common to use only the single and the double excitations. This restriction leads to the method CISD, which stands for Configuration Interaction Single and Double. However, a severe drawback of the CISD method is that due to the truncation of excitations, the method is not size-consistent anymore. This means that calculating two systems separately and adding the energy leads to different amounts of energy than calculating them at the same time. This size consistency is a property often beneficial in computational studies.

2.2.7 Coupled Cluster

Coupled Cluster (CC) [28, 29] is used to expand on a reference wave function $|\phi_0\rangle$, including missing electronic correlations. Typically, the HF state is chosen as the reference state $|\phi_0\rangle$ for it has heuristically a good overlap with the ground state. Mathematically, the CC includes the electronic correlation by applying all possible excitations using an exponential ansatz

$$|\Phi\rangle_{\mathrm{CC}} = e^{\hat{T}} |\phi_0\rangle . \tag{2.35}$$

The parameterized ansatz $\hat{T}$

$$\begin{aligned} \hat{T} = &\sum_{i<a} t_i^a \hat{a}_a^\dagger \hat{a}_i + \sum_{i,j<a,b} t_{i,j}^{a,b} \hat{a}_a^\dagger \hat{a}_b^\dagger \hat{a}_i \hat{a}_j + ... \\ &a, b, \cdots \in \{unoccupied\}, i, j, \cdots \in \{occupied\}. \end{aligned} \tag{2.36}$$

Different truncations of $\hat{T}$ are possible. Typically, Coupled Cluster is used with Single and Double (CCSD) excitations, truncating the ansatz operator $\hat{T}$ at the two body terms. The parameters of the ansatz t_i^a and $t_{i,j}^{a,b}$ need to be optimized to find the appropriate wave function. $\hat{a}^\dagger$ and $\hat{a}$ are the creation and annihilation operators. Our notation enumerates occupied orbitals as $i, j...$ and unoccupied orbitals as $a, b....$ The parameters $t_i^a, t_{i,j}^{a,b}, t_{ij...}^{ab...}$ can be determined solving the equations

$$E_{\mathrm{CC}} = \langle \phi_0 | \, e^{-\hat{T}} \hat{H} e^{\hat{T}} \, |\phi_0\rangle , \tag{2.37}$$

$$0 = \left\langle \phi_{ij...}^{ab...} \right| e^{-\hat{T}} \hat{H} e^{\hat{T}} \, |\phi_0\rangle , \tag{2.38}$$

where E_{CC} is the ground state energy and $\left|\phi_{ij\ldots}^{ab\cdots}\right\rangle = \hat{a}_a^\dagger \hat{a}_b^\dagger \ldots \hat{a}_i \hat{a}_j \ldots |\phi_0\rangle$ are excited Slater determinants. Using the similarity-transformed Hamiltonian $\bar{H} = e^{-\hat{T}} \hat{H} e^{\hat{T}}$ in these functions naturally factors out redundant excitations significantly reduces the computational cost.

The asymmetrical energy Eq. (2.37) makes the energy not variational. Implying that the predicted energy is not an upper bound to the true ground state energy when a truncation is used. This can be seen in highly correlated systems such as N_2, where CCSD produces energies below the exact FCI solution.

Variational Coupled Cluster

The Variational Coupled Cluster (VCC) [53–63] is an alternative to the CC theory that does not break for highly correlated systems. It uses a symmetric expectation value, which takes the form

$$E_{\mathrm{VCC}} = \frac{\langle \phi_0 | \, e^{\hat{T}^\dagger} \hat{H} e^{\hat{T}} \, | \phi_0 \rangle}{\langle \phi_0 | \, e^{\hat{T}^\dagger} e^{\hat{T}} \, | \phi_0 \rangle}. \tag{2.39}$$

The parameters are found by minimizing the expectation value E_{VCC} in an iterative manner.

The ansatz operator $\hat{T}$ in Eq. (2.36) acts as a nilpotent operator on the qubits. We can see this directly when we consider it in the matrix representation. $\hat{T}$ is a sum of $\hat{a}_a^\dagger \hat{a}_i$ and $\hat{a}_a^\dagger \hat{a}_b^\dagger \hat{a}_i \hat{a}_j$ terms. Using the JW transformation, these summands take the form

$$\hat{a}_a^\dagger \hat{a}_i = \frac{(\hat{X}_a - i\hat{Y}_a)}{2} \otimes \hat{Z}_{a-i} \otimes \frac{(\hat{X}_i + i\hat{Y}_i)}{2} \tag{2.40}$$

and

$$\begin{aligned} \hat{a}_a^\dagger \hat{a}_b^\dagger \hat{a}_i \hat{a}_j = \frac{(\hat{X}_a - i\hat{Y}_a)}{2} \otimes \hat{Z}_{a-b} \otimes \frac{(\hat{X}_b - i\hat{Y}_b)}{2} \\ \otimes \frac{(\hat{X}_i + i\hat{Y}_i)}{2} \otimes \hat{Z}_{i-j} \otimes \frac{(\hat{X}_j + i\hat{Y}_j)}{2}. \end{aligned} \tag{2.41}$$

In both expressions, the first term $(\hat{X}_a - i\hat{Y}_a)/2$ is nilpotent, leading to the tensor product being nilpotent. Keep in mind that all excitations are from occupied to unoccupied; therefore, the indices $a, b > i, j$. A sum of upper triangle nilpotent matrices is again nilpotent.

Since $\hat{T}$ is nilpotent, a polynomial approximations of $e^{\hat{T}} = \sum_{i=0}^{d} c_i \hat{T}^i$ can be exact when a sufficient high polynomial degree d is used. To determine the maximal power k when $\hat{T}^k = 0$, we can consider the behavior of the smallest body term in powers of $\hat{T}$. The smallest body term occurring is a direct result of the product of the single body terms in $\hat{T}^i$. All terms of $\hat{T}^i$ become 0 when the smallest body terms exceed the available occupied or unoccupied orbitals. In that case, at least two excitation or de-excitation operators act on the same orbital. Since $\hat{a}_a^\dagger * \hat{a}_a^\dagger = 0 = \hat{a}_i * \hat{a}_i$, we can conclude that

$$d_{\max} = \min(\#\text{ of occupied orbitals}, \#\text{ of unoccupied orbitals}). \tag{2.42}$$

Unitary Coupled Cluster

With the rise of quantum computing, the unitary ansatz gained a lot of traction, especially in the context of VQE. In contrast to the VCC, the Unitary Coupled Cluster (UCC) [70] ansatz uses the anti-Hermitian operator $\hat{T} - \hat{T}^\dagger$ in the exponent. The expectation value is given by

$$E_{\mathrm{UCC}} = \langle \phi_0 | \, e^{\hat{T}^\dagger - \hat{T}} \hat{H} e^{\hat{T} - \hat{T}^\dagger} \, | \phi_0 \rangle \, . \tag{2.43}$$

The wave function $e^{\hat{T} - \hat{T}^\dagger} \, |\phi_0\rangle$ is normalized by construction.

Variational versus Unitary Coupled Cluster

The VCC and the UCC share many similarities. However, Harsha et al. showed in their work [61] following the work of Pal et al. [71] the difference between VCC and UCC mathematically. It can be shown that some of the energy terms vanish for the UCC compared to the VCC. This difference can lead to significant differences in the accuracy of the methods. Multiple numerical experiments have shown that the difference is most notable in strongly correlated systems [57, 61]. In their work, they showed energy differences between UCC and VCC using several molecules. VCC constantly produced more reliable results, with energy differences up to several mH.

2.3 Fundamentals of Quantum Computing

Quantum computing utilizes quantum mechanical effects such as entanglement and superposition in order to increase computational capabilities. Since a quantum computer behaves itself in a quantum mechanical way, it is more capable of representing a quantum state than a classical computer.

Quantum computing evolves an initial state using a unitary transformation to a final point in the Hilbert space. The unitary transformation represents the algorithm executed on a quantum computer. To learn about the produced state, one can measure an observable. This happens projectively, meaning that measuring the observable collapses the system's state to an eigenvector of the observable.

Multiple approaches exist to represent a quantum algorithm. However, the most used method is to use gates to represent the circuit. We used this model in this thesis, so we will discuss it in more detail. In this model, the quantum computer can execute predefined unitary operations. This operations are called gates. The gates available on a quantum device depend on the concrete implementation. In Sec. 2.3.2 we will discuss the most common used gates.

2.3.1 Qubits

The smallest unit in a quantum computer is a qubit. It is the equivalent of a bit on a classical computer. However, in contrast to a classical bit that can represent

the states 0 and 1, a qubit can hold the states $|0\rangle$ and $|1\rangle$ in a superposition. For a pure state, the state can be written as

$$|\phi\rangle = a\,|0\rangle + b\,|1\rangle\,. \tag{2.44}$$

The state is normalized by imposing the restriction

$$|a|^2 + |b|^2 = 1, a, b \in \mathbb{C} \tag{2.45}$$

on the coefficients a and b.

2.3.2 Gates

In this section, we introduce the most common gates. Gates are predefined operations executable on a quantum computer. We summarize the most common gates in Tab. 2.1, showing the symbols used in a quantum circuit as well as their matrix representation. It should be noted that a quantum computer does not need to be able to execute all of these gates since some of them can be constructed from a combination of the other gates.

2.3.3 Fermion to Qubit Mapping

Quantum computers operate using qubits, which are two-level systems and can naturally represent spin-$\frac{1}{2}$ systems. However, simulating this spin-$\frac{1}{2}$ systems is still challenging since the operators need to follow the non-trivial commutation relationships we have mentioned in Eq. (2.29). In this thesis, we used the JW [65] mapping. It creates a one-to-one mapping of spin-orbitals to qubits and ensures that the operators follow the correct commutation rules. The creation and annihilation operator can be mapped to the qubit system on a quantum computer following these rules

$$\hat{a}_j^\dagger \mapsto \frac{1}{2}(\mathbb{1}^{\otimes j-1}) \otimes (\hat{X}_j - i\hat{Y}_j) \otimes \hat{Z}^{\otimes N-j-1} \tag{2.46}$$

and

$$\hat{a}_j \mapsto \frac{1}{2}(\mathbb{1}^{\otimes j-1}) \otimes (\hat{X}_j + i\hat{Y}_j) \otimes \hat{Z}^{\otimes N-j-1}, \tag{2.47}$$

where $\hat{X}, \hat{Y}, \hat{Z}$ are the Pauli operators and $\mathbb{1}$ is the identity matrix.

However, the JW transformation is not the only encoding strategy. Other also exist such as the Parity encoding or the Bravyi-Kitaev encoding. These encodings could lead to more compact representations of the creation and annihilation operator; however, the correspondence between fermion occupation and qubit configurations is not as straightforward as in JW. These methods are explained in detail in Ref. [72].

Operator	Gate(s)	Matrix
Pauli-X (X)		$\begin{pmatrix} 0 & 1 \\ 1 & 0 \end{pmatrix}$
Pauli-Y (Y)	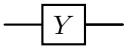	$\begin{pmatrix} 0 & -i \\ i & 0 \end{pmatrix}$
Pauli-Z (Z)	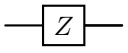	$\begin{pmatrix} 1 & 0 \\ 0 & -1 \end{pmatrix}$
Hadamard (H)	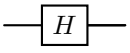	$\frac{1}{\sqrt{2}}\begin{pmatrix} 1 & 1 \\ 1 & -1 \end{pmatrix}$
Phase (S, P)	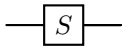	$\begin{pmatrix} 1 & 0 \\ 0 & i \end{pmatrix}$
$\pi/8$ (T)	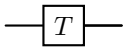	$\begin{pmatrix} 1 & 0 \\ 0 & e^{i\pi/4} \end{pmatrix}$
Controlled Not (CNOT, CX)	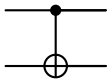	$\begin{pmatrix} 1 & 0 & 0 & 0 \\ 0 & 1 & 0 & 0 \\ 0 & 0 & 0 & 1 \\ 0 & 0 & 1 & 0 \end{pmatrix}$
Controlled Z (CZ)		$\begin{pmatrix} 1 & 0 & 0 & 0 \\ 0 & 1 & 0 & 0 \\ 0 & 0 & 1 & 0 \\ 0 & 0 & 0 & -1 \end{pmatrix}$
SWAP		$\begin{pmatrix} 1 & 0 & 0 & 0 \\ 0 & 0 & 1 & 0 \\ 0 & 1 & 0 & 0 \\ 0 & 0 & 0 & 1 \end{pmatrix}$
Toffoli (CCNOT, CCX, TOFF)	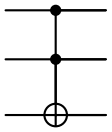	$\begin{pmatrix} 1 & 0 & 0 & 0 & 0 & 0 & 0 & 0 \\ 0 & 1 & 0 & 0 & 0 & 0 & 0 & 0 \\ 0 & 0 & 1 & 0 & 0 & 0 & 0 & 0 \\ 0 & 0 & 0 & 1 & 0 & 0 & 0 & 0 \\ 0 & 0 & 0 & 0 & 1 & 0 & 0 & 0 \\ 0 & 0 & 0 & 0 & 0 & 1 & 0 & 0 \\ 0 & 0 & 0 & 0 & 0 & 0 & 0 & 1 \\ 0 & 0 & 0 & 0 & 0 & 0 & 1 & 0 \end{pmatrix}$
$R_x(\theta)$	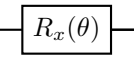	$\begin{pmatrix} \cos(\theta/2) & -i\sin(\theta/2) \\ -i\sin(\theta/2) & \cos(\theta/2) \end{pmatrix}$
$R_y(\theta)$	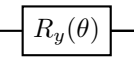	$\begin{pmatrix} \cos(\theta/2) & -\sin(\theta/2) \\ \sin(\theta/2) & \cos(\theta/2) \end{pmatrix}$
$R_z(\theta)$	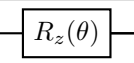	$\begin{pmatrix} e^{-i\theta/2} & 0 \\ 0 & e^{i\theta/2} \end{pmatrix}$

Table 2.1: Quantum Logic Gates

2.4 Quantum and Quantum-Classical Algorithms

2.4.1 Variational Quantum Eigensolver

The variational quantum eigensolver (VQE) [14–16] algorithm solves an eigenvalue problem using a classical and a quantum computer. Its goal is to find the lowest eigenvalue $E^{(G)}$ and the corresponding ground state. The VQE is an iterative algorithm. We show a single iteration step in Fig. 2.1. A parameterized ansatz $\hat{U}(\vec{\theta}^n)$ is used to generate a trial state $|\phi_n\rangle$ of the ground state on a quantum computer. Here, the index n indicates that we are in the n-th iteration. Usually, the HF state $|\mathrm{HF}\rangle$ is selected as the reference state $|\phi_0\rangle$.

$$|\phi_n\rangle = \hat{U}(\vec{\theta}^n)\,|\phi_0\rangle\,. \tag{2.48}$$

The literature uses multiple different ansatzes, such as hardware-efficient or the chemically inspired UCC ansatz. In this thesis, we used the Unitary Coupled Cluster with Single and Double excitations (UCCSD) ansatz.

VQE measures the energy $E^{(n)}$ of the trial state in a variational way

$$E^{(n)} = \langle\phi_n|\,\hat{H}\,|\phi_n\rangle \equiv E^{(n)} \geq E^{(G)}. \tag{2.49}$$

Therefore, the measured energy $E^{(n)}$ is always greater or equal to the ground state energy $E^{(G)}$. A classical computer is used to interpret the measured energy and update the parameters $\vec{\theta}^n \to \vec{\theta}^{n+1}$ accordingly to an optimization algorithm. In this thesis, we often used the L-BFGS algorithm, which is a classical gradient descent optimization procedure. The VQE was developed in 2014 by Peruzzo et al. [14]. It is an alternative approach to QPE or Imaginary Time Evolution (ITE) [73–77], which both require long coherence times and high-fidelity gates. The VQE, being a quantum-classical hybrid algorithm, is expected to require more shallow circuits and be, therefore, better suited for the NISQ era of quantum computing.

2.4.2 Quantum Singular Value Transformation

This section reviews the quantum singular value transformation (QSVT) [64] algorithm. We follow the notation of Ref. [78], which includes a great pedagogical tutorial. QSVT is a quantum algorithm allowing to perform a polynomial transformation $\mathrm{Poly}^{(\mathrm{SV})}(A)$ on the singular values of a matrix A. Here $\mathrm{Poly}^{(\mathrm{SV})}(A)$ indicates that the singular values of matrix A get transformed according to a polynomial. QSVT can often be used as a subroutine in algorithms [78–81]. The achievable polynomials are restricted by

$$\begin{aligned} &\deg(\mathrm{Poly}^{(\mathrm{SV})}) \leq d, \\ &\mathrm{Poly}^{(\mathrm{SV})} \text{ has parity } d \bmod 2, \\ &\forall x \in [-1,1],\ |\mathrm{Poly}^{(\mathrm{SV})}(x)|^2 \leq 1. \end{aligned} \tag{2.50}$$

The expression $\deg(\mathrm{Poly}^{(\mathrm{SV})})$ indicates the degree of the applied polynomial. Given a matrix $A = \sum_k \sigma_k\,|w_k\rangle\,\langle v_k|$ with $|w_k\rangle\,, |v_k\rangle$ being its left and right

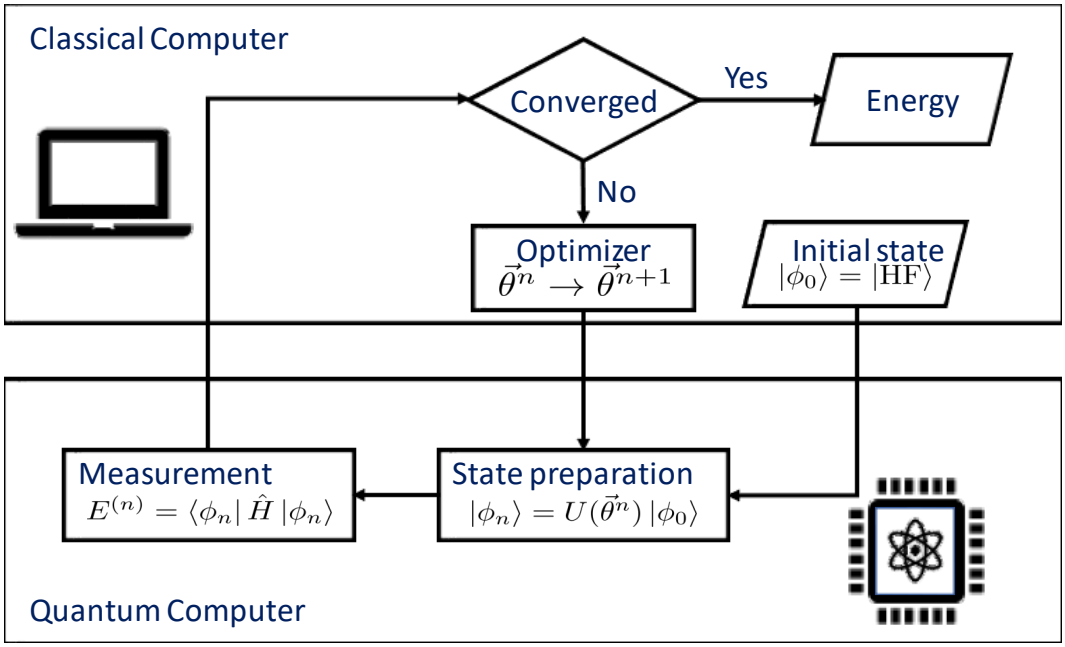

Figure 2.1: Variational Quantum Eigensolver of a single iteration. A parameterized ansatz is applied on an initial state $|\phi_0\rangle$ to create a trial state $|\phi_n\rangle$ on a quantum computer. The measured energy is returned to a classical computer, which updates the parameters $\vec{\theta}^n$ to lower the trial energy according to a classical optimizer. This process is repeated until the energy converges.

singular vectors and σ_k its singular values. The $\text{Poly}^{(\text{SV})}(A)$ is defined depending on whether it has even or odd parity as

$$\begin{aligned} \text{Poly}^{(\text{SV})}_{\text{odd}}(A) &= \sum_k \text{Poly}(\sigma_k) \left|w_k\right\rangle \left\langle v_k\right|, \\ \text{Poly}^{(\text{SV})}_{\text{even}}(A) &= \sum_k \text{Poly}(\sigma_k) \left|v_k\right\rangle \left\langle v_k\right|. \end{aligned} \tag{2.51}$$

When matrix A is Hermitian, the right and left eigenvectors are equivalent, and the matrix can be written as $A = \sum_k \sigma_k \left|v_k\right\rangle \left\langle v_k\right|$. In such a case, the singular and eigenvalue transformations are equivalent.

The QSVT achieves this transformation by first encoding matrix A into a unitary operator $\hat{U}$ using block-encoding [82–84]. This is done so that A can be executed on a quantum computer.

$$\hat{U} = \begin{bmatrix} A & \cdot \\ \cdot & \cdot \end{bmatrix}. \tag{2.52}$$

For the sake of readability, we omitted some entries of $\hat{U}$ and replaced them with $\cdot$. These entries are needed to ensure that $\hat{U}$ is unitary and are determined in the block-encoding algorithm. The QSVT algorithm transforms the operator $\hat{U}$ into the form

$$\text{QSVT}(\hat{U}) = \begin{bmatrix} \text{Poly}^{(\text{SV})}(A) & \cdot \\ \cdot & \cdot \end{bmatrix}, \tag{2.53}$$

using the quantum circuits [78]

$$\begin{aligned} \text{QSVT}_{\text{odd}} &= \tilde{\Pi}_{\Psi_1} \hat{U} \left[\prod_{k=1}^{(d-1)/2} \Pi_{\Psi_{2k}} \hat{U}^\dagger \tilde{\Pi}_{\Psi_{2k+1}} \hat{U} \right], \\ \text{QSVT}_{\text{even}} &= \left[\prod_{k=1}^{d/2} \Pi_{\Psi_{2k-1}} \hat{U}^\dagger \tilde{\Pi}_{\Psi_{2k}} \hat{U} \right]. \end{aligned} \tag{2.54}$$

$\Pi_\Psi = e^{2i\Psi \sum_k \left|v_k\right\rangle \left\langle v_k\right|}, \tilde{\Pi}_\Psi = e^{2i\Psi \sum_k \left|w_k\right\rangle \left\langle w_k\right|}$ are rotations round the subspace defined by the right and left singular vector of the matrix A. From Eq. (2.54), we see that the length of the QSVT algorithm scales polynomially with the degree d of the polynomial, allowing it to be applied to high-degree polynomials. The challenge in using QSVT is to find the appropriate angles Ψ to execute the correct transformation. Using the strategies discussed in [64, 85, 86], the angles can be determined efficiently using a classical computer.

In order to lift some of the restrictions on $\text{Poly}^{(\text{SV})}(A)$ defined in Eq. (2.50), we can combine multiple QSVT, allowing us to perform real polynomial transitions of indifferent parity. We can combine multiple QSVT using a linear combination of unitaries [87] approach.

Chapter 3

Local Bases of Deep Variational Quantum Eigensolver for Quantum Chemistry

In this Chapter, we address the limited resource problem with a divide-and-conquer approach. In particular, we work with the deep VQE algorithm. Deep VQE splits the molecule into subsystems and solves them individually using VQE. The individual subsystem grounds states are used as a starting point to form a reduced Hilbert space for the full system. We examined different strategies to form the reduced Hilbert space in the deep VQE algorithm. Using numerical experiments, we show that the different strategies differ in accuracy and ability to reduce the number of needed qubits. Therefore, selecting a basis-forming strategy is an essential part of the deep VQE algorithm. Selecting an appropriate strategy, we were able to approximate the ground state within chemical accuracy for some of the examined quantum systems. This Chapter is based on [Erhart, Mitarai, Mizukami, and Fujii, Phys. Rev. Applied 18, 064051].

3.1 Introduction

Quantum algorithms have better asymptotic behavior than classical alternatives for some of today's most challenging and intriguing calculation problems. Outstanding examples are factorization of large integers using the Shor algorithm [2, 3], linear algebraic processes (matrix inversion) [4, 64, 88], as well as promising results in quantum machine learning [89]. Quantum chemistry will, however, arguably be the research field that gets impacted most by quantum computing [90]. Simulating large molecules using a quantum computer will push our

understanding of nature to new levels and significantly affect today's society. A specific intent in quantum chemistry is to calculate the electronic ground state of a molecule. Since the dimension of the Hilbert space grows exponentially to the system size, a molecular electronic structure can be exceedingly complex to solve on a classical computer.

Despite recent developments [91–93], we anticipate that quantum computers in the near future still have a limited number of qubits and only partial error resistance. Therefore, the number of operations on a quantum device is limited, as the errors are building up to a point where we can not receive meaningful results. These restrictions confine us to the area of so-called NISQ algorithms [10].

The VQE algorithm is a promising approach for overcoming these obstacles. VQE is a method designed to find the ground state of a chemical system. One uses a parameterized variational circuit, or ansatz, on a quantum device to prepare a trial state whose energy gets measured. A classical computer sets the parameters for the ansatz following some optimizer rules. By looping between the quantum device and a classical computer, one tries to minimize the energy. Using such an approach, it is possible to find a good approximation of the ground state. The states created in such a way can be classically hard to represent. Depending on the ansatz, this only requires a circuit with a modest number of gates. Therefore, it is possible that VQE could be running on an NISQ device.

The system size solvable by the VQE is essentially limited by the number of qubits on the quantum device, making it challenging to apply it to large-scale systems. In classical quantum chemistry methods, fragmentation techniques [94] proved to be highly successful in reducing the computational requirement to handle large-scale molecules. Recently, divide-and-conquer techniques in quantum computing also got much attention to potentially solve the problem of the limited quantum resource [17–20]. They aim to decrease the number of qubits needed to solve complex problems. These techniques separate the original system into subsystems and solve them individually. The subsystem solutions set the starting point to formulate a meaningful result of the original problem in the next step.

One such method is the deep VQE [20]. It first separates the target quantum system into subsystems and obtains their approximate ground states by the usual VQE. The next step constructs a basis set for each subsystem by applying specific excitation operators to the subsystem ground states. The basis set is later used to form an effective Hamiltonian of the whole system. Another VQE can then solve the effective Hamiltonian to obtain a ground state of the target system. This process can be repeated multiple times to solve increasingly large systems. The performance of the deep VQE has been analyzed for spin systems [20] and periodic materials [17], which have suggested that the deep VQE can produce accurate results while reducing the number of needed qubits simultaneously. However, only systems with minimal interactions between subsystems have been examined. Molecules are highly complex systems for which the Hamiltonian consists of many terms with various strengths. Such complex systems provide a unique set of challenges for the deep VQE. It is, therefore, vital to examine the performance of the deep VQE for such systems.

In this Chapter, we propose multiple methods to create the search-able subspace and compare their influence on the accuracy of the deep VQE using tree-like molecules as a testbed. A 10-atom, and a 13-atom dendrimer-like molecule only consisting of hydrogen atoms, were chosen as the tree-molecules in question. Additionally to these toy-models we also apply the deep VQE to retinal to examine its performance on a natural molecule. Retinal is a natural occurring molecule of considerable size and is therefore a good indicator for the performance of deep VQE on a real complex molecule. The strategy for creating a subsystem basis ultimately limits the deep VQE performance as it determines which subspace of the entire Hilbert space can be explored to express the ground state. To examine the impact of different bases on the deep VQE, we tested three strategies to select excitation operators to form the subsystem basis. The first method followed the original paper and is based on the interaction operators. The second technique uses single-qubit Pauli operators to create a basis set, whereas the third obtains a basis using single-electron excitation and deexcitation operators. Additionally to the different basis creation methods, we propose multiple techniques to control the needed qubits. This shows the remarkable accuracy and reduction of qubits the deep VQE offers for even complex quantum systems. We find that the deep VQE can simulate the electron-correlation energy of the ground state to an error of below 1%, thus helping us reach chemical accuracy in some cases. Our understanding of the various basis creation methods and the comparison of their performance provides an essential recipe for determining the bases of subsystems for the use of deep VQE in larger molecules of even more practical importance.

3.2 Theory

3.2.1 Deep VQE

The deep VQE [20] is an algorithm of the divide and conquer family. Its purpose is to calculate the ground state of a quantum system. We review the algorithm of the original deep VQE, which can treat spin Hamiltonians consisting of 2-local interactions. In deep VQE, we first divide the system into M subsystems. The problem Hamiltonian with 2-local interactions can consequently be written in the form of,

$$\hat{H} = \sum_{i=1}^{M} \hat{H}_i + \sum_{i,j=1}^{M} \hat{V}_{ij}, \tag{3.1}$$

where $\hat{H}_i$ acts on subsystem i and $\hat{V}_{ij}$ on subsystems i and j. The interaction term $\hat{V}_{ij}$ decompose into operators $\hat{V}_{\mu,i}$ acting only on single subsystems i:

$$\hat{V}_{ij} = \sum_{\mu} \lambda_{ij}^{\mu} \hat{V}_{\mu,i} \hat{V}_{\mu,j}, \tag{3.2}$$

where μ indicates the different interaction terms. The deep VQE first finds ground states $|G_i\rangle$ of each subsystem Hamiltonian $\hat{H}_i$ using a VQE algorithm.

Then we build a subsystem basis $\{|b_{i,k}\rangle\}_{k=1}^{K_i}$ for each subsystem i with dimensions K_i by acting with certain excitation operators $\mathcal{B}_i = \{B_{i,k}\}$ that $|G_i\rangle$. The selection of the excitation operators $B_{i,k}$ is a crucial step which determines the performance of the deep VQE, and we will discuss it in detail in Sec. 3.3. To ensure the created basis set $\{|b_{i,k}\rangle\}_{k=1}^{K_i}$ is orthogonal a Gram-Schmidt orthogonalization is applied.

In the next step, we construct an effective Hamiltonian $\hat{H}^{\text{eff}}$ by projecting the original Hamiltonian $\hat{H}$ to the subspace spanned by $\bigotimes_i \{|b_{i,k}\rangle\}_{k=1}^{K_i}$. This can be achieved by measuring all matrix elements $\langle b_{i,k}| \hat{H}_i |b_{i,l}\rangle$ as well as $\langle b_{i,k}| \langle b_{j,l}| \hat{V}_{i,j} |b_{i,p}\rangle |b_{j,q}\rangle = \sum_\mu \lambda_{i,j}^\mu \langle b_{i,k}| \hat{V}_{\mu,i} |b_{i,p}\rangle \langle b_{j,l}| \hat{V}_{\mu,j} |b_{j,q}\rangle$. Notice that calculating the expectation values only involves one subsystem, which can be calculated separately on a quantum computer. Now, we represent each subsystem by $N_i = \lceil \log_2 K_i \rceil$ qubits, and we again utilize the VQE using $N_{\text{tot}} = \sum_i \lceil \log_2 K_i \rceil$ qubits to search for the ground state of $\hat{H}^{\text{eff}}$. Even though $\hat{H}^{\text{eff}}$ whose dimension is $d = \prod_i K_i$ could, in principle, be mapped to $\lceil \log_2 d \rceil \leqslant N_{\text{tot}}$ qubits, it is beneficial to map each subsystem individually since it preserves the locality of the Hamiltonian. The deep VQE algorithm can be repeated iteratively to treat larger and larger systems on a qubit-limited quantum computer.

3.2.2 Deep VQE for Fermionic System

The central problem in quantum chemistry is finding the first-principles Hamiltonian's ground state, which describes interacting electrons. In the second quantization, the Hamiltonian can be written in the form

$$\hat{H} = \sum_{o,p=1}^{N} h_{o,p} \hat{a}_o^\dagger \hat{a}_p + \sum_{q,r,s,t=1}^{N} h_{q,r,s,t} \hat{a}_q^\dagger \hat{a}_r^\dagger \hat{a}_s \hat{a}_t. \tag{3.3}$$

where N is the number of orbitals of the molecule. Here, we consider how to apply the deep VQE to this Hamiltonian.

A frequent approach to treat the Hamiltonian of Eq. (3.3) on a quantum computer is to map the fermionic operators $\hat{a}_o^\dagger$ and $\hat{a}_o$ to qubit operators through, e.g., JW transformation. This leads to a Hamiltonian in the form of,

$$\hat{H} = \sum_i h_i P_i, \tag{3.4}$$

where P_i is a Pauli string, $P_i \in \{\hat{I}, \hat{X}, \hat{Y}, \hat{Z}\}^{\otimes N}$, and h_i is a real coefficient. The obstacle to applying the deep VQE is that P_i is not 2-local but can be nonlocal when using JW transformation, as we will see below.

After partitioning the system into M subsystems and M_{int} interaction terms, we can write the Hamiltonian in Eq. (3.4) in the form of

$$\hat{H} = \sum_{i=1}^{M} \hat{H}_i + \sum_{\mu=1}^{M_{\text{int}}} \lambda^\mu \hat{V}_{\mu,1} \otimes \hat{V}_{\mu,2} \otimes \cdots \otimes \hat{V}_{\mu,M}, \tag{3.5}$$

where $\hat{H}_i$ and $\hat{V}_{\mu,i}$ is an operator acting only on the i-th subsystem, and μ indexes different interaction terms. To perform the deep VQE, we construct the effective Hamiltonian $\hat{H}^{\text{eff}}$ using the subsystem basis $\{|b_{i,k}\rangle\}_{k=1}^{K_i}$. To do this, we measure the matrix elements $(\hat{H}_i{}^{\text{eff}})_{k,l} = \langle b_{i,k}| \hat{H}_i |b_{i,l}\rangle$ and $(\hat{V}^{\text{eff}}_{\mu,1})_{k,l} = \langle b_{i,k}| \hat{V}_{\mu,i} |b_{i,l}\rangle$ for all combinations of i, k, l, and μ. Let $\hat{H}_i{}^{\text{eff}}$ and $\hat{V}^{\text{eff}}_{\mu,i}$ be $n_i = \lceil \log_2 K_i \rceil$-qubit operators with the evaluated matrix elements. The total effective Hamiltonian can be written as

$$\hat{H}^{\text{eff}} = \sum_{i=1}^{M} \hat{H}_i{}^{\text{eff}} + \sum_{\mu=1}^{M_{\text{int}}} \lambda^\mu \hat{V}^{\text{eff}}_{\mu,1} \otimes \hat{V}^{\text{eff}}_{\mu,2} \otimes \cdots \otimes \hat{V}^{\text{eff}}_{\mu,M}. \tag{3.6}$$

If we wish to perform the VQE of $\hat{H}^{\text{eff}}$, we must be able to efficiently measure the expectation value $\langle \hat{H}^{\text{eff}} \rangle = \langle \psi | \hat{H}^{\text{eff}} |\psi\rangle$ for a given state $|\psi\rangle$ prepared on a quantum computer. A usual approach to measure the expectation value of a Hamiltonian is to expand it into Pauli operators. However, if we do so in Eq. (3.6), the number of Pauli operators grows exponentially to M due to its nonlocality, which blocks efficient evaluation of $\langle \hat{H}^{\text{eff}} \rangle$.

We must avoid this exponential growth to apply the deep VQE to fermionic systems. To this end, we first diagonalize $\hat{V}^{\text{eff}}_{\mu,i}$ classically and obtain unitary $U_{\mu,i}$ such that

$$\hat{V}^{\text{eff}}_{\mu,i} = U^\dagger_{\mu,i} \text{diag}(\boldsymbol{v}_{\mu,i}) U_{\mu,i}, \tag{3.7}$$

where $\boldsymbol{v}_{\mu,i}$ are eigenvalues of $\hat{V}^{\text{eff}}_{\mu,i}$. Note that this process can be performed in time $2^{O(n_i)}$ and that it is natural to assume n_i is a small constant in the deep VQE. We can also construct a quantum circuit to realize a 2^{n_i}-dimensional unitary $U_{\mu,i}$ in time $2^{O(n_i)}$. Therefore, we can measure $\langle \hat{V}^{\text{eff}}_{\mu,1} \otimes \cdots \otimes \hat{V}^{\text{eff}}_{\mu,M} \rangle$ for a given $\sum_{i=1}^{M} n_i$-qubit state $|\psi\rangle$ by first applying $U_{\mu,1} \otimes \cdots \otimes U_{\mu,M}$ to $|\psi\rangle$ and then measuring it in the computational basis. Therefore, the required measurements to determine the expectation value of the interaction term scale linearly with the number of interactions in the system. Thereby, we can efficiently measure $\langle \hat{V}^{\text{eff}}_{\mu,1} \otimes \cdots \otimes \hat{V}^{\text{eff}}_{\mu,M} \rangle$ and hence $\langle \hat{H}^{\text{eff}} \rangle$ as well.

Note that we prefer JW transformation for applying deep VQE to fermionic systems because it directly maps the i-th orbital to the i-th qubit; if the i-th qubit is $|1\rangle$, it indicates that an electron occupies the i-th orbital. This property allows us to split systems naturally into subsystems using localized orbitals. Although other techniques, such as Bravyi-Kitaev transformation, relax the locality of Pauli strings down to $O(\log N)$, the correspondence between fermion occupation and qubit configurations is not straightforward. Note that the above technique may also be used for BK-transformation-based deep VQE to obtain the expectation values efficiently.

Table 3.1: Description of basis sets with starting vector and excitations. n_i number of qubits in subsystem i. A_i number of qubits involved in strongest interaction. In Interactions fix qubits method ε_{adapt} is selected such that the generated basis set is of fixed dimension. Otherwise, a fixed ε was chosen for the interaction-based methods.

Method	**Start vectors**	**Applied excitation** $B_{i,k}$
Interactions	$\left\|G_i^0\right\rangle$	$\forall \hat{V}_{\mu,i} \in \hat{V}_{i,j,...} \quad \lambda^\mu > \varepsilon$
Interactions & excited	$\left\|G_i^e\right\rangle \ \forall e < l$	$\forall \hat{V}_{\mu,i} \in \hat{V}_{i,j,...} \quad \lambda^\mu > \varepsilon$
Interactions fix qubits	$\left\|G_i^0\right\rangle$	$\forall \hat{V}_{\mu,i} \in \hat{V}_{i,j,...} \quad \lambda^\mu > \varepsilon_{adapt}$
Single Pauli	$\left\|G_i^0\right\rangle$	$P_s \quad s \in \{1, ..., n_i\}$
Single Pauli & excited	$\left\|G_i^e\right\rangle \ \forall e < l$	$P_s \quad s \in \{1, ..., n_i\}$
Single Pauli edge	$\left\|G_i^0\right\rangle$	$P_s \quad s \in A_i$
Particle conserving	$\left\|G_i^0\right\rangle$	$\mathrm{SWAP}_{s,s'}$, $\hat{a}_s, \hat{a}_s^\dagger \quad s, s' \in \{1, ..., n_i\}$
Particle conserving edge	$\left\|G_i^0\right\rangle$	$\mathrm{SWAP}_{s,s'}$, $\hat{a}_s, \hat{a}_s^\dagger \quad s \in A_i$

3.3 Method

3.3.1 Basis Creation Strategies

Choosing a basis set impacts the performance of the deep VQE. It ultimately determines the number of qubits needed to run the algorithm and the accuracy of the result. It is, therefore, vital to make an educated decision about the method used.

Below, we examine different procedures to generate the basis sets, which are summarized in Tab. 3.1 as well as their scaling in Tab. 3.2. In the single Pauli method, we use the set of the Pauli operators X, Y, Z acting on each qubit as $\mathcal{B}_i$. In the interactions approach, we apply all $\hat{V}_{\mu,i}$ in Eq. (3.6) to the subsystem i to create a basis, this leads to $\mathcal{B}_i = \{\hat{V}_{\mu,i}\}_{\mu=1}^{M_{\mathrm{int}}}$. For the particle conserving approach, we apply the excitation $\hat{a}_s^\dagger$ or the de-excitation operators $\hat{a}_s$ to every qubit s of the n_i qubits of the subsystem. Additionally, to capture effects inside the subsystems, we applied swap gates between different qubits belonging to the same subsystem to create a basis. Therefore, in this approch, $\mathcal{B}_i = \{\hat{a}_s\}_{s=1}^{n_i} \cup \{\hat{a}_s^\dagger\}_{s=1}^{n_i} \cup \{\mathrm{SWAP}_{s,s'}\}_{s,s'=1}^{n_i}$.

We also use additional low-lying energy eigenstates $|G_i^e\rangle$ to generate the basis sets instead of using only $|G_i\rangle$ as has been done in the original paper [20]. The superscript e marks the e-th excited state and we define $\left|G_i^0\right\rangle := |G_i\rangle$. Note that if the subsystem Hamiltonian has degenerate ground states, $|G_i^e\rangle$ does not necessarily have a different energy than $\left|G_i^0\right\rangle$. Such excited states can be constructed with an algorithm like the subspace-search VQE [95]. After applying $\mathcal{B}_i$ to $\{|G_i^e\rangle\}_{e=1}^{l}$, we use the Gram-Schmidt algorithm to ensure that the created basis is orthogonal and minimal with K_i elements.

The number of basis vectors determines how many qubits we need to run the deep VQE algorithm. We, therefore, also examine different approaches to reduce the dimensionality of the basis. For the interaction-based methods,

we only consider interactions between subsystems with λ^μ exceeding a certain threshold $\varepsilon > 0$. In the numerical experiments that follow, we examine the results for $\varepsilon = 10^{-2}$ if not stated otherwise. This selection was necessary since otherwise, the interaction-based methods would lead to basis sets that resemble no reduction from the entire Hilbert space. This was caused due to the numerous interaction terms between the subsystems for the molecular Hamiltonian.

The particle conserving and single Pauli methods as well can produce basis sets with a dimensionality that is challenging to represent on a quantum machine. We, therefore, also examine methods to truncate their basis sets. Our approach aimed to reduce the number of participating qubits in the subsystems for the basis-creating step, leading to a subset of the entire basis. To do so, we select the interaction $\bigotimes_{i=1}^{M} \lambda^\mu \hat{V}_{\mu,i}$ which has the largest absolute λ^μ. Let us denote the set of qubits involved in this interaction by A_i for each subsystem i. We then apply the corresponding excitation operators of the particle conserving or single Pauli methods to the qubits in A_i to create the basis. We call these methods particle conserving edges and single Pauli edges, respectively. Mathematically, the former method uses $\mathcal{B}_i = \{\hat{a}_s\}_{s\in A_i} \cup \{\hat{a}_s^\dagger\}_{s\in A_i} \cup \{\mathrm{SWAP}_{s,s'}\}_{s,s'\in A_i}$ and the latter uses $\mathcal{B}_i = \{\hat{X}_s, \hat{Y}_s, \hat{Z}_s\}_{s\in A_i}$. The dimensionalities K_i for the different strategies scale differently with increasing system sizes, which are summarized in Tab. 3.2. These methods will be compared numerically in Sec. 3.4.3.

The above strategies can reduce the number of qubits but in a hardware-agnostic way. In practice, a quantum computer has a fixed number of qubits, and we wish to use as many qubits as possible within the hardware limitation. With this in mind, we also propose an adaptive interaction-based strategy to create a basis set. We first order the interactions between the subsystems based on the interaction strength. By gradually increasing the threshold ε_{adapt}, we find a basis set of the desired dimensionality. This selection of thresholds can be performed for each subsystem independently. We will present the numerical demonstration of this method in Sec. 3.4.4.

Table 3.2: Upper bound of the number of independent vectors K_i in sub-system i. n_i number of qubits in subsystem i. A_i number of qubits involved in strongest interaction.

Method	K_i
Interaction	$\mathcal{O}(\#\text{Interactions} > \varepsilon)$
Single Pauli	$\mathcal{O}(n_i)$
Single Pauli edge	$\mathcal{O}(A_i)$
Particle conserving	$\mathcal{O}(n_i^2)$
Particle conserving edge	$\mathcal{O}(A_i^2)$

3.3.2 Remarks on Degenerate Eigenstates of Subsystems

A subsystem Hamiltonian having degenerate ground states can lead to unexpected results. A VQE then cannot find a unique ground state. The found ground state would be semi-random and depends on multiple factors, such as the starting condition of the VQE and the noise in the quantum device. In principle, all linear combinations of the degenerate ground states are possible solutions to the VQE without any treatment. This results in an instability of the deep VQE since the random starting vectors, in general, lead to different basis sets and consequently to different $\hat{H}^{\text{eff}}$.

This dependency on the starting vector set is tricky as, without supplementary knowledge about the system, there is no justification for favoring one sub-vector set over the other without running it through the deep VQE first. Therefore, the deep VQE must consider all degenerate vectors as starting vectors to ensure that the result is independent of the randomness of the first VQE. Alternatively, we should design the first VQE to return a unique solution for the reproducibility of the experiment by, for example, unfolding the degeneracy with constrained VQE [96].

3.4 Numerical Simulation

3.4.1 Setup

Tree-like Molecules

We apply the deep VQE to two different toy models of tree-like molecules in Fig. 3.1, a 10-atom and a 13-atom version. We describe the geometry of the tree-like molecules in the Appendix 6, notice that their geometry were not optimized rather it was chosen, to have an angle of 120 degrees and a torsions of 30 degrees. Nakatani and Chan have used a similar molecule for benchmarking tree tensor network [97], however the distance between atoms were chosen different. Since a tree-like molecule naturally separates into different branch-like subsystems, it is also an ideal benchmark molecule for the deep VQE. These molecules are the first step to calculating dendrimers or Cayley tree-like molecules. Today's industry frequently uses dendrimers, e.g., for pharmaceuticals [98]. Understanding dendrimers better would allow us to tailor them specifically to the applications. We repeated the deep VQE simulation multiple times, enlarging the distance between atoms by applying a stretching factor ranging from 0.9 to 2.0 to all Cartesian coordinates, simulating the performance of deep VQE under the influence of different interaction strengths between subsystems.

Using STO-3G minimal basis set, the molecules in Fig. 3.1 (a) and Fig. 3.1 (b) respectively have 20 and 26 spin-orbitals. The Hamiltonians of the molecules are obtained with PySCF [99]. We map it to a qubit system by JW transformation implemented in OpenFermion [100], resulting in 20- and 26-qubit Hamiltonians.

For simulating the quantum states of these molecules on a classical machine, we use the Python library Qulacs [101].

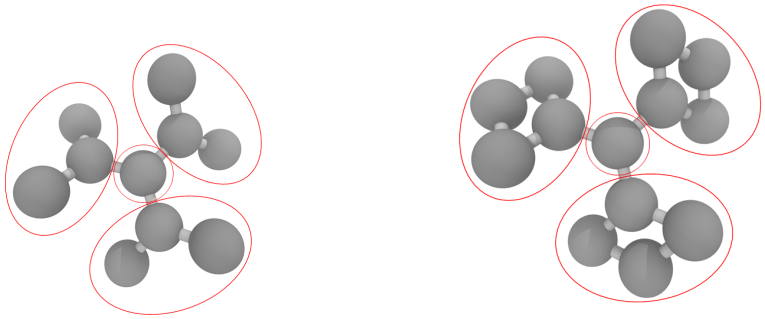

(a) 10 Hydrogen atom tree-like molecule

(b) 13 Hydrogen atom tree-like molecule

Figure 3.1: Toy-model molecules for deep VQE. Red circles indicate the partition of subsystems.

Fig. 3.1 shows the separation of the tree-like molecule into subsystems. Other selections of subsystems would be possible and an exciting research topic; however, we have to leave it to future research as it would exceed the scope of this Chapter. We use localized orbitals to define the subsystems based on the distance between their associated atoms. The Löwdin orthogonalization method is employed to create well-localized orbitals.

We use the FCI to solve the molecules' ground state. The FCI solution was used as a reference for the performance of deep VQE. Additionally, we show the energy of the "combined subsystem" solution, which is the product state of all individual subsystem solutions, as well as the restricted HF solution. HF is a standard mean-field method that cannot account for the electron-correlation energy in the molecule.

The performance of deep VQE depends partially on the subroutine VQE algorithm employed. However, here we aim to compare the different basis creation methods. Therefore, we replaced all VQE subroutines with direct diagonalizations of the matrix representation of the observable to find the ground state of the subsystem and the effective Hamiltonian. This replacement assures us that we find accurate eigenstates of the systems equivalent to having performed an FCI calculation. Additionally, the direct diagonalization replacement allows us to compare the different basis sets without the additional effects a realistic VQE algorithm would add, such as the noise of the quantum system. The ground state solution of the subsystems, as well as for the $\hat{H}^{\text{eff}}$, was determined using the exact diagonalization with SciPy [102].

We find that the ground state of each subsystem of the 10-atom molecule shown in Fig. 3.1 (a) has a two-fold degeneracy for all stretching factors. We

suspect that this degeneracy of the subsystems is due to a degeneracy of the spin eigenstates. For the 13-atom tree molecule shown in Fig. 3.1 (b), each subsystem, except for the central hydrogen atom, has a unique ground state, but their first excited states are three-fold degenerate. We also consider how this degeneracy affects the overall result in Sec. 3.4.2.

The following subsections show the energy difference between the different basis sets and the FCI solution for the 10 and 13-atom tree molecules. To better compare the different methods, we also show the weighted mean error of correlation energies over the different stretching factors and the required number of qubits to run the deep VQE on a quantum machine. We define the weighted mean error of correlation energies as,

$$\begin{matrix}\text{Weighted mean error}\\ \text{of correlation energies}\end{matrix} = \frac{1}{|X|}\sum_{x\in X}\frac{E(x)-E_{\text{FCI}}(x)}{E_{\text{subsystems}}(x)-E_{\text{FCI}}(x)}, \tag{3.8}$$

where $E(x)$, $E_{\text{FCI}}(x)$, and $E_{\text{subsystems}}(x)$ are the energy obtained by the deep VQE using particular strategies, the FCI energy, and the energy of the "combined subsystem" solution at a stretching factor x. X denotes the set of stretching factors for which we perform the calculations, and $|X|$ indicates the number of elements in X. Here, X is $\{0.9, 1.0, 1.1, 1.2, 1.3, 1.4, 2.0\}$. We applied the weight $E_{\text{subsystems}}(x) - E_{\text{FCI}}(x)$ to the correlation energy error to take into account the difference in magnitude over the stretching factors.

Retinal

Additional to the toy tree-like molecules, we also apply the deep VQE algorithm to a natural molecule, retinal. Retinal is essential in visual phototransduction, where visible light gets detected in our eyes. We use library Gaussian 16 [103] at a B3LYP/6-31G** level of theory to find the optimized geometry of the retinal. We show the geometry in the Appendix 6. Retinal consists of 20 carbons, 28 Hydrogen, and one Oxygen. The number of orbitals in the STO-3G basis for the molecule forced us to calculate the ground state in an active space. We started by forming 20 π-orbitals using the PiOS [104] function of PySCF. 10 electrons are considered for this calculation. The π-orbitals take part in forming double bonds between the carbons in retinal. Then we localize the obtained π-orbitals using the Cholesky localisation method [105]. The localized orbitals were used as the active space for molecules. As a reference for the deep VQE result we used a CASCI calculation. CASCI calculates the molecule's ground energy in the active space without optimizing the orbitals as CASSCF would do and is, therefore, less system-dependent. The Hamiltonian in this active space was mapped to a qubit system by a JW transformation using OpenFermion resulting in a 20 qubit Hamiltonian. We split the molecule into 2 subsystems of each 10 spin orbitals and 5 electrons as indicated in Fig. 3.2. Again, this split is by no means unique, and other separations could be examined. Both subsystems produced double degenerate eigenstates. This degeneracy is most likely due to a degeneracy of the spin eigenstates. In the case, we only considered one starting

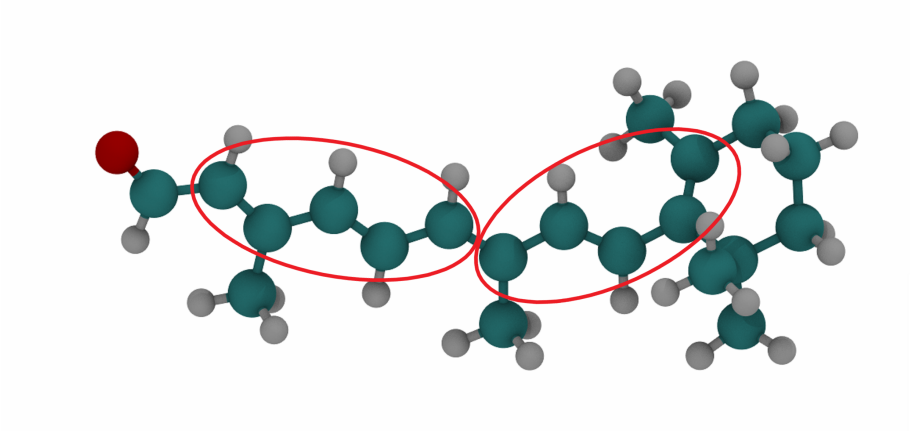

Figure 3.2: Retinal for deep VQE. Red circles indicate the partition of subsystems. Retinal was calculated using 20 π-orbitals, splitting it equally into subsystems of 10 orbitals.

vector, we selected the spin $\downarrow$ ground state as the starting vector. The results are shown in Sec. 3.4.5. In the case of the edge methods, we used the bordering spin orbitals as the active qubits in the basis state finding method.

3.4.2 Influence of Starting Vector for Degenerate Subsystems

First, we discuss the dependency of the deep VQE on the starting vector. For the sake of readability, we only show the results using the particle conserving method to produce the basis in the deep VQE. We show the 10-atom tree molecule results in Fig. 3.3. The ground states of all the subsystems of the 10-atom tree molecule are doubly degenerate. The ground state found by the VQE or, in our case, the direct diagonalization is therefore not unique. We use the spin state to distinguish the degenerate states. We mark the spin-up ground state with $\uparrow$ and the spin-down ground state with $\downarrow$. We only show a selection of all possible spin configurations due to redundancy resulting from the symmetry in the molecule. We observe two distinct resulting energy levels, indicating that the stating vector $|G_i\rangle$ can considerably influence which Hilbert space can be searched for the overall ground state and, therefore, the performance of the deep VQE.

The choice of the starting vector is not trivial, and without further knowledge of the system, all possible starting vectors have to be considered. Additional starting vectors, however, come at the cost of requiring additional qubits to represent $\hat{H}^{\text{eff}}$.

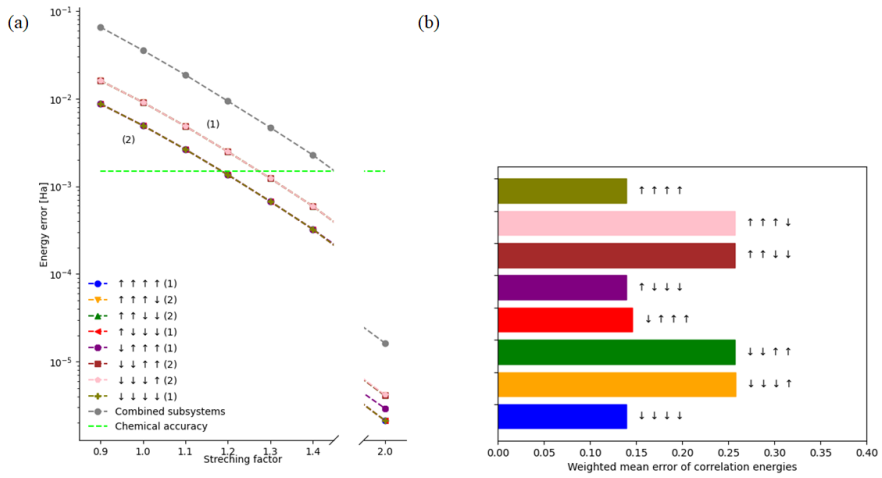

Figure 3.3: (a) Performance of the particle conserving edges method with different incomplete starting vector compositions. The results are for the 10-atom tree molecule, which has a two degenerate ground state. The first marker describes the spin state of the central subsystem starting vector, whereas the three following markers indicate the spin state of the branch-like subsystems starting vectors. Since the results overlap in two lines, we introduce the labels (1) and (2) to indicate to which line the result belongs. (b) Weighted mean error of correlation energies for the particle conserving edges method with different incomplete starting vectors composition (1111).

3.4.3 Different Basis Methods

Next, we compare the performance of different basis methods with different starting vectors introduced in Sec. 3.3 using the tree-like molecules. We compare two choices of starting vectors. The first choice uses single ground states of each subsystem, whereas the second uses additional eigenstates of each subsystem. In the former case, we chose the spin configuration $\downarrow\downarrow\downarrow\downarrow$ for the starting vectors for a 10-atom tree molecule since we had degenerate eigenstates. In the case of the 13-atom tree molecule, only the central subsystem had a two-fold degeneracy, and we also chose the spin $\downarrow$ ground state as the starting vector. For the interaction method, an $\epsilon = 10^{-2}$ was chosen for the 10-atom tree molecule and an $\epsilon = 10^{-3}$ for the 13-atom tree molecule. The number of considered starting vectors is indicated in the method's name in the bracket. The first digit indicates the number of starting vectors for the central subsystem, whereas the three following digits count the starting vectors for the branch-like subsystems.

Fig. 3.4 (a) and Fig. 3.4 (b) show the corresponding results for the 10-atom

tree system. We also show the number of qubits needed for each method in Tab. 3.3. We note that we are unable to perform the calculation for the particle conserving method with additional starting vectors due to its sizeable computational requirement. The particle conserving methods with only one starting vector per subsystem performed exceptionally well in terms of accuracy. For all tested basis creation methods, including an additional eigenstate significantly increased the accuracy of the deep VQE. This is a consequence of the expanded Hilbert space that can be explored.

Unlike the other methods, we observe that the interaction methods with a fixed truncation have a decreasing accuracy with increasing stretching factors. More concretely, the energy obtained by interaction methods jumps to the combined subsystem's energy at the stretching factor of 1.4. The interaction methods also display different behavior regarding the saved qubits, showing a significant dependence on the stretching factor as shown in Tab. 3.3. This dependence is due to our selection process of the interactions to generate a basis set. We set a fixed cut-off of the interaction strength λ^{μ} for the interactions involved in the basis creation step. Consequently, as the interactions between subsystems become weaker by stretching the molecule, more interactions are disregarded. Lowering the dimensionality of the basis sets allows us to save more qubits but comes at the cost of lowering the method's accuracy.

Fig. 3.5 (a) and Fig. 3.5 (b) show the results for the 13-atom tree molecule. Here, only the central subsystem was doubly degenerate, and the first excited state of the branch subsystems for the 13-atom tree molecule is a triplet. To see the effect of adding additional excited states as starting vectors on the performance of the deep VQE, we considered all three states as additional starting vectors. Due to the high computational cost of the other methods, only the single Pauli edges and the particle conserving edges methods could be prepared with additional starting vectors. For both methods, the additional starting vectors were able to increase the accuracy of the deep VQE, but this came at the expense of requiring extra qubits (see Tab. 3.4 for the exact number of qubits required for each method). The particle conserving edges methods performed slightly better than others. This is consistent with the case of the 10-atom tree molecule, indicating an advantage of using the particle conserving approach in deep VQE for chemistry problems.

3.4.4 Interaction Based Deep VQE with Fixed Qubit Numbers

We show the results for the fixed qubit numbers approach in Fig. 3.6 and Fig. 3.7. We fix the number of qubits to 11, 14, and 17. For the 13-atom tree molecule, we could not produce an 11-qubit version as already including only the strongest interaction strength results in a basis set requiring more than 11 qubits. The qubit number is increased by three per step to take into account that there are three equivalent branch-like subsystems of the molecules.

In Fig. 3.6 and Fig. 3.7, we see that if we define a fixed number of qubits, we can avoid the decreasing accuracy for increasing stretching factors. However, if

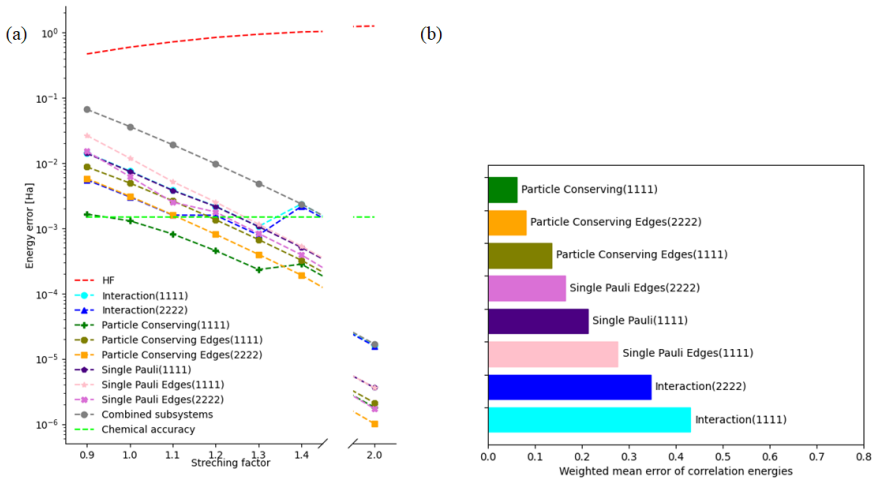

Figure 3.4: (a) The energy difference between FCI and the deep VQE for the 10-atom tree molecule. We compare the different basis creation methods when using a single starting vector marked as (1111) and a complete degenerate basis set indicated by (2222). The first digit indicates the number of starting vectors for the central subsystem, whereas the three following digits count the starting vectors for the branch-like subsystems. (b) Weighted mean error of correlation energies for all methods for the 10-atom tree molecule.

the number of qubits is too restrictive, we cannot improve the result from the "combined subsystems". We see this behavior for the interaction(2222) method with 11 qubits for the 10-atom tree molecule in Fig. 3.6.

3.4.5 Retinal

Additional to the toy model of a 10 and 13-atom hydrogen trees, we also applied the deep VQE algorithm to retinal to examine the performance on a natural molecule. We applied different basis forming strategies and compared them based on their accuracy and the number of qubits in Tab. 3.5. The calculation was performed with no stretching factors applied. The molecule was separated into two 10-qubit subsystems. With such a division, the eigenstates of the subsystems are double degenerate. In the case when only one starting vector for the basis forming step was considered, we chose the spin-down starting vector.

Deep VQE proves to be effective in treating such a molecule as retinal. Especially the addition of additional states as starting vectors seems to be a valid strategy. For both the 12 and the 14 qubit interaction treatment, the addition of a second starting vector resulted in a significantly better ground state energy ap-

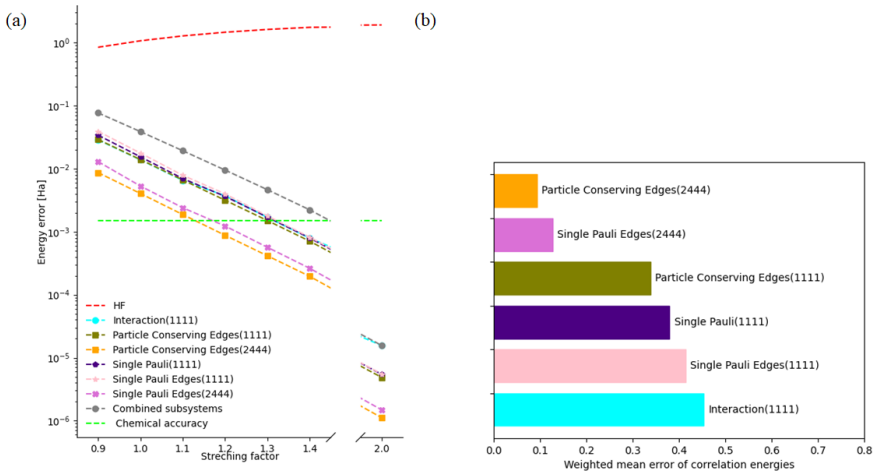

Figure 3.5: (a) The energy difference between FCI and the deep VQE for the 13-atom tree molecule. We compare the different basis creation methods when using a single starting vector marked as (1111) and a full degenerate basis set indicated by (2444). The first digit indicates the number of starting vectors for the central subsystem, whereas the three following digits count the starting vectors for the branch-like subsystems. (b) Weighted mean error of correlation energies for all methods for the 13-atom tree molecule.

proximation. This can be a consequence of the doubly degenerate ground state of the individual subsystems. The particle conserving edges method with each 10 starting vectors performed again exceptionally well and was able to approximate the ground state energy in the STO-3G basis within chemical accuracy while saving 8 qubits.

3.4.6 Performance Comparison

Overall we achieved similar accuracy for the 10 and the 13-atom tree molecules (see Fig. 3.4 and Fig. 3.5). We expect this from the minor influence the newly added outer atoms have on the overall ground state. This behavior would also explain the remarkable success the edge methods provide, saving up to 15 qubits with comparable accuracy to the other methods (see Tab. 3.4). All methods were able to produce lower energies than the HF method. Multiple methods were able to approximate the ground state energies within an error of below 1% of the electron correlation energy of the molecule. The electron correlation energy is equivalent to the error of the HF method shown in Fig. 3.4 and Fig. 3.5 and represents the error due to the mean-field approximation of HF.

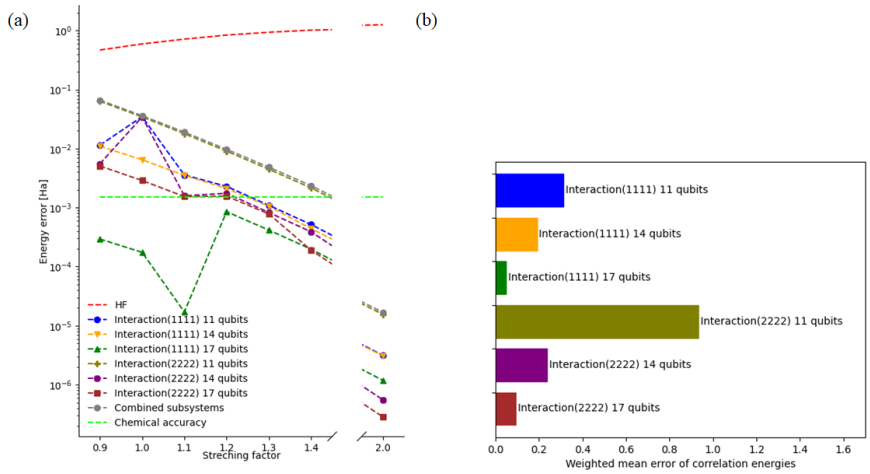

Figure 3.6: (a) The energy difference between FCI and the deep VQE for the 10-atom tree molecule. We compare the interaction fixed methods with a different number of qubits. The fully degenerate basis set is indicated by (2222). The first digit indicates the number of starting vectors for the central subsystem, whereas the three following digits count the starting vectors for the branch-like subsystems. (b) Weighted mean error of correlation energies for the interaction based method with fixed number of qubits for the 10-atom tree molecule.

This improvement helped us reach chemical accuracy for some stretching factors. The particle conserving edges method performed exceptionally well both for the tree-like molecules as well for retinal. Especially the use of additional starting vectors proved to be beneficial for retinal. Using an edge method allows us to focus on changes affecting the orbitals involved in the most substantial interaction. We expect electrons occupying such orbitals to experience the most dramatic changes from the individual subsystem solutions when forming a bond with the other subsystems. To use the computational resources offered most effectively, it is advisable to use basis sets that focus on exploring the changes to the occupation of the most involved orbitals.

In contrast to the other methods, the interaction methods with a fixed truncation for the participating interactions significantly depended on the stretching factor. The number of qubits decreased with increasing distance. This reduction allows us to save more and more qubits but comes at the cost of decreasing accuracy. However, we consider this is not preferable if we have access to a quantum device with a fixed number of qubits. It seems unreasonable to not use all of them. The fixed number qubits interaction method we propose in this Chapter seems a more reasonable approach as it allows the use of all qubits.

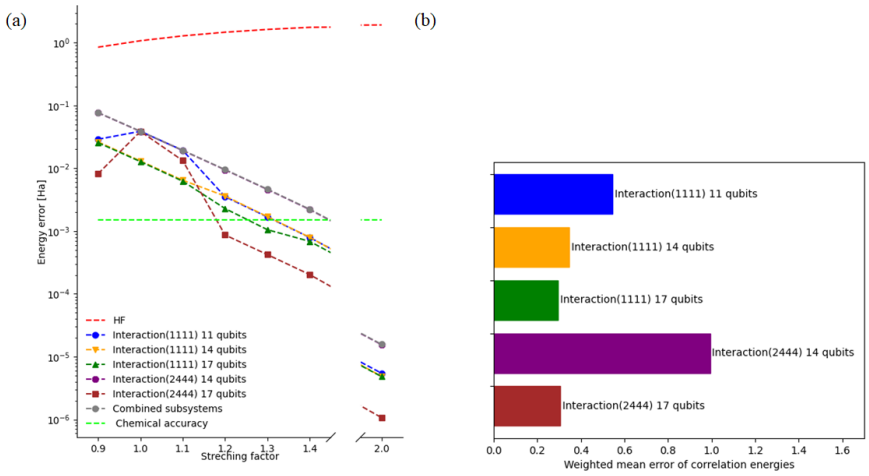

Figure 3.7: (a) The energy difference between FCI and the deep VQE for the 13-atom tree molecule. We compare the interaction fixed methods with a different number of qubits. The fully degenerate basis set is indicated by (2444). The first digit indicates the number of starting vectors for the central subsystem, whereas the three following digits count the starting vectors for the branch-like subsystems. (b) Weighted mean error of correlation energies for the interaction based method with fixed number of qubits for the 13-atom tree molecule.

It also performs more stable for less interacting systems, not suffering from decreasing accuracy.

3.5 Conclusion and Discussion

The deep VQE approach successfully reduced the number of qubits to calculate a ground state of a complex chemical molecule. Notice that we have not exploited any symmetries in the molecules. Using such could be a further way to make deep VQE more efficient. All different basis creation methods we tested could create a ground state energy within a few mHa of the FCI/CASCI solution. However, they showed a significant difference in the accuracy and the number of qubits they could save. We discussed the challenges of degenerate subsystems and provided a solution in the form of additional stating vectors or marking the single starting vector by its spin state. We also showed that adding additional low-lying states as starting vectors for the basis-creation method can improve the accuracy. However, the approximation of such states can be costly. Therefore, further research is needed to determine if this accuracy can

Table 3.3: Qubits needed to represent the $\hat{H}^{\text{eff}}$ of the 10-atom tree molecule for the different basis creation methods. The number of considered starting vectors is indicated in the method's name in the bracket. The first digit indicates the number of starting vectors for the central subsystem, whereas the three following digits count the starting vectors for the branch-like subsystems.

Stretching factor	**0.9**	**1.0**	**1.1**	**1.2**	**1.3**	**1.4**	**2.0**
Interaction(1111)($\lambda^{\mu} > 10^2$)	17		14	11			7
Interaction(2222)($\lambda^{\mu} > 10^2$)	17		14			10	
Particle conserving(1111)	17						
Particle conserving edges(1111)	11						
Particle conserving edges(2222)	14						
Single Pauli(1111)	17		14				
Single Pauli edges(1111)	11						
Single Pauli edges(2222)	14						

Table 3.4: The numbers of qubits needed to represent the $\hat{H}^{\text{eff}}$ of the 13-atom tree molecule for the different basis creation methods. The number of considered starting vectors is indicated in the method's name in the bracket. The first digit indicates the number of starting vectors for the central subsystem, whereas the three following digits count the starting vectors for the branch-like subsystems.

Stretching factor	**0.9**	**1.0**	**1.1**	**1.2**	**1.3**	**1.4**	**2.0**
Interaction(1111)($\lambda^{\mu} > 10^3$)	17			11			7
Particle conserving edges(1111)	11						
Particle conserving edges(2444)	17						
Single Pauli(1111)	17						
Single Pauli edges(1111)	11						
Single Pauli edges(2444)	17						

be achieved using other basis creation methods. A possible approach would be to consider double Pauli excitation compared to the here used single Pauli method. Another exciting way to think about a new basis creation method is its similarity to the VQE ansatz. A new basis creation method could be created using a VQE ansatz with discrete fixed parameters. We also proposed methods to upper bound the number of qubits by using edge methods or selection of interaction in the interaction-based approach. These methods have proven effective strategies to reduce the number of needed qubits for the deep VQE. With these modifications to the deep VQE and a proper basis set, we believe that using deep VQE in a quantum chemistry setting can be highly beneficial.

Table 3.5: The numbers of qubits needed to represent the $\hat{H}^{\text{eff}}$ of retinal for the different basis creation methods. The number of considered starting vectors is indicated in the methods name in the bracket. Δ E indicated the energy error of the method compared to the CASCI solution.

Method	**Qubits**	**Energy (Ha)**	**Δ E (mHa)**
Interaction(1,1) 12 qubits	12	-838.2504	42.41
Interaction(1,1) 14 qubits	14	-838.2832	9.578
Interaction(2,2) 12 qubits	12	-838.2911	1.759
Interaction(2,2) 14 qubits	14	-838.2924	0.362
Particle Conserving (1,1)	14	-838.2821	10.75
Particle Conserving Edges(10,10)	12	-838.2921	0.710
Single Edges(8,8)	12	-838.2909	1.897
CASCI		-838.2928	
HF		-838.1550	

Chapter 4

Coupled Cluster Method Tailored with Quantum Computing

In this Chapter, we show how an active space solution on a quantum computer can be combined with a classical computer used to incorporate classical dynamic correlation. To solve the active space on a quantum computer, we are free to choose the algorithm we use. Our method is, therefore, applicable to the NISQ era as well as the FTQC era. After solving the active space, we use the CBT to determine the CI parameters of the produced state. These parameters can be used to tailor some of the CC amplitude on the classical hardware. The remaining CC amplitudes are then determined on the classical computer. We could show that our method successfully incorporates missing electron correlation into the active space solution, increasing its accuracy. We show this using multiple numerical experiments. This Chapter is based on [Erhart, Yoshida, Khinevich and Mizukami, Phys. Rev. Research 6, 023230].

4.1 Introduction

Quantum chemistry is expected to be an application of quantum computing where it could be possible to outperform its classical counterpart [90]. Quantum computers can hold and manipulate a superposition of an exponential number of electronic configurations using a polynomial number of quantum bits (qubits). They are, therefore, considered particularly suitable for simulations of strongly correlated systems, where the nature of quantum superpositions, often difficult to handle using current classical computers, is of essential importance.

Nevertheless, for the foreseeable future, quantum computers are limited in the number of qubits they have. In most cases, they cannot handle all the electronic degrees of freedom (orbitals and electrons) of a targeted molecule on

a quantum computer. Furthermore, even if the number of qubits in a quantum computer increases sufficiently in the future, it is known that there will still be practical limits on the number of electrons and orbitals that a quantum computer can handle because of the slow clock speed of fault-tolerant quantum computers [106, 107]. Given these limitations, it is expected that quantum computers can only be applied to what is known as the 'active space,' which is a user-defined, chemically important space around the Fermi level of a molecular electronic structure.

Active spaces are designed to consider only the most important orbitals for treating the strong correlation of electrons (i.e., static correlation). The active spaces, however, naturally ignore the remaining weak correlation (i.e., dynamical correlation) resulting from the non-active orbitals. Moreover, as the selection of an active space is more or less based on the chemical intuition of the user, there is often a degree of arbitrariness. This user dependency can have a significant impact on the accuracy of the methods using an active space. Recently automated active space selection procedures have been proposed to reduce user bias and improve the reliability of results [104, 108–114]. The active space approximation has been extensively discussed and addressed in traditional quantum chemistry [115–121].

In quantum computing, various approaches have been proposed to incorporate ignored electron correlation [30–52]. These approaches fall into two broad categories. The first involves constructing models incorporating weak electron correlation during the development of effective Hamiltonians, which are then solved using quantum computers. This method is often called the 'perturb-then-diagonalize' approach. The second category improves the results based on an active space Hamiltonian solution obtained by quantum computers and is known as the 'diagonalize-then-perturb' approach. The former requires an up-front estimation of the electron correlation outside the active space, which introduces some arbitrariness. The latter commonly uses the internally-contracted multireference perturbation theory or multireference configuration interaction, and there have already been proposals for implementation using quantum computing results. However, these classical computing methods require higher-order Reduced Density Matrices (RDMs), leading to prohibitive measurement costs on quantum computers and seem impractical [41, 122–124]. Consequently, there is an increasing demand for methods considering weak electron correlation without relying on higher-order RDMs.

One of the practical and easy-to-use approaches to account for dynamical correlation from outside the active space without using higher-order RDMs is TCC. In TCC, after finding the ground state of an active space Hamiltonian by the CASCI method, the lost dynamical correlation in the CASCI calculation is described in an additional CCSD optimization of the whole space while keeping the static correction of the CASCI solution. TCC can be worked with not only CASCI but also other quantum chemical theories such as DMRG [125], FCIQMC [126, 127], and pair coupled cluster doubles [128–131]. It should be noted that there is another method, known as the externally corrected coupled cluster method, which is similar to the TCC in its conceptual framework [132–

139].

In this Chapter, we propose to combine TCC and quantum computing to recover dynamical correlation from excluded orbitals outside the active space. Our practical method is a two-step approach using a quantum computer to solve the static correlation and add the remaining dynamical correlation using classical computers. This method requires only a limited number of qubits to mainly solve the static correlation, while the relatively computationally cheap consideration of weak correlation can be performed on classical hardware. To extract the solved quantum state from a quantum computer, we use a CBT. CBT is based on computational basis sampling [27] and is an effective strategy when only a small number of Slater determinants are non-negligible, as is often the case in quantum chemistry. Additionally, a method is proposed, in which we utilize the direct access to the energy of the active space and add our newly determined electron correlation outside the active space. The accuracy of the proposed method is further enhanced using this approach.

We demonstrate that our approach can produce accurate PECs for LiH, H_2O, and N_2. As CBT is naturally a statistical process that uses measurements to determine a quantum state, we investigate the number of measurement dependencies in CBT on LiH, H_2O, and N_2. Finally, to demonstrate the analysis of a realistic chemical reaction, we estimate the activation energy of the Cope rearrangement of 1,5-hexadiene.

The remainder of this Chapter is organized as follows: We discuss the relevant theories of TCC, CBT, and our new approach QC-CBT-TCC in Sec. 4.2. The numerical results for the PECs of LiH, H_2O, and N_2 are shown in Sec. 4.3, as well as the influence of different numbers of measurements in CBT have on the confidence of our approaches. Additionally, we determined the activation energy of the Cope rearrangement using our method and presented the results in Sec. 4.3. In Sec. 4.4, we summarize our findings.

4.2 Theory

4.2.1 Tailored Coupled Cluster

The TCC proposed by Kinoshita et al. [21] is a two-step theory designed to incorporate strong correlation into the standard CC theory, particularly the CCSD model. CCSD often breaks down when strong electron correlation exists. The main idea behind TCC is to split the CC parameters into those for strongly-correlated electrons in the active space and those for weakly-correlated electrons. They can then be determined individually. This gives rise to a formulation, as shown in the following equation

$$|\psi_{\mathrm{TCC}}\rangle = e^{\hat{T}^{\mathrm{rest}}(\theta^{\mathrm{rest}})} e^{\hat{T}^{\mathrm{active}}(\theta^{\mathrm{active}})} |\psi_0\rangle \,. \tag{4.1}$$

The operators $e^{\hat{T}^{\mathrm{active}}}$ act exclusively on the active space. The other operators $e^{\hat{T}^{\mathrm{rest}}}$ also act on the rest of the space. For CCSD, those operators are written

as

$$\hat{T}^{\text{active}}(\theta) = \sum_{i,a} \hat{T}_i^a(\theta_i^a) + \sum_{i,j,a,b} \hat{T}_{i,j}^{a,b}(\theta_{i,j}^{a,b}) \quad i,j,a,b \in \text{active space}, \tag{4.2}$$

$$\hat{T}^{\text{rest}}(\theta) = \sum_{i,a} \hat{T}_i^a(\theta_i^a) + \sum_{i,j,ab} \hat{T}_{i,j}^{a,b}(\theta_{i,j}^{a,b}) \quad \{i,j,a,b\} \not\subset \text{ active space}, \tag{4.3}$$

where $\hat{T}_i^a$ and $\hat{T}_{i,j}^{a,b}$ are the single and double excitation CC operators. Say, $\hat{T}_{i,j}^{a,b}$ excites electrons from the occupied orbitals i and j to the unoccupied orbitals a, b. The brackets $\{\}$ in Eq. (4.3) indicate that at least one of the i, j, a, b orbitals is not present in the active space.

In the first step of TCC, the molecule is described using a variational method using an active space approximation, such as the CASCI approach. This step aims to incorporate strong correlation by assuming that all the strongly correlated degrees of freedom are involved in the active space. Electron configurations' coefficients of the variational wavefunction $\left|\psi_{\text{variational}}^{\text{active}}\right\rangle$ can be mapped directly to CC amplitudes through the known relationship between their corresponding CC and CI operators

$$\hat{T}_1^{\text{active}} = \hat{C}_1, \tag{4.4}$$

$$\hat{T}_2^{\text{active}} = \hat{C}_2 - \frac{1}{2}\hat{C}_1^2, \tag{4.5}$$

where $\hat{C}_1$ and $\hat{C}_2$ are the CI operators to create single and double excitations, respectively. This procedure allows us to approximately reconstruct the variational wavefunction $\left|\psi_{\text{variational}}^{\text{active}}\right\rangle$ in the CCSD ansatz.

The second step is the optimization of the remaining operators $e^{\hat{T}^{\text{rest}}(\theta^{\text{rest}})}$, while the active space operators are kept fixed during the optimization. This preserved the description of static correlation. The optimized operator $e^{\hat{T}^{\text{rest}}(\theta^{\text{rest}})}$ incorporates the previously missing dynamic correlation into the solution.

Additionally, given that TCC is a method rooted in CCSD, after optimizing the CCSD operator $e^{\hat{T}^{\text{rest}}(\theta^{\text{rest}})}$, one can further improve accuracy by perturbatively incorporating the effects of the three-body excitation operator in the same way as in CCSD(T). So, we denote TCC with the (T) correction as TCC(T) in this thesis. For TCC(T), all active single and double amplitudes must be set to zero during the (T) correction calculation to prevent double-counting [23, 140].

4.2.2 Computational Basis Tomography

Computational Basis Tomography (CBT) is an estimation method to determine a quantum state prepared on a quantum computer using the computational

basis sampling method proposed by Kohda et al. [27]. In this section, we briefly review how CBT estimates a quantum state $|\Psi\rangle$ on a quantum computer.

Let us call the estimated state CBT state $|\Psi_{\mathrm{CBT}}\rangle$. Its definition is given as

$$|\Psi_{\mathrm{CBT}}\rangle = \frac{1}{\mathcal{N}} \sum_{i=1}^{R} \langle k_i|\Psi\rangle |k_i\rangle, \tag{4.6}$$

where $1/\mathcal{N}$ is the normalization constant and $|k_i\rangle$ is a computational basis (i.e., Slater determinants or electron configuration) listed in the order of the absolute values of the coefficients $\langle k_i|\Psi\rangle$. The coefficients $\langle k_i|\Psi\rangle$ are equivalent to the CI coefficients. The parameter R is introduced to truncate the trivial computational basis; therefore, R needs to be chosen large enough in order to adequately approximate the original quantum state $|\Psi\rangle$. We tentatively consider the upper limit of R to be around 1000-10000, this is limited by the number of measurements possible on a current quantum computer. By keeping the number of extracted coefficients R constant, the method sacrifices some accuracy but enables scalability to large systems.

CBT aims to estimate the quantum state via measurements rather than the expectation value of an observable. The coefficients are expressed as follows:

$$\langle k_i|\Psi\rangle = |\langle k_i|\Psi\rangle| e^{i\phi_i}. \tag{4.7}$$

To get the coefficients, we must determine their absolute values and the phases ϕ_i. The absolute value $|\langle k_i|\Psi\rangle|$ can be readily obtained using projective measurements; we show it in a later stage. However, a more detailed method is required to determine the phase. Instead of determining the phase directly, Kohda's computational basis sampling approach enables the efficient determination of CI coefficients through the observation of phase differences. We can use the following relationship to determine the phase difference between two computational bases $|k_i\rangle$ and $|k_j\rangle$

$$e^{i(\phi_i - \phi_j)} = \frac{\langle k_i|\Psi\rangle\langle\Psi|k_j\rangle}{|\langle k_i|\Psi\rangle||\langle\Psi|k_j\rangle|}. \tag{4.8}$$

As the global phase of a state can be neglected, we can freely set the phase for one coefficient to zero and determine the relative phase differences for the remaining basis states using Eq. (4.8). As described later, the absolute value of the coefficient $|\langle k_i|\Psi\rangle|$ and what we call the interference factor $\langle k_i|\Psi\rangle\langle\Psi|k_j\rangle$ can be determined relatively easily by projective measurements, thus allowing the estimation of phase differences.

When a sufficient number of samplings N_{sample} are performed, the squared weight of $\langle k_i|\Psi\rangle$ is estimated as

$$|\langle k_i|\Psi\rangle|^2 \simeq \frac{N_i}{N_{\mathrm{sample}}}, \tag{4.9}$$

where N_i is the number of times the outcome k_i is obtained. This directly gives us an approximation for the absolute values of the coefficients.

To determine the phase factor, we need to measure the interference factors $\langle k_i|\Psi\rangle\langle\Psi|k_j\rangle$. In the case $k_i = k_j$ this is equivalent to a determine $|\langle k_i|\Psi\rangle|^2$. When $k_i \neq k_j$, we can rewrite the interference factor as

$$\begin{aligned}\langle k_i|\Psi\rangle\langle\Psi|k_j\rangle = |\langle 0|U_{k_i,k_j}|\Psi\rangle|^2 + i|\langle 0|V_{k_i,k_j}|\Psi\rangle|^2 \\ - \frac{1+i}{2}(|\langle k_i|\Psi\rangle|^2 + |\langle k_j|\Psi\rangle|^2),\end{aligned} \tag{4.10}$$

where U_{k_i,k_j} and V_{k_i,k_j} are unitary operators acting in the following way

$$U_{k_i,k_j}\left(\frac{|k_i\rangle + |k_j\rangle}{\sqrt{2}}\right) = |0\rangle\,, V_{k_i,k_j}\left(\frac{|k_i\rangle - |k_j\rangle}{\sqrt{2}}\right) = |0\rangle\,. \tag{4.11}$$

How to construct the circuits U_{k_i,k_j} and V_{k_i,k_j} was discussed in Ref. [19, 27]. Using the relation

$$\langle k_i|\Psi\rangle\langle\Psi|k_j\rangle = \frac{(\langle k_1|\Psi\rangle\langle\Psi|k_i\rangle)^*\langle k_1|\Psi\rangle\langle\Psi|k_j\rangle}{|\langle k_1|\Psi\rangle|^2}, \tag{4.12}$$

we note that we only need to measure the case for $k_i = k_1$ and $k_j \neq k_1$ and can recover the remaining interference factors. We explicitly write the cases $k_i = k_1$ and $k_j \neq k_1$ as

$$\begin{aligned}\langle k_1|\Psi\rangle\langle\Psi|k_j\rangle = |\langle 0|U_{k_1,k_j}|\Psi\rangle|^2 + i|\langle 0|V_{k_1,k_j}|\Psi\rangle|^2 \\ - \frac{1+i}{2}(|\langle k_1|\Psi\rangle|^2 + |\langle k_j|\Psi\rangle|^2).\end{aligned} \tag{4.13}$$

The first term in Eq. (4.13) is estimated as

$$|\langle 0|U_{k_1,k_j}|\Psi\rangle|^2 \simeq \frac{N_0}{N_U}, \tag{4.14}$$

where N_0 is the count that we obtain the outcome zero and N_U is the total amount of samplings. Similarly, when N_V is the number of measurements used to determine the second term in Eq. (4.13). The second term is estimated as

$$|\langle 0|V_{k_1,k_j}|\Psi\rangle|^2 \simeq \frac{N_0'}{N_V}, \tag{4.15}$$

where N_0' is the count of the times we obtained the outcome zero. The remaining terms of Eq. (4.13) can be determined similarly, as in Eq. (4.9).

In summary, the truncation number R and the numbers of the three types of measurements N_{sample}, N_U, and N_V play vital roles in CBT.

4.2.3 QC-CBT-TCC

In this section, we discuss our quantum-classical hybrid tailored coupled cluster theory with CBT method, which we denoted as QC-CBT-TCC. This method aims to include dynamic correlations for quantum computing while using an

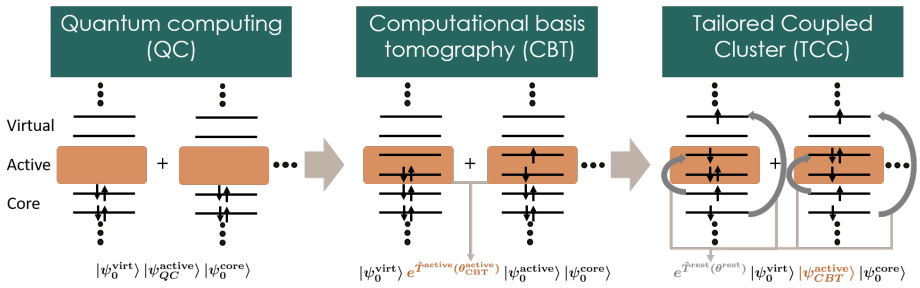

Figure 4.1: Schematic depiction of QC-CBT-TCC. In the first step, we determine the ground state solution of the active space using a quantum computer. As the state is classically inaccessible, we indicate this by not showing the concrete electronic structure of the active space. To determine the relevant CI-coefficients of the state, we use a CBT method and tailor the corresponding CCSD coefficients. In the last step, we optimize the remaining CCSD coefficients while keeping the active space coefficients constant.

active space. QC-CBT-TCC uses a quantum computer to consider the strong correlation and then describes the remaining dynamic correlation using a classical device. In our framework, the CBT method is used to transfer the quantum solution onto a classical device. We present a graphical representation of our method in Fig. 4.1 and explain it in more detail in the following.

In the first step, we determine the active-space ground state $\left|\psi_{\mathrm{QC}}^{\mathrm{active}}\right\rangle$ using a quantum computer. Different quantum (or quantum-classical hybrid) algorithms, such as VQE, QPE, or ITE can be used in this step.

In the second step, CBT is used to determine the most significant CI coefficients of the produced ground state on a quantum computer $\left|\psi_{\mathrm{QC}}^{\mathrm{active}}\right\rangle$. Using the obtained CI coefficients, the ground state of the active space $\left|\psi_{\mathrm{QC}}^{\mathrm{active}}\right\rangle$ is approximately converted to a CC ansatz. Mapping the CI operators to their CC counterparts follows the same relationship as already described in Sec. 4.2.1 in equation (4.4) to (4.5). As the wavefunction parmameters θ^{active} for $\left|\psi_{\mathrm{QC}}^{\mathrm{active}}\right\rangle$ are practically approximated by CBT, we call them $\theta_{\mathrm{CBT}}^{\mathrm{active}}$. The obtained approximate active-space ground state wavefunction in the CC is written as

$$\left|\psi_{\mathrm{CBT}}^{\mathrm{active}}\right\rangle = e^{\hat{T}^{\mathrm{active}}(\theta_{\mathrm{CBT}}^{\mathrm{active}})}\left|\psi_0\right\rangle . \tag{4.16}$$

In the third step, the remaining θ^{rest} coefficients are optimized by solving the standard projected CC equations. During the optimization, the amplitudes of the active space operators are held constant. This procedure allows the addition of dynamical correlation descriptions while conserving that of static correlation. The final produced state of QC-CBT-TCC $\left|\psi_{\text{QC-CBT-TCC}}\right\rangle$ can be written as

$$\begin{aligned}\left|\psi_{\text{QC-CBT-TCC}}\right\rangle =& e^{\hat{T}^{\mathrm{rest}}(\theta^{\mathrm{rest}})} e^{\hat{T}^{\mathrm{active}}(\theta_{\mathrm{CBT}}^{\mathrm{active}})}\left|\psi_0\right\rangle \\ =& e^{\hat{T}^{\mathrm{rest}}(\theta^{\mathrm{rest}})}\left|\psi_{\mathrm{CBT}}^{\mathrm{active}}\right\rangle .\end{aligned} \tag{4.17}$$

The QC-CBT-TCC energy $E_{\text{QC-CBT-TCC}}$ is then given by the following projected energy:

$$E_{\text{QC-CBT-TCC}} = \langle \psi_0 | \hat{H} | \psi_{\text{QC-CBT-TCC}} \rangle . \tag{4.18}$$

4.2.4 Enhanced QC-CBT-TCC

One of the issues associated with QC-CBT-TCC is the lack of assurance that the energy obtained via QC-CBT-TCC will outperform classical algorithms in accuracy. This arises because of the approximate nature of both CBT and TCC methodologies. The TCC approach employs the standard CCSD ansatz to approximate the active space wavefunction, which implies that it does not incorporate information about higher-order excitations, such as triple and quadruple excitations, obtained from a quantum computer. Furthermore, CBT is a statistical method, and its inherent statistical nature introduces additional errors. To address this problem, we introduce a correction method as described below. The corrected energy $E_{\text{QC}-\text{CBT}-\text{TCC(c)}}$ is defined as

$$\begin{aligned} E_{\text{QC-CBT-TCC(c)}} = {} & E_{\text{QC}}^{\text{active}} \\ & + (E_{\text{QC-CBT-TCC}} - E_{\text{QC-CBT-TCC}}^{\text{active}}). \end{aligned} \tag{4.19}$$

The first term $E_{\text{QC}}^{\text{active}}$ in Eq. (4.19) represents the expectation value of the active space Hamiltonian via quantum computing such as QPE. The difference in the second term corresponds to the additional correlation added to the active space solution using the QC-CBT-TCC technique. $E_{\text{QC-CBT-TCC}}$ is the predicted energy using the QC-CBT-TCC method, whereas

$$E_{\text{QC-CBT-TCC}}^{\text{active}} = \langle \psi_0 | \hat{H} e^{\hat{T}^{\text{active}}(\theta_{\text{CBT}}^{\text{active}})} | \psi_0 \rangle , \tag{4.20}$$

is the CCSD energy after dressing the CCSD amplitudes but before the remaining CCSD optimization. In that case, the remaining operators $e^{\hat{T}^{\text{rest}}}$ are equivalent to the identity. Since the same error arises in $E_{\text{QC-CBT-TCC}}$ and $E_{\text{QC-CBT-TCC}}^{\text{active}}$, taking the difference between these terms removes the errors in the active-space electron correlation inherent to the QC-CBT-TCC method.

Note that Izsák et al. have already employed a similar extrapolative correction method in Ref. [141] in the context of using quantum computers for quantum chemistry as well as Daniel Kats and his co-workers for FCIQMC-TCC [126].

4.3 Results and Discussion

This section describes our new method, QC-CBT-TCC, and the QC-CBT-TCC(c) approach's performance. Sec. 4.3.1 presents the PECs for three molecules, LiH, H_2O, and N_2. In Sec. 4.3.2, we conducted multiple experiments at different interatomic distances for each molecule to discuss the reliability of CBT, as CBT

is a statistical method and QC-CBT-TCC is influenced by the statistical errors of CBT. In Sec. 4.3.3, we apply our method to a prototype organic reaction, the Cope rearrangement of 1,5-hexadiene.

The computational details are as follows: A chemqulacs [142] library was used to simulate quantum circuits on classical hardware. We employed disentangled UCCSD as an ansatz for VQE and BFGS as an optimizer. CCSD, CCSD(T), CASCI, and FCI were calculated using PySCF [143]. The MR-CISD+Q method was employed to obtain reference data for the PECs of H_2O and N_2 because the FCI calculation was too computationally demanding for the hardware at hand. This method was implemented in the ORCA quantum chemistry program Version 5.0.3 [144]. All calculations for the PECs in this Chapter were performed using the cc-pVDZ basis set. In Sec. 4.3.3, we used the 6-31G$*$ basis set to compute the activation energy for the Cope rearrangement. We used the canonical orbitals for all molecules except for LiH, which was calculated using the natural orbitals provided by a CCSD calculation. This, however, is an approximation because the CCSD implementation of PySCF used assumes canonical orbitals, so off-diagonal terms in the Fock matrix are ignored. The active spaces were determined using the lowest energy level unoccupied orbitals and the highest energy occupied orbitals from the HF calculation. To transfer the CI coefficients determined by CBT to the amplitudes for CCSD, only the real parts were considered. This was necessary because usually the CCSD for a non-relativistic or non-periodic Hamiltonian expects real coefficients. The CI coefficients were normalized to ensure the normalization. Unless otherwise indicated, we applied the parameters $R = 100$, $N_{\text{sample}} = 10^6$, $N_U = 10^6$, and $N_V = 10^6$ for all the CBT calculations.

4.3.1 Potential Energy Curves

First, we investigated the PEC of the LiH molecule. In addition to the QC-CBT-TCC(c), we show the results for QC-CBT-TCC, active space UCCSD, and FCI, as well as HF, CCSD, CCSD(T) and orbital-optimized-UCCSD [43, 44]. The selected active spaces for these calculations were two electrons and two spatial orbitals, the highest occupied and the lowest unoccupied orbitals.

Fig. 4.2 (a) shows the PEC of the LiH molecule. All considered methods followed the qualitative features of the FCI energy curve shape, except for HF. The active space UCCSD increased the accuracy compared to that of the HF solution. This behavior is most notable in the bond dissociation region. At the equilibrium bond length, the active space UCCSD can capture some dynamic correlation. Active space OO-UCCSD produced almost identical energies to the active space UCCSD. We assume this results from using natural orbitals in the case of UCCSD, which are already a good choice of orbitals to capture some of the electron correlation effects. The QC-CBT-TCC and its enhanced version, the QC-CBT-TCC(c), further increased the computed energy's accuracy. This indicates that additional dynamical correlations outside the active space are required to reach good ground state energy. CCSD and CCSD(T) both gave energies very similar to FCI. In the high dissociation regime, where static

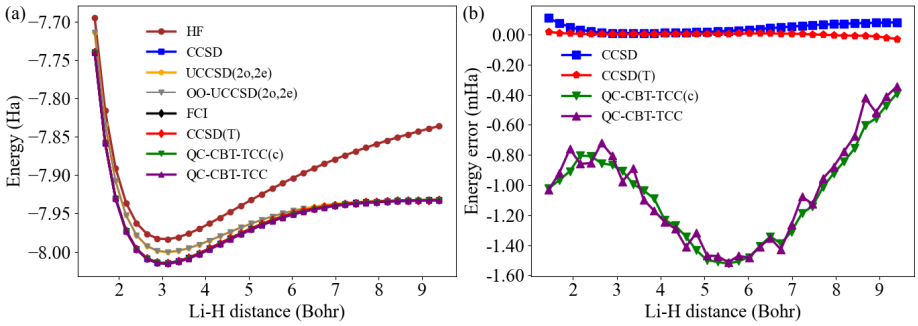

Figure 4.2: (a) Potential energy curves of LiH using the cc-pVDZ basis sets. The CCSD natural orbitals were employed for the VQE and subsequent QC-CBT-TCC and QC-CBT-TCC(c) calculations. An active space consisting of 2 orbitals and 2 electrons [i.e., (2o, 2e).] was used. (b) Deviations from the FCI potential energy curve.

correlation dominates, all methods except for HF gave similar results.

We focus on the energy errors of the CC and present methods compared with the FCI energy in Fig. 4.2 (b). CCSD and CCSD(T) showed better accuracy throughout the tested bond lengths than the QC-CBT-TCC and QC-CBT-TCC(c). This can be attributed to the small static correlation within the molecule. For such a system, CCSD and CCSD(T) can capture electron correlation up to high accuracy. The energy difference between the QC-CBT-TCC and QC-CBT-TCC(c) was small. However, the QC-CBT-TCC(c) appears to produce a smoother energy error. We assume that some errors in the QC-CBT-TCC did cancel out when the QC-CBT-TCC(c) was constructed. QC-CBT-TCC and QC-CBT-TCC(c) produced energies that are lower than the FCI energy. This is possible since QC-CBT-TCC tailors the classical CC equations, which are not variational.

Secondly, we observed the two-bond dissociation behavior of H_2O. We simultaneously increased the two H-O distances while leaving the HOH angle constant at 104.52°. Such a treatment can be understood as an example of a doubly bond dissociation [21]. We selected an active space of eight electrons and six spatial orbitals of the four highest occupied and two lowest unoccupied orbitals. The MR-CISD+Q calculation was based on preliminary state-specific CASSCF(6o,8e).

As shown in Fig. 4.3 (a), QC-CBT-TCC and QC-CBT-TCC(c) reproduce the quantitative features of the MR-CISD+Q calculation and show good accuracy throughout the observed bond distances. The CCSD energy curve, on the other hand, shows less accurate results but still follows the MR-CISD+Q energy curve. This contrasts with CCSD(T), which fails to compute the energy in the high dissociation region. At the equilibrium point, the active space UCCSD(6o,8e) and HF estimated similar energies. For long bond distances, UCCSD gave more accurate energies than HF. OO-UCCSD(6o,8e) consistently

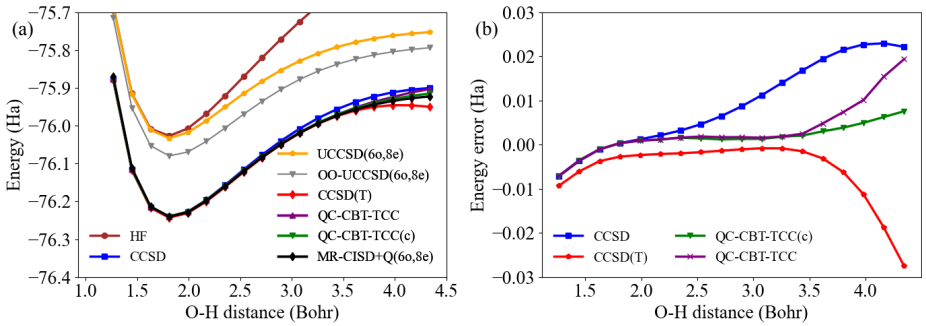

Figure 4.3: (a) Potential energy curves of the double dissociation of the water molecule's OH bonds using the cc-pVDZ basis sets. An active space consisting of 6 orbitals and 8 electrons [i.e., (6o, 8e)] was used. (b) Deviations from the MR-CISD+Q potential energy curve of the double dissociation of the water molecule's OH bonds.

produced more accurate energy than active space UCCSD(6o,8e), indicating that optimizing the orbitals structure allows for more electronic correlation to be considered. Treating the molecule within natural orbitals would probably increase the accuracy of the UCCSD(6o,8e). Methods that included out-of-active space correlation produced significantly more accurate results than the UCCSD(6o,8e) or the OO-UCCSD(6o,8e). This shows that such correlation must be included to obtain an accurate ground state description.

In Fig. 4.3 (b), we show the explicit error of the presented methods compared to MR-CISD+Q. CCSD(T), and arguably CCSD, also break in the highly entangled region. QC-CBT-TCC and the QC-CBT-TCC(c) can give accurate energies. However, in the high dissociation region, QC-CBT-TCC's error increases, whereas that of QC-CBT-TCC(c) shows this effect is reduced, indicating that the QC-CBT-TCC(c) method produces more stable energies.

Finally, we investigated the PEC of N_2 as an example of a triple-bonded molecule. We used the three highest occupied and three lowest unoccupied orbitals for the active space to perform the active space UCCSD calculations. The MR-CISD+Q calculations were performed following the state-specific CASSCF (10o,10e).

Fig. 4.4 (a) shows that the QC-CBT-TCC(c) reproduces the MR-CISD+Q PEC well. However, there is an almost constant, small energy gap between the two PECs in the region of approximately more than 4.0 Bohr. We expect this gap to result from the different active spaces selected for the QC-CBT-TCC(c) and MR-CISD+Q calculations. CCSD and CCSD(T) failed to reproduce the triple-bond breaking for extensive bond lengths as well known. They exhibited unnatural behavior and overestimated the correlation energy. The energy of active space UCCSD increased the accuracy compared with the HF energy because it could consider electron correlation inside the active space. OO-UCCSD(6o,6e) consistently produced more accurate energy than active space UCCSD(6o,6e),

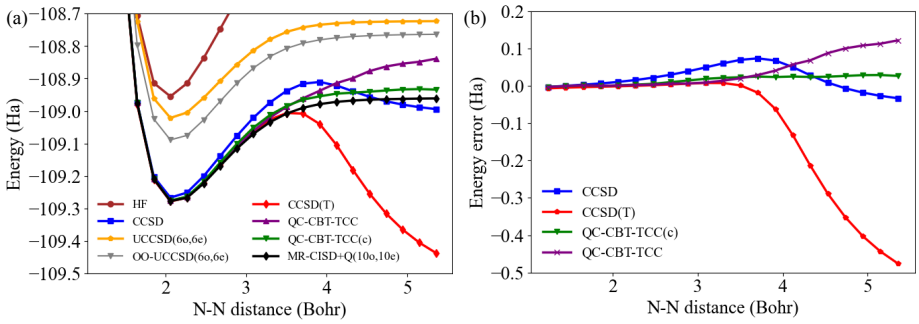

Figure 4.4: (a) Potential energy curves of N_2 using the cc-pVDZ basis sets. UCCSD calculations employed the active space consisting of 6 orbitals and 6 electrons [i.e., (6o, 6e)], while MR-CISD+Q calculations used CASSCF with the active space of 10 orbitals and 10 electrons as a reference wavefunction. (b) Deviations from the MR-CISD+Q potential energy curve of N_2.

indicating that optimizing the orbitals structure allows for more electronic correlation to be considered. Like the previous results, the additional dynamical correlation from non-active space affected the QC-CBT-TCC energy, and QC-CBT-TCC(c) further demonstrates the significant accuracy.

The error of the observed methods compared with that of MR-CISD+Q is shown in Fig. 4.4 (b). Only the QC-CBT-TCC(c) provided a good solution for all observed distances. As well known, CCSD and CCSD(T) fail to predict accurate energies for N_2 for considerable bond lengths, but also QC-CBT-TCC started to produce unfaithful results in the high dissociation limit. This effect suggests that the QC-CBT-TCC(c) can cancel out some errors resulting from the transition from the quantum device to the CCSD ansatz and is a genuine improvement of the method.

4.3.2 Number of Shot Dependency of QC-CBT-TCC

CBT used in our method adds a certain level of uncertainty to our computed energies. Determining the CASCI coefficients using CBT is a statistical process. To investigate this statistical behavior, we examined for the molecules LiH, H_2O, and N_2 the impact of varying measurement repetitions in CBT on the QC-CBT-TCC(c). We considered two constellations, one for the molecules at the equilibrium bond length [21] and one for a bond length of twice the equilibrium bond distance. Note that the geometries were not optimized. To ensure statistical significance, we repeated each measurement setup 1000 times and showed its effect on the QC-CBT-TCC(c). The parameter R, used to truncate the trivial computational basis in CBT, is set as 100. The behavior of LiH was similar to that of H_2O and N_2, and the results are shown in the Appendix. We demonstrated the effect using a box blot to demonstrate numerical data graphically.

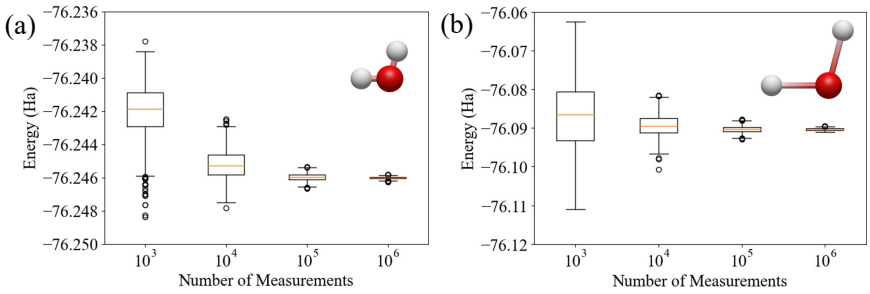

Figure 4.5: Energy insecurity of QC-CBT-TCC(c) for H_2O with a different number of measurements for CBT. N_{sample}, N_U, and N_V were all measured in the specified quantities in the figure as the X-axis values. CBT was performed 1000 times for each setting to obtain an estimate for the statistical errors. The box indicates the range from the first to the third quartile, called the inter-quartile range (IQR), with the median drawn in the middle. The box contains 50% of the data. Whiskers are the lines extending 1.5 times the IQR from the first and third quantiles. Data points that exceed the whiskers are considered outliers (fliers) and are represented as single dots. (a) Number of measurements dependency at an equilibrium distance of 1.808 Bohr. (b) Number of measurements dependency at 3.617 Bohr, twice the equilibrium distance.

Fig. 4.5 (a) and Fig. 4.5 (b) discuss the influence of the number of CBT measurements for QC-CBT-TCC(c) for H_2O. The two graphs show the differences in the bond lengths between oxygen and hydrogen. The boxes become smaller in both cases. Thus, the uncertainty decreases with an increased number of measurement repetitions. This effect is more prevalent in Fig. 4.5 (b), which was expected as the electronic structure of the ground state in the dissociation region is more complex and involves more relevant electron configurations than those around the equilibrium point. The greater complexity in the dissociation region requires more measurements to determine all relevant CI coefficients accurately. Statistical errors are smaller at the equilibrium point because the HF state, a single computational basis state, is already a good approximation.

The results for N_2 show a behavior similar to that of H_2O in that increasing the number of measurements reduces the QC-CBT-TCC(c) energy distribution, as seen in Fig. 4.6 (a) and Fig. 4.6 (b). This behavior can be explained by the higher accuracy and decreased uncertainty in determining the CBT state coefficients. Consequently, the produced state is more consistent; therefore, the energy expectancy can be determined with a higher degree of confidence.

These observations show the importance of accounting for the complexity of electronic structures when applying CBT. This becomes increasingly important in the high dissociation region when the states become more entangled. A large number of measurements are necessary to accurately determine all the relevant coefficients.

To estimate the number of shots needed to reach sub-mH standard devia-

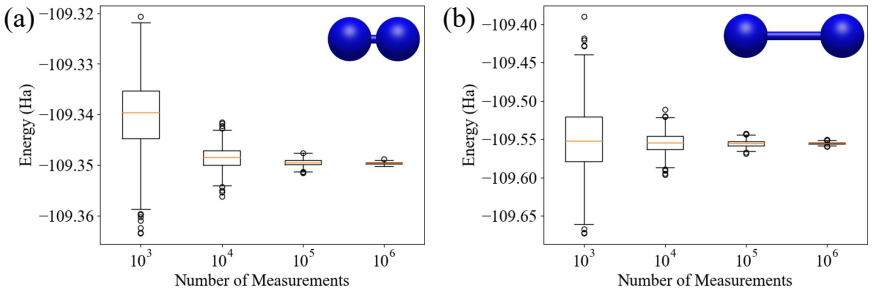

Figure 4.6: Energy insecurity of QC-CBT-TCC(c) for N_2 with a different number of measurements for CBT. N_{sample}, N_U, and N_V were all measured in the specified quantities in the figure as the X-axis values. CBT was performed 1000 times for each setting to obtain an estimate for the statistical errors. The box indicates the range from the first to the third quartile, called the inter-quartile range (IQR), with the median drawn in the middle. The box contains 50% of the data. Whiskers are the lines extending 1.5 times the IQR from the first and third quantiles. Data points that exceed the whiskers are considered outliers (fliers) and are represented as single dots. (a) Number of measurements dependency at an equilibrium distance of 2.060 Bohr. (b) Number of measurements dependency at 4.119 Bohr, twice the equilibrium distance.

tion of the predicted energy, we performed further calculations for the N_2 at 5.355 Bohr. This system is the most challenging system for CBT we examined. The other molecules need considerably fewer measurements. A standard derivation of 0.61 mH using QC-CBT-TCC(c) can be reached using $3\times 10^7 (N_{\text{sample}} = 10^7, N_U = 10^7$, and $N_V = 10^7)$ shots. This is in reach for today's quantum hardware and similar to the predicted shot counts reported by Scheurer et al. [145] using the matchgate classical shadows to extract CI coefficients from a quantum computer.

4.3.3 Application to Cope Rearrangement

Our dynamical correlation correction allows the analysis of realistic chemical processes using quantum computers. We estimated the activation energy of the Cope rearrangement using our method. Cope rearrangements are well-known organic chemical reactions. In this reaction, the carbon chain of 1,5-hexadiene is rearranged in a concerted way to convert into itself via the transition state of the chair form.

We considered the energy difference between the 1,5-hexadiene and its chair-form transition state, which are C_i symmetry structures. Their geometric structures are shown in Fig. 4.7 (a) and Fig. 4.7 (b). We performed QC-CBT-TCC(c) with the perturbative tripled corrections, denoted as QC-CBT-TCC(T)(c), to evaluate the activation energy.

For the chair and hexadiene (C_i symmetry) geometries, we used the opti-

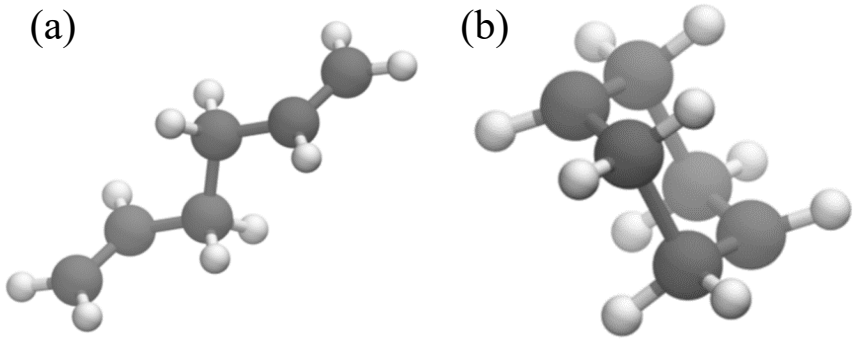

Figure 4.7: (a) 1,5-hexadiene in the C_i symmetry structure. (b) Transition state of Cope rearrangement of 1,5-hexadiene in the chair-form.

mized structures from Ref. [146]; they used the analytic MR-CISD and multireference averaged quadratic coupled-cluster (MR-AQCC) gradient methods [147] to optimize the structures with a reference space of complete active space (6o,6e) in a 6-31G$*$ basis set.

The result is shown in Tab. 4.1. Our newly proposed method agrees well with the experimental value in Ref. [148] and the value of MR-AQCC [146]. We observed that methods that ignore outside-of-active space correlation, such as HF, CASCI, and the active space UCCSD, failed to compute a reasonable activation energy. Including the dynamical correlation significantly improved the accuracy of these methods. The QC-CBT-TCC(T)(c) produced comparable results to the MR-AQCC method. This result demonstrates our method's potential for simulating complex chemical processes with strong correlation.

Table 4.1: Activation energies in kcal/mol for 1,5-hexadiene Cope rearrangement calculated in the 6-31G$*$ basis set. The VQE calculations used the disentangled UCCSD ansatz and an active space consisting of 6 orbitals and 6 electrons [i.e., (6o, 6e)]. The experimental values were obtained from the computational study in Ref. [148], which was based on the experimentally measured enthalpy from Ref. [149]

Methods	Activation energy
HF	66.0
CASCI(6o, 6e)	59.0
UCCSD(6o, 6e)	60.1
QC-CBT-TCC(T)(c)	38.7
MR-AQCC [146]	37.3
Experiment [148]	35.0

4.4 Conclusion

In this Chapter, we combine the TCC approach with quantum computing. The TCC approach separates the active space from the remaining orbitals. This allows for a more rigorous active space treatment while maintaining the dynamic correlation from the out-of-active space orbitals. Computing an eigenvalue of an active space Hamiltonian using a quantum computer is desirable because it is expected that they can simulate much larger quantum systems. We tailor the CCSD approach using the quantum state of the active space determined on a quantum computer. We use this approach to describe the dynamical correlation from the out-of-active space orbitals on the quantum solution. We employ CBT to determine the relevant CCSD amplitudes using a quantum computer. This makes our method universally usable for all quantum algorithms that produce an eigenstate of an active-space Hamiltonian.

The QC-CBT-TCC was applied to three small molecules, LiH, H_2O, and N_2. In the LiH case, where static correction is less important, our method may improve the accuracy compared to the active space UCCSD, and we observe that our method with correction scheme, QC-CBT-TCC(c), works well to cancel out the error of QC-CBT-TCC. In the H_2O and N_2 cases, our method improved the accuracy and could provide suitable quantitative PECs, even when standard CCSD or CCSD(T) fails. Hence, our method has the potential to practically include the lacking dynamical correlation into a static correlated active space solution of quantum computation.

We investigated the influence of the different number of measurements for the CBT on our method's uncertainty. We conclude that determining the correct coefficients becomes more challenging in the high dissociation region with large static correlation. A sufficient number of measurements must be performed to determine the CCSD amplitudes with sufficient accuracy. For the investigated molecules, a total of $R = 100$, $N_{\text{sample}} = 10^6$, $N_U = 10^6$, and $N_V = 10^6$ measurements were appropriate to predict energies with a high level of confidence.

In addition, we applied our method with the perturbative triples correction to Cope-rearrangement, a well-known organic reaction. We demonstrated that our method produced activation energy comparable to MR-AQCC. This showed our method's potential for complex chemical reactions.

Nevertheless, for more complex systems or in the presence of real device errors such as depolarising noise, further verification is required to determine the extent to which QC-CBT-TCC works well. Although, in this Chapter, we utilized the CBT method to approximate the wavefunction on the quantum computer, it is possible to explore extensions that combine TCC with methods that are more resilient to noise and statistical errors, such as quantum selected configuration interaction [150, 151]. Another potential avenue for further development of this method is to create a self-consistent version [152, 153] that iterates between the calculation of the active space wavefunction and the optimization of the CC amplitudes in the outside of the active space, although such a self-consistent approach multiplies the computational cost associated with the method.

Finally, the performance of a tomography method depends heavily on the number of shots available. Matchgate/Fermionic shadows has good asymptotic scaling and can be highly efficient if enough shots are available [50, 154]. On the other hand, these shadow tomography methods may not always be the best approach given realistic shot budgets [124]. We chose CBT because it requires shallower circuits and can be effective with small shot budgets by adjusting the R parameter. Nevertheless, it is an open question as to which method is better for extracting CI coefficients with a limited number of shots.

Chapter 5

Variational Coupled Cluster Method for Quantum Computer

In this Chapter, we show how we can prepare an approximation of the VCCSD state on a quantum computer. This has multiple benefits. A VCCSD state could present itself as a suitable initial state for QPE, allowing for exact determination of the ground state. Additionally, the VCCSD and the CCSD parameters are connected. This can be helpful when we want to predetermine some of the VCCSD parameters on a classical computer or when we extract information on the produced state of the quantum computer since we can directly use the VCC parameters as the parameters of CCSD on a classical computer. To implement the VCCSD, we utilized the Chebyshev expansion to approximate the ansatz as a polynomial and applied it using QSVT. In multiple numerical experiments, we were able to produce ground state energies in agreement with VCCSD. This Chapter is based on [Erhart, Yoshida, Khinevich, and Mizukami, arXiv:2406.07364].

5.1 Introduction

The CC theory is a highly effective framework for quantum chemical calculations [29]. For weakly correlated systems, the CCSD(T) is widely known to achieve chemical accuracy. The development of CC methods has progressed steadily within the quantum chemistry community, making them applicable to a wide range of systems. In 2013, a CC calculation of an entire small protein was achieved [155]. In recent years, applications have extended beyond molecular systems to include solid-state and surface systems under periodic boundary conditions [156, 157]. CCSD and CCSD(T) are routinely used as reference methods and have been actively utilized for creating datasets for machine learning,

especially in recent times [158–160].

However, it is well known that CC methods do not work well for strongly correlated systems. CC methods assume weak electron correlations and are not variational; therefore, they break down for complicated electronic structures. If CC methods could be solved variationally, their range of applicability would greatly expand. Solving VCC on a classical computer requires an exponential computational cost, making VCC calculations virtually impossible for most molecules.

This situation changed in 2014 when it was revealed that UCC, a variational version of the CC theory, could be solved in polynomial time using the quantum-classical hybrid algorithm VQE. This study triggered extensive research on UCC and related theories using quantum computers. Over the past decade, numerous studies have revealed several practical problems with VQE [16]. One major issue is the enormous measurement cost (sampling cost) required to calculate energies with the accuracy needed for chemistry [122]. Another problem is the lack of efficient algorithms for optimizing the parameters of nonlinear wavefunction models. Parameter optimization requires repeated energy calculations, and a large number of optimization steps means that high-cost energy calculations must be repeated, making parameterization of wavefunctions such as UCC using VQE difficult [161].

To address this problem, it is desirable to determine as many parameters as possible in advance using a classical computer. This requires a wavefunction ansatz that can be optimized on a classical computer. For example, Matrix Product States [162] can be optimized classically and are easy to implement on quantum computers. However, UCC is different from classical CC, and while some approximate parameters can be prepared on a classical computer, it is difficult to ensure sufficient correspondence. If CC could be directly implemented on a quantum computer, this issue would be greatly improved.

Another issue is that VQE and QPE generally require more than twice the number of qubits as spatial orbitals. When using basis functions of the size needed for quantitative calculations, the number of required qubits becomes very large. Therefore, in VQE and QPE, it is inevitable that the application of quantum computers will be limited to essential degrees of freedom, necessitating the introduction of the active space orbital approximation. The electron correlation in other degrees of freedom outside the active space must be considered using a classical computer before or after the quantum computation. In this case, the information from the wavefunction on the quantum computer needs to be transferred to the classical computer. However, measuring high-order RDMs is unrealistic due to the enormous measurement cost [41, 122–124], and approximate tomography methods [27, 163] also require repeating a considerable number of measurements. In contrast, if a common ansatz could be used for both classical and quantum computers, such as implementing CC on a quantum computer, the wavefunction information could be directly transferred to the classical computer from the parameters of the quantum circuit. Therefore, realizing the widely used non-unitary CC on classical computers as a quantum circuit, which connects quantum and classical methods, is significant.

In this Chapter, we aimed to implement non-unitary CC theory on quantum computers. Specifically, we proposed an approximated VCC theory by expanding the exponential ansatz in Chebyshev polynomials. We also developed a method for Chebyshev expansion based on the decomposition of the cluster operator into Hermitian and anti-Hermitian parts and showed its implementation in a quantum circuit.

The structure of this Chapter is organized as follows: In Sec. 5.2, we provide an overview of the VCC theory and the Chebyshev expansion method. We explain the method of Chebyshev expansion based on Hermitian cluster operators and its implementation in a quantum circuit. In Sec. 5.3, we detail the numerical simulations, including the software, algorithms, and computational conditions used. In Sec. 5.4, we present the results of the numerical verification for small molecules and evaluate the accuracy of VCC using Chebyshev expansion. Finally, in Sec. 5.5, we summarize this Chapter and discuss future prospects.

5.2 Methods

5.2.1 Review of Variational Coupled Cluster

VCC [53–63] is a variant of CC. The energy expression of VCC is given by

$$E_{\mathrm{VCC}} := \frac{\langle\Psi_0|\, e^{\hat{T}^\dagger} \hat{H} e^{\hat{T}} \,|\Psi_0\rangle}{\langle\Psi_0|\, e^{\hat{T}^\dagger} e^{\hat{T}} \,|\Psi_0\rangle}, \tag{5.1}$$

where $|\Psi_0\rangle$ is the reference wave function, usually the HF state. The operators $\hat{H}$ and $\hat{T}$ are the electronic Hamiltonian and the cluster operator. The cluster operator $\hat{T}$ comprising single and double excitation operators is expressed as

$$\hat{T} = \sum_{i,a} t_i^a \hat{a}_a^\dagger \hat{a}_i + \sum_{i<j,\, a<b} t_{ij}^{ab} \hat{a}_a^\dagger \hat{a}_b^\dagger \hat{a}_i \hat{a}_j, \tag{5.2}$$

where $\hat{a}_a^\dagger$ and $\hat{a}_i$ are the creation and annihilation operators of the a-th and i-th orbitals, respectively. The indices i, j, $\cdots$ and a, b, $\cdots$ correspond to the occupied and unoccupied orbitals, respectively. The coefficients t_i^a and t_{ij}^{ab} are known as the cluster amplitudes. The exponential ansatz with the single and double cluster operators is called the CCSD ansatz.

In Variational Coupled Cluster Singles and Doubles (VCCSD), these parameters are variationally optimized to minimize the energy of Eq. (5.1) and, therefore, produce an upper bound for the exact ground state energy. However, it has to be mentioned that if the normalization factor $\langle\Psi_0|\, e^{\hat{T}^\dagger} e^{\hat{T}} \,|\Psi_0\rangle$ becomes small, the variance of this method could increase. Additionally, computing the VCC energy on classical computers is known to require exponential computational costs. This is because the Baker–Campbell–Hausdorff expansion of $\langle\Psi_0|\, e^{\hat{T}^\dagger} \hat{H} e^{\hat{T}} \,|\Psi_0\rangle$ is not terminated. To address this issue, the standard CC

method employs the following energy expression based on the similarity transformation

$$E_{\mathrm{CC}} := \langle \Psi_0 | \, e^{-\hat{T}} \hat{H} e^{\hat{T}} \, | \Psi_0 \rangle \, . \tag{5.3}$$

This approach allows the computation of CC energy and the determination of the cluster amplitudes with polynomial costs on classical computers. One drawback of this method is that the energy is no longer variational and breaks down when the overlap between the reference wavefunction and the target wavefunction is small.

5.2.2 Chebyshev Expansion of VCC towards Quantum Computing Applications

Evaluating E_{VCC} is challenging, even using quantum computers, due to the non-unitary nature of $e^{\hat{T}}$. Here, we introduce the Chebyshev expansion of $e^{\hat{T}}$ for implementation on a quantum computer, where QSVT is employed to prepare Chebyshev polynomials. The Chebyshev expansion and the QSVT algorithm have been discussed in Chapter 2.

Chebyshev Expansion of $e^{\hat{T}}$

The exponential ansatz $e^{\hat{T}}$ can be expanded using Chebyshev polynomials

$$e^{\hat{T}} = \sum_{n=0}^{N} c_n \mathcal{T}_n(\hat{T}/\tau), \tag{5.4}$$

where $\mathcal{T}_n$ and c_n are the n-th degree Chebyshev polynomials of the first kind and their real coefficients, respectively. N denotes the number of electrons. Since the Chebyshev expansion of a function $f(x)$ is only defined for $|x| \leq 1$, the cluster operator $\hat{T}$ is normalized with $\tau = |\hat{T}|$, when $|\hat{T}| > 1$. The Chebyshev polynomial coefficients c_n are determined for the Chebyshev expansion of $f(x) = (e^{\tau})^x$ to compensate for the normalization of the cluster operator $\hat{T}$.

We truncate the Chebyshev polynomial expansion in Eq. (5.4) at $n = d$ to reduce computational costs. Henceforth, we will denote the Chebyshev polynomial expansion of $e^{\hat{T}}$ truncated at the d-th degree as $\hat{A}^{(d)}(\hat{T})$. For example, the low-degree truncated ansatzes of the Chebyshev polynomial expansion of $e^{\hat{T}}$ are represented as

$$\hat{A}^{(0)}(\hat{T}) = c_0, \tag{5.5}$$

$$\hat{A}^{(1)}(\hat{T}) = c_0 + c_1 \hat{T}/\tau, \tag{5.6}$$

$$\hat{A}^{(2)}(\hat{T}) = (c_0 - c_2) + c_1 \hat{T}/\tau + 2c_2(\hat{T}/\tau)^2. \tag{5.7}$$

In this manuscript, we refer to the Chebyshev expansion of VCCSD with degree d as C^d-VCCSD. The ansatzes $\hat{A}^{(d)}(\hat{T})$ truncated at low degrees correspond

to well-known quantum chemical theories. By substituting the 0-degree ansatz $\hat{A}^{(0)}(\hat{T})$ for $e^{\hat{T}}$ into Eq. (5.1), it is evident that the energy expectation value of the HF state is obtained. Applying the 1-degree ansatz $\hat{A}^{(1)}(\hat{T})$ enables the wave function to incorporate single and double excitations and assume the same form as CISD

$$\begin{aligned}&\hat{A}^{(1)}(\hat{T})\,|\Psi_0\rangle \\ &\quad = c_0\,|\Psi_0\rangle + c_1/\tau \sum_{i,a} t_i^a\,|\Psi_i^a\rangle + c_1/\tau \sum_{i<j,a<b} t_{ij}^{ab}\,\left|\Psi_{ij}^{ab}\right\rangle,\end{aligned} \tag{5.8}$$

where $|\Psi_i^a\rangle$ and $\left|\Psi_{ij}^{ab}\right\rangle$ are the singly and doubly excited configurations, respectively.

Chebyshev Expansion of $e^{\hat{T}}$ based on a decomposed Hermitian cluster operator

The implementation of the truncated Chebyshev expansion of the VCC ansatz on a quantum computer requires an additional approximation. QSVT does not allow for making a polynomial of any matrix on quantum computers. The matrix for QSVT should be Hermitian. However, the cluster operator $\hat{T}$ is nilpotent, making QSVT not directly applicable for constructing $\mathcal{T}_n(\hat{T}/\tau)$.

To address this issue, we consider the following approximated form of the VCC ansatz

$$e^{\hat{T}} = e^{\frac{1}{2}(\hat{T}-\hat{T}^\dagger)+\frac{1}{2}(\hat{T}+\hat{T}^\dagger)} \approx e^{\frac{1}{2}(\hat{T}-\hat{T}^\dagger)} e^{\frac{1}{2}(\hat{T}+\hat{T}^\dagger)}. \tag{5.9}$$

In this approach, the cluster operator is decomposed into the anti-Hermitian $\frac{1}{2}(\hat{T}-\hat{T}^\dagger)$ and Hermitian parts $\frac{1}{2}(\hat{T}+\hat{T}^\dagger)$. In this thesis, we call the ansatz as a *trotterized* VCC ansatz. The exponential function of the anti-Hermitian part $\frac{1}{2}(\hat{T}-\hat{T}^\dagger)$ is unitary and closely resembles the UCC theory. The implementation of a UCC ansatz in a quantum circuit has been extensively researched. The disentangled UCC ansatz [164, 165] can be utilized to implement the former part

$$e^{\frac{1}{2}(\hat{T}-\hat{T}^\dagger)} \approx \prod_\mu e^{\frac{1}{2}(\hat{T}_\mu-\hat{T}_\mu^\dagger)}, \tag{5.10}$$

where $\hat{T}_\mu$ denotes each term of the cluster operator $\hat{T}$ such as $t_i^a \hat{a}_a^\dagger \hat{a}_i$ and $t_{ij}^{ab} \hat{a}_a^\dagger \hat{a}_b^\dagger \hat{a}_i \hat{a}_j$.

The Chebyshev expansion is applied to the latter part $e^{\frac{1}{2}(\hat{T}+\hat{T}^\dagger)}$. As mentioned in the previous subsection, we normalize the operator $\frac{1}{2}(\hat{T}+\hat{T}^\dagger)$ with the spectral norm $\kappa = |\frac{1}{2}(\hat{T}+\hat{T}^\dagger)|$, when $\kappa > 1$ to ensure the condition of the Chebyshev expansion. The resulting Chebyshev expansion truncated at $n = d$ is expressed as

$$e^{\frac{1}{2}(\hat{T}+\hat{T}^\dagger)} \approx \sum_{n=0}^{d} c_n \mathcal{T}_n \left(\frac{1}{2}(\hat{T}+\hat{T}^\dagger)/\kappa\right). \tag{5.11}$$

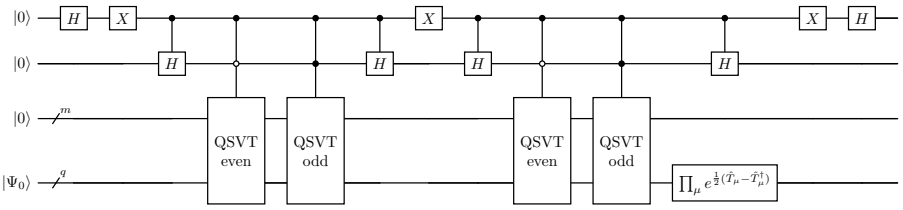

Figure 5.1: Quantum circuit to execute the HC^d-VCC ansatz for a q-qubit system. QSVT even and QSVT odd apply the corresponding part of the Chebychev polynomial with even/odd parity, respectively. The block encoding of $\frac{1}{2}(\hat{T}+\hat{T}^\dagger)$ in QSVT is performed using m-ancilla qubits. A linear combination of unitaries structure with two ancilla qubits is required to perform the real polynomial of indifferent parity resulting from the Chebyshev expansion.

An approximate VCC ansatz that can be implemented in a quantum circuit is

$$e^{\hat{T}} \approx \prod_{\mu} e^{\frac{1}{2}(\hat{T}_\mu - \hat{T}_\mu^\dagger)} \left(\sum_{n=0}^{d} c_n \mathcal{T}_n \left(\frac{1}{2}(\hat{T}+\hat{T}^\dagger)/\kappa \right) \right). \tag{5.12}$$

We refer to this ansatz as the Hermitian-part Chebyshev approximation with degree d of VCC or HC^d-VCC in the remainder of this thesis.

5.2.3 The QSVT Implementation of HC^d-VCC Ansatz

The quantum circuit used to perform VCC for a q-qubit system is shown in Fig. 5.1. The parity of the polynomials generated by a QSVT circuit is restricted; a single QSVT function can return only even or odd polynomials. Therefore, it is necessary to combine two QSVT circuits, each responsible for even or odd polynomials, to realize the Chebyshev expansion. This combination was achieved using a linear combination of unitaries [87], requiring two ancilla qubits. Additionally, additional m-ancilla qubits are required to realize block-encoding [82–84] of $\frac{1}{2\kappa}(\hat{T}+\hat{T}^\dagger)$ in QSVT. After the Chebyshev expansion of $e^{\frac{1}{2}(\hat{T}+\hat{T}^\dagger)}$, the disentangled UCC part $\prod_\mu e^{\frac{1}{2}(\hat{T}_\mu - \hat{T}_\mu^\dagger)}$ may be applied to the system state, finalizing the HC^d-VCC ansatz.

5.3 Computational Details

Here, we provide the computational details of the proof-of-principle numerical simulations of our methods. We implemented the circuit shown in Fig. 5.1 in Python using Pennylane, version 0.34.0 [166]. The angles for the QSVT were determined using the algorithm implemented in Pyqsp, version 0.1.6 [64, 78, 167, 168]. It should be noted that, in this manuscript, the exact $e^{\frac{1}{2}(\hat{T}-\hat{T}^\dagger)}$ matrix was used instead of the disentangled UCC ansatz.

We computed the PECs of N_2, linear H_4 and H_6 molecules to assess the accuracy of our methods. All calculations utilized the minimal basis set STO-3G, with the HF state serving as the reference state. Variational parameters were optimized using the L-BFGS-B algorithm [169]. For comparison, we performed FCI or exact diagonalization. When using the active space approximation, the CASCI was employed to obtain reference energies. Classical algorithms were executed using the PySCF program, version 2.3.0 [143].

5.4 Results and Discussion

5.4.1 Chebyshev Approximation of VCCSD

First, we discuss the accuracy of the truncated Chebyshev expansion VCCSD, denoted as C^d-VCCSD, compared to the exact VCCSD and its dependence on the degree d. The simulation results are presented in Fig. 5.2. The C^0-VCCSD and C^1-VCCSD are equivalent to HF and CISD, respectively. As expected, these two methods show significant deviations from the exact VCCSD. However, the C^d-VCCSD rapidly converges to the exact VCCSD as d increases.

The right panels of Fig. 5.2 illustrate the truncation errors for cases where $d \geq 2$. The truncation error increases with the interatomic distance R but decreases rapidly with the increase of the degree of truncation. For the linear H_4 molecule, the C^4-VCCSD shows slight errors. Since H_4 is a 4-electron system, the C^4-VCCSD is expected to be exact. These observed errors likely stem from numerical inaccuracies in the parameter gradients during the optimization process. For H_6 and N_2, both 6-electron systems, the C^5-VCCSD exhibits sub-milliHartree (mHa) errors. These results suggest that the C^d-VCCSD with $d < N$ can sufficiently reproduce the exact VCCSD.

5.4.2 Robustness of *Trotterized* VCCSD

Next, we validate the *trotterized* VCCSD ansatz in Eq. (5.9). Fig. 5.3 compares the *trotterized* VCCSD PECs with the exact VCCSD. Note that the *trotterized* VCCSD does not employ a Chebyshev expansion, so any deviation from the exact VCCSD is solely due to trotterization. When using the parameters from the exact VCCSD ansatz, the deviation increased in the strongly correlated regime. However, the variationally optimized *trotterized* VCCSD significantly reduced the error, indicating that most Trotter errors can be absorbed into the variational parameters. A similar observation has been made in the context of the UCC ansatz [170]. Nonetheless, for longer bond lengths, the Trotter error remains non-negligible. This error may be further reduced using a higher-order Trotter-Suzuki approximation [171, 172], though at the expense of increased computational costs.

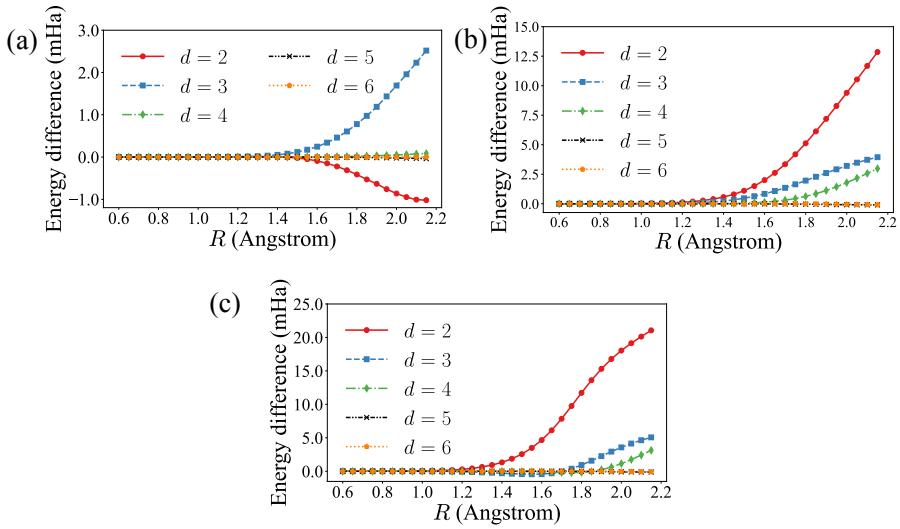

Figure 5.2: Convergence of C^d-VCCSD to exact VCCSD as the degree of truncation in the Chebyshev expansion. The three rows correspond to the results for linear H_4, H_6, and N_2, respectively. The left panels display the PECs of C^d-VCCSD, exact VCCSD, and FCI/CASCI for each molecule. The right panels illustrate the energy difference between C^d-CCSD and exact VCCSD. The horizontal axes represent the inter-atomic distance R between neighboring atoms. All calculations use the STO-3G basis set, with the active space for N_2 set to (6e, 6o).

5.4.3 Numerical Verification of HC^d-VCCSD

Fig. 5.4 shows the performance of the HC^d-VCCSD ansatz. The PECs of the linear H_4 and H_6 molecules have been simulated. The errors in the HC^d-VCCSD ansatz stem from two sources: the Chebyshev expansion errors (Fig. 5.2) and the Trotterization errors (Fig. 5.3). For the H_4 molecule, where Trotterization errors are negligible, the Chebyshev expansion error is smaller in HC^d-VCCSD than in C^d-VCCSD. For instance, at an H-H distance of 2.0 Angstrom, the HC^2-VCCSD error is approximately 1/4 of the C^2-VCCSD error. This result is because HC^d-VCCSD does not use the Chebyshev expansion for the disentangled UCC ansatz. In the H_6 molecule, for $d = 4$ or higher, the main source of error is Trotterization, with the Chebyshev expansion error being small and non-dominant.

5.5 Conclusions

In this Chapter, we proposed an approach to implementing the VCC theory on quantum computers by expanding the exponential cluster operator using Chebyshev polynomials. We introduced the Chebyshev approximated VCC (C^d-VCC)

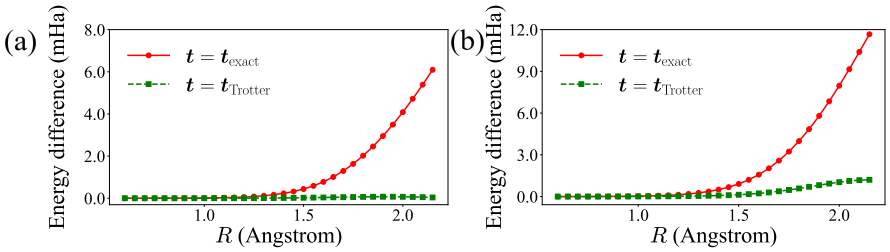

Figure 5.3: Energy errors in *trotterized* VCCSD using amplitudes optimized for exact VCCSD, $\boldsymbol{t} = \boldsymbol{t}_{\text{exact}}$, and *trotterized* VCCSD, $\boldsymbol{t} = \boldsymbol{t}_{\text{Trotter}}$. Panels (a) and (b) represent the results for linear H_4 and H_6, respectively. The distance R specifies the interatomic distance between neighboring hydrogens. All calculations were performed using the STO-3G basis set.

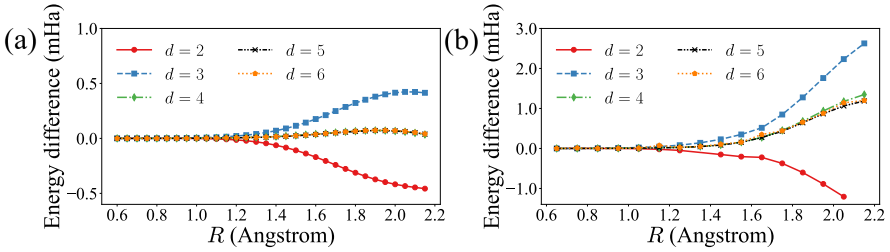

Figure 5.4: Convergence of HC^d-VCCSD to exact VCCSD as the degree of truncation in the Chebyshev expansion increases from $d = 2$ to $d = 6$. HC^d-VCCSD was implemented using QSVT. The two rows correspond to the results for linear H_4 and H_6. The left panels display the PECs of HC^d-VCCSD, exact VCCSD, and FCI for each molecule. The right panels illustrate the energy difference between HC^d-CCSD and exact VCCSD. The distance R specifies the interatomic distance between neighboring hydrogens. All calculations were performed using the STO-3G basis set.

and investigated its accuracy and convergence with respect to the truncation degree d. Numerical simulations demonstrated that the C^d-VCC rapidly converges to the exact VCC with increasing d, and the C^d-VCC with $d < N$, where N is the number of electrons, reproduced the exact VCC with sufficient accuracy.

Implementing the C^d-VCC itself on quantum computers is not straightforward because the cluster operator is not diagonalizable. When an operator is not diagonalizable, quantum algorithms such as QSVT cannot be directly applied. To address this issue, we developed the Hermitian-part Chebyshev approximated VCC (HC^d-VCC) ansatz, which decomposes the cluster operator into anti-Hermitian and Hermitian parts. The anti-Hermitian part is represented by the well-known disentangled UCC ansatz, while the Hermitian part is approximated using the Chebyshev expansion. For Hermitian operators, their Chebyshev polynomials can be realized on quantum circuits using the QSVT technique. Numerical simulations revealed that the HC^d-VCC ansatz can effectively reduce the Chebyshev expansion error compared to the C^d-VCC, as it does not employ the Chebyshev expansion for the UCC part.

Implementing non-unitary CC wave functions on quantum computers has the potential to simplify the process of initial state preparation on quantum devices, as it is expected that the circuit parameters with small rotation angles can be determined on classical computers [173]. Furthermore, this method may also facilitate the efficient extraction of quantum state information, which is essential for post-processing tasks on classical computers following quantum computations. For example, the quantum circuit parameters (i.e., CC amplitudes) in the active space can be directly used in the framework of tailored or externally-corrected CC methods with quantum inputs [145, 174], efficiently considering the electron correlations ignored in quantum computing on a classical computer. Existing such post-processing methods require many repeated measurements, while the present method allows us to extract the cluster amplitudes without any measurement.

Chapter 6

Conclusion

After a short introduction to the field of quantum computing in Chapter 1, we introduced in Chapter 2 some of the background needed to follow this thesis. In Chapters 3-5, we discussed in detail the advantages of our developed quantum-classical hybrid algorithms. In this Chapter, we will summarize our findings and put them in the context of today's status of quantum computing.

A major advantage of calculating electronic structures using quantum computing is effectively representing quantum states using qubits. The difficulties of operating stable qubits challenge this fundamental advantage. Even when tremendous efforts have been made to develop quantum computers that can execute algorithms with high fidelity, the currently available qubits remain limited. Implementing error correction codes can only be a partial answer due to the significant overhead required. This resource limitation led to the fact that, as of today, quantum computers can only be used to calculate the electronic structure of relatively simple molecules. There are currently multiple different approaches to improving electronic structure algorithms to put them within reach of today's and future improved quantum computers. We reached the conclusion that in the context of resource-limited quantum computers, it is advantageous to execute an algorithm that partly runs on a quantum computer and partly on a classical computer. In this sense we speak of such algorithms as a quantum-classical hybrid algorithm. Using such a concept, we effectively increase the degrees of freedom manageable by quantum computers by using the quantum-classical optimization method deep VQE. In a second approach, for molecules requiring a number of degrees of freedom that quantum computers can not handle, we develop the quantum-classical correction method QC-CBT-TCC, mitigating the error from ignored electronic correlation. A third approach to using the concept of quantum-classical hybrid algorithms opens opportunities for an approximated ansatz of the CC theory usable by both quantum and classical computers.

Deep VQE is a known method that combines the quantum-classical hybrid algorithm VQE with the divide-and-conquer concept. It divides the full system into subsystems and solves them individually using VQE. The found ground

states are the foundation for building a reduced basis in which the full system is represented. The system can then be calculated on a reduced basis using a finalizing VQE. To effectively increase the degrees of freedom manageable by quantum computers, we focused in Chapter 3 on optimizing to build an effective basis set to represent the ground state of the recombined molecule. Selecting a suitable basis set reduces the number of qubits needed in the finalizing VQE, without sacrificing accuracy. Deep VQE optimized with our basis forming methods produces results within a few mHa of the reference methods FCI or CASCI, often achieving chemical accuracy. We showed that including additional low-laying energy states can be beneficial when forming the effective basis set, especially when degenerate ground states are occurring. A future research direction could consider an adaptive approach for building the basis sets sequentially.

The active space approximation is a widely used method in quantum chemistry calculations. It reduces the computational cost by selecting the molecule's most relevant orbitals and electrons for calculating the electronic structure. It is well-known that such a reduction suffers from lost electronic correlation and needs to be corrected. In classical computation chemistry, the TCC is such a correction method. In Chapter 4, we combined the TCC approach with quantum computing, creating a quantum-classical hybrid algorithm. This allows us to calculate effectively the active space on a quantum computer and correct the effect from the missing electron correlation using a CC ansatz on a classical computer. We utilized CBT to determine the relevant CC amplitudes to map the active space solution from the quantum computer to the classical computer. We could show that we successfully reintroduced the missed electron correlation in the active space solution for multiple molecules and were even able to estimate the activation energy of the 1,5-hexadiene Cope rearrangement in good agreement with MR-AQCC. A possible way to improve the efficiency of this method is to develop a parameterized ansatz on the quantum computer that allows the transfer of the state via the coefficients directly to the classical computer. This would allow us to circumvent the costly CBT method. We investigated such a method in Chapter 5.

In Chapter 5, we proposed a method to enhance the connection between quantum and classical computers. We achieve this with an approximation version of the parameterized VCC on the quantum computer. We realized that the approximation needed to execute the non-unitary algorithm on a quantum computer can be largely absorbed during the classical optimization step of the methods's parameters. The similarity with the CC that can be executed on a classical computer allows us to freely exchange the parameters between the classical executable CC and the quantum computer approximated VCC. This development further enhances the impact of quantum-classical hybrid algorithms since it allows the extraction of information on the produced quantum state and allows the pre-optimization of the VCC parameters on a classical computer, leading to faster convergence. This makes quantum-classical hybrid algorithm an even stronger choice to solve electronic structure problems with resource-limited quantum computers and classical computers.

We determined the performance of all the methods we developed in this thesis by considering a noise-free quantum computer. This ignores that the quantum calculation part of our quantum-classical hybrid algorithms on a real quantum computer is suffering from external noise. Using a real quantum computer would require the utilization of error correction or error mitigation. However, the overhead demanded to execute such codes often exceeds the number of qubits available on a quantum device.

For quantum computing to be a viable tool for electronic structure calculations, it will be fundamentally important to develop scalable fault-tolerant qubits. We assume that if this necessary condition is met, there will be good reasons to use quantum-classical hybrid algorithms to find the solution for complex chemical structures. In this sense, it is sufficient to use new high-potential quantum algorithms, which are in part supported by already-developed classical algorithms, allowing for improved results. When these necessary and sufficient conditions are fulfilled, quantum computing has gone from basic research to a practical tool for electronic structure calculations. We believe quantum-classical hybrid algorithms could be the key to this goal since they combine the best of two worlds.

Bibliography

[1] R. P. Feynman, "Simulating physics with computers", International Journal of Theoretical Physics **21**, 467–488 (1982).

[2] P. Shor, "Algorithms for quantum computation: discrete logarithms and factoring", in Proceedings 35th annual symposium on foundations of computer science (1994), pp. 124–134.

[3] P. W. Shor, "Polynomial-Time Algorithms for Prime Factorization and Discrete Logarithms on a Quantum Computer", SIAM Journal on Computing **26**, 1484–1509 (2006).

[4] A. W. Harrow, A. Hassidim, and S. Lloyd, "Quantum Algorithm for Linear Systems of Equations", Physical Review Letters **103**, 150502 (2009).

[5] A. Y. Kitaev, *Quantum measurements and the abelian stabilizer problem*, 1995, arXiv:`quant-ph/9511026 [quant-ph]`.

[6] D. S. Abrams and S. Lloyd, "Quantum algorithm providing exponential speed increase for finding eigenvalues and eigenvectors", Phys. Rev. Lett. **83**, 5162 (1999).

[7] A. Aspuru-Guzik, A. D. Dutoi, P. J. Love, and M. Head-Gordon, "Simulated quantum computation of molecular energies", Science **309**, 1704–1707 (2005).

[8] M. Reiher, N. Wiebe, K. M. Svore, D. Wecker, and M. Troyer, "Elucidating reaction mechanisms on quantum computers", Proceedings of the National Academy of Sciences **114**, 7555–7560 (2017).

[9] N. Yoshioka, T. Okubo, Y. Suzuki, Y. Koizumi, and W. Mizukami, "Hunting for quantum-classical crossover in condensed matter problems", npj Quantum Information **10**, 45 (2024).

[10] J. Preskill, "Quantum Computing in the NISQ era and beyond", Quantum **2**, 79 (2018).

[11] A. Kandala, A. Mezzacapo, K. Temme, M. Takita, M. Brink, J. M. Chow, and J. M. Gambetta, "Hardware-efficient variational quantum eigensolver for small molecules and quantum magnets", Nature **549**, 242–246 (2017).

[12]G. A. Quantum, Collaborators*†, F. Arute, K. Arya, R. Babbush, D. Bacon, J. C. Bardin, R. Barends, S. Boixo, M. Broughton, B. B. Buckley, D. A. Buell, B. Burkett, N. Bushnell, Y. Chen, Z. Chen, B. Chiaro, R. Collins, W. Courtney, S. Demura, A. Dunsworth, E. Farhi, A. Fowler, B. Foxen, C. Gidney, M. Giustina, R. Graff, S. Habegger, M. P. Harrigan, A. Ho, S. Hong, T. Huang, W. J. Huggins, L. Ioffe, S. V. Isakov, E. Jeffrey, Z. Jiang, C. Jones, D. Kafri, K. Kechedzhi, J. Kelly, S. Kim, P. V. Klimov, A. Korotkov, F. Kostritsa, D. Landhuis, P. Laptev, M. Lindmark, E. Lucero, O. Martin, J. M. Martinis, J. R. McClean, M. McEwen, A. Megrant, X. Mi, M. Mohseni, W. Mruczkiewicz, J. Mutus, O. Naaman, M. Neeley, C. Neill, H. Neven, M. Y. Niu, T. E. O'Brien, E. Ostby, A. Petukhov, H. Putterman, C. Quintana, P. Roushan, N. C. Rubin, D. Sank, K. J. Satzinger, V. Smelyanskiy, D. Strain, K. J. Sung, M. Szalay, T. Y. Takeshita, A. Vainsencher, T. White, N. Wiebe, Z. J. Yao, P. Yeh, and A. Zalcman, "Hartree-fock on a superconducting qubit quantum computer", Science **369**, 1084–1089 (2020), eprint: https://www.science.org/doi/pdf/10.1126/science.abb9811.

[13]Y. Kim, A. Eddins, S. Anand, K. X. Wei, E. van den Berg, S. Rosenblatt, H. Nayfeh, Y. Wu, M. Zaletel, K. Temme, and A. Kandala, "Evidence for the utility of quantum computing before fault tolerance", Nature **618**, 500–505 (2023).

[14]A. Peruzzo, J. McClean, P. Shadbolt, M. H. Yung, X. Q. Zhou, P. J. Love, A. Aspuru-Guzik, and J. L. O'Brien, "A variational eigenvalue solver on a photonic quantum processor", Nature Communications **5**, 4213 (2014).

[15]D. A. Fedorov, B. Peng, N. Govind, and Y. Alexeev, "Vqe method: a short survey and recent developments", Mater Theory **6**, 2 (2022).

[16]J. Tilly, H. Chen, S. Cao, D. Picozzi, K. Setia, Y. Li, E. Grant, L. Wossnig, I. Rungger, G. H. Booth, and J. Tennyson, "The variational quantum eigensolver: a review of methods and best practices", Phys. Rep. **986**, 1–128 (2022).

[17]K. Mizuta, M. Fujii, S. Fujii, K. Ichikawa, Y. Imamura, Y. Okuno, and Y. O. Nakagawa, "Deep variational quantum eigensolver for excited states and its application to quantum chemistry calculation of periodic materials", Physical Review Research **3**, 043121 (2021).

[18]Y. Zhang, L. Cincio, C. F. A. Negre, P. Czarnik, P. Coles, P. M. Anisimov, S. M. Mniszewski, S. Tretiak, and P. A. Dub, *Variational Quantum Eigensolver with Reduced Circuit Complexity*, June 2021, arXiv:2106.07619 [quant-ph].

[19]A. Eddins, M. Motta, T. P. Gujarati, S. Bravyi, A. Mezzacapo, C. Hadfield, and S. Sheldon, "Doubling the size of quantum simulators by entanglement forging", PRX Quantum **3**, 010309 (2022).

[20]K. Fujii, K. Mizuta, H. Ueda, K. Mitarai, W. Mizukami, and Y. O. Nakagawa, *Deep variational quantum eigensolver: a divide-and-conquer method for solving a larger problem with smaller size quantum computers*, 2020, arXiv:2007.10917 [quant-ph].

[21]T. Kinoshita, O. Hino, and R. J. Bartlett, "Coupled-cluster method tailored by configuration interaction", J. Chem. Phys. **123**, 074106 (2005).

[22]O. Hino, T. Kinoshita, G. K.-L. Chan, and R. J. Bartlett, "Tailored coupled cluster singles and doubles method applied to calculations on molecular structure and harmonic vibrational frequencies of ozone", J. Chem. Phys. **124**, 114311 (2006).

[23]D. I. Lyakh, V. F. Lotrich, and R. J. Bartlett, "The 'tailored' ccsd(t) description of the automerization of cyclobutadiene", Chem. Phys. Lett. **501**, 166–171 (2011).

[24]A. Melnichuk and R. J. Bartlett, "Relaxed active space: Fixing tailored-CC with high order coupled cluster. I", J. Chem. Phys. **137**, 214103 (2012).

[25]A. Melnichuk and R. J. Bartlett, "Relaxed active space: Fixing tailored-CC with high order coupled cluster. II", J. Chem. Phys. **140**, 064113 (2014).

[26]M. Mörchen, L. Freitag, and M. Reiher, "Tailored coupled cluster theory in varying correlation regimes", J. Chem. Phys. **153**, 244113 (2020).

[27]M. Kohda, R. Imai, K. Kanno, K. Mitarai, W. Mizukami, and Y. O. Nakagawa, "Quantum expectation-value estimation by computational basis sampling", Phys. Rev. Res. **4**, 033173 (2022).

[28]T. D. Crawford and H. F. Schaefer III, "An introduction to coupled cluster theory for computational chemists", in *Reviews in computational chemistry* (John Wiley & Sons, Ltd, 2000), pp. 33–136.

[29]R. J. Bartlett and M. Musiał, "Coupled-cluster theory in quantum chemistry", Rev. Mod. Phys. **79**, 291–352 (2007).

[30]S. McArdle and D. P. Tew, *Improving the accuracy of quantum computational chemistry using the transcorrelated method*, 2020, arXiv:2006.11181 [quant-ph].

[31]A. Kumar, A. Asthana, C. Masteran, E. F. Valeev, Y. Zhang, L. Cincio, S. Tretiak, and P. A. Dub, "Quantum simulation of molecular electronic states with a transcorrelated hamiltonian: higher accuracy with fewer qubits", J. Chem. Theory Comput. **18**, 5312–5324 (2022).

[32]I. O. Sokolov, W. Dobrautz, H. Luo, A. Alavi, and I. Tavernelli, "Orders of magnitude increased accuracy for quantum many-body problems on quantum computers via an exact transcorrelated method", Phys. Rev. Res. **5**, 023174 (2023).

[33]N. P. Bauman, E. J. Bylaska, S. Krishnamoorthy, G. H. Low, N. Wiebe, C. E. Granade, M. Roetteler, M. Troyer, and K. Kowalski, "Downfolding of many-body Hamiltonians using active-space models: Extension of the sub-system embedding sub-algebras approach to unitary coupled cluster formalisms", J. Chem. Phys. **151**, 014107 (2019).

[34]M. Metcalf, N. P. Bauman, K. Kowalski, and W. A. De Jong, "Resource-efficient chemistry on quantum computers with the variational quantum eigensolver and the double unitary coupled-cluster approach", J. Chem. Theory Comput. **16**, 6165–6175 (2020).

[35]B. Nicholas P., J. Chládek, L. Veis, J. Pittner, and K. Karol, "Variational quantum eigensolver for approximate diagonalization of downfolded hamiltonians using generalized unitary coupled cluster ansatz", Quantum Sci. Technol. **6**, 034008 (2021).

[36]R. Huang, C. Li, and F. A. Evangelista, "Leveraging small-scale quantum computers with unitarily downfolded hamiltonians", PRX Quantum **4**, 020313 (2023).

[37]N. P. Bauman and K. Kowalski, "Coupled cluster downfolding theory: towards universal many-body algorithms for dimensionality reduction of composite quantum systems in chemistry and materials science", Mater Theory **6**, 17 (2022).

[38]N. T. Le and L. N. Tran, "Correlated reference-assisted variational quantum eigensolver", J. Phys. Chem. A **127**, 5222–5230 (2023).

[39]H. Ma, N. Sheng, M. Govoni, and G. Galli, "Quantum embedding theory for strongly correlated states in materials", J. Chem. Theory Comput. **17**, 2116–2125 (2021).

[40]A. Tammaro, D. E. Galli, J. E. Rice, and M. Motta, "N-electron valence perturbation theory with reference wave functions from quantum computing: application to the relative stability of hydroxide anion and hydroxyl radical", J. Phys. Chem. A **127**, 817–827 (2023).

[41]S. Nishio, Y. Oba, and Y. Kurashige, "Statistical errors in reduced density matrices sampled from quantum circuit simulation and the impact on multireference perturbation theory", Phys. Chem. Chem. Phys. **25**, 30525–30535 (2023).

[42]T. Takeshita, N. C. Rubin, Z. Jiang, E. Lee, R. Babbush, and J. R. McClean, "Increasing the representation accuracy of quantum simulations of chemistry without extra quantum resources", Phys. Rev. X **10**, 011004 (2020).

[43]W. Mizukami, K. Mitarai, Y. O. Nakagawa, T. Yamamoto, T. Yan, and Y.-y. Ohnishi, "Orbital optimized unitary coupled cluster theory for quantum computer", Phys. Rev. Res. **2**, 033421 (2020).

[44]I. O. Sokolov, P. K. Barkoutsos, P. J. Ollitrault, D. Greenberg, J. Rice, M. Pistoia, and I. Tavernelli, "Quantum orbital-optimized unitary coupled cluster methods in the strongly correlated regime: Can quantum algorithms outperform their classical equivalents?", J. Chem. Phys. **152**, 124107 (2020).

[45]J. S. Kottmann, P. Schleich, T. Tamayo-Mendoza, and A. Aspuru-Guzik, "Reducing qubit requirements while maintaining numerical precision for the variational quantum eigensolver: a basis-set-free approach", J. Phys. Chem. Lett. **12**, 663–673 (2021).

[46]P. Schleich, J. S. Kottmann, and A. Aspuru-Guzik, "Improving the accuracy of the variational quantum eigensolver for molecular systems by the explicitly-correlated perturbative [2]r12-correction", Phys. Chem. Chem. Phys. **24**, 13550–13564 (2022).

[47]M. Rossmannek, P. K. Barkoutsos, P. J. Ollitrault, and I. Tavernelli, "Quantum HF/DFT-embedding algorithms for electronic structure calculations: Scaling up to complex molecular systems", J. Chem. Phys. **154**, 114105 (2021).

[48]W. J. Huggins, B. A. O'Gorman, N. C. Rubin, D. R. Reichman, R. Babbush, and J. Lee, "Unbiasing fermionic quantum monte carlo with a quantum computer", Nature **603**, 416–420 (2022).

[49]Y. Zhang, Y. Huang, J. Sun, D. Lv, and X. Yuan, *Quantum computing quantum monte carlo*, 2023, arXiv:2206.10431 [quant-ph].

[50]K. Wan, W. J. Huggins, J. Lee, and R. Babbush, "Matchgate shadows for fermionic quantum simulation", Commun. Math. Phys. **404**, 629–700 (2023).

[51]P. Verma, L. Huntington, M. P. Coons, Y. Kawashima, T. Yamazaki, and A. Zaribafiyan, "Scaling up electronic structure calculations on quantum computers: The frozen natural orbital based method of increments", J. Chem. Phys. **155**, 034110 (2021).

[52]E. Xu, Y. Shimomoto, S. L. Ten-no, and T. Tsuchimochi, "Many-body-expansion based on variational quantum eigensolver and deflation for dynamical correlation", J. Phys. Chem. A **128**, 2507–2521 (2024).

[53]J. B. Robinson and P. J. Knowles, "Quasi-variational coupled cluster theory", J Chem Phys **136**, 054114 (2012).

[54]R. J. Bartlett and J. Noga, "The expectation value coupled-cluster method and analytical energy derivatives", Chem. Phys. Lett. **150**, 29–36 (1988).

[55]W. Kutzelnigg, "Error analysis and improvements of coupled-cluster theory", Theor. Chim. Acta **80**, 349–386 (1991).

[56]P. G. Szalay, M. Nooijen, and R. J. Bartlett, "Alternative ansätze in single reference coupled-cluster theory. III. A critical analysis of different methods", J. Chem. Phys. **103**, 281–298 (1995).

[57]B. Cooper and P. J. Knowles, "Benchmark studies of variational, unitary and extended coupled cluster methods", J. Chem. Phys. **133**, 234102 (2010).

[58]P. J. Knowles and B. Cooper, "A linked electron pair functional", J. Chem. Phys. **133**, 224106 (2010).

[59]F. A. Evangelista, "Alternative single-reference coupled cluster approaches for multireference problems: The simpler, the better", J. Chem. Phys. **134**, 224102 (2011).

[60]J. B. Robinson and P. J. Knowles, "Approximate variational coupled cluster theory", J. Chem. Phys. **135**, 044113 (2011).

[61] G. Harsha, T. Shiozaki, and G. E. Scuseria, "On the difference between variational and unitary coupled cluster theories", J. Chem. Phys. **148**, 044107 (2018).

[62] T. Van Voorhis and M. Head-Gordon, "Benchmark variational coupled cluster doubles results", J. Chem. Phys. **113**, 8873 (2000).

[63] A. Marie, F. Kossoski, and P.-F. Loos, "Variational coupled cluster for ground and excited states", J. Chem. Phys. **155**, 104105 (2021).

[64] A. Gilyén, Y. Su, G. H. Low, and N. Wiebe, "Quantum singular value transformation and beyond: exponential improvements for quantum matrix arithmetics", in Proceedings of the 51st annual acm sigact symposium on theory of computing, STOC 2019 (2019), pp. 193–204.

[65] P. Jordan and E. P. Wigner, "Über das paulische äquivalenzverbot", in *The collected works of eugene paul wigner: part a: the scientific papers*, edited by A. S. Wightman (Springer Berlin Heidelberg, Berlin, Heidelberg, 1993), pp. 109–129.

[66] B. P. Pritchard, D. Altarawy, B. Didier, T. D. Gibson, and T. L. Windus, "New basis set exchange: an open, up-to-date resource for the molecular sciences community", Journal of Chemical Information and Modeling **59**, 4814–4820 (2019).

[67] W. J. Hehre, R. F. Stewart, and J. A. Pople, "Self-Consistent Molecular-Orbital Methods. I. Use of Gaussian Expansions of Slater-Type Atomic Orbitals", The Journal of Chemical Physics **51**, 2657–2664 (1969).

[68] R. Ditchfield, W. J. Hehre, and J. A. Pople, "Self-Consistent Molecular-Orbital Methods. IX. An Extended Gaussian-Type Basis for Molecular-Orbital Studies of Organic Molecules", The Journal of Chemical Physics **54**, 724–728 (1971).

[69] J. Dunning Thom H., "Gaussian basis sets for use in correlated molecular calculations. I. The atoms boron through neon and hydrogen", The Journal of Chemical Physics **90**, 1007–1023 (1989).

[70] A. Anand, P. Schleich, S. Alperin-Lea, P. W. K. Jensen, S. Sim, M. Díaz-Tinoco, J. S. Kottmann, M. Degroote, A. F. Izmaylov, and A. Aspuru-Guzik, "A quantum computing view on unitary coupled cluster theory", Chem. Soc. Rev. **51**, 1659–1684 (2022).

[71] S. Pal, M. D. Prasad, and D. Mukherjee, "On certain correspondences among various coupled-cluster theories for closed-shell systems", Pramana **18**, 261–270 (1982).

[72] J. T. Seeley, M. J. Richard, and P. J. Love, "The Bravyi-Kitaev transformation for quantum computation of electronic structure", The Journal of Chemical Physics **137**, 224109 (2012).

[73] S. McArdle, T. Jones, S. Endo, Y. Li, S. C. Benjamin, and X. Yuan, "Variational ansatz-based quantum simulation of imaginary time evolution", npj Quantum Information **5**, 75 (2019).

[74]M. Motta, C. Sun, A. T. K. Tan, M. J. O'Rourke, E. Ye, A. J. Minnich, F. G. S. L. Brandão, and G. K.-L. Chan, "Determining eigenstates and thermal states on a quantum computer using quantum imaginary time evolution", Nat. Phys. **16**, 205–210 (2020).

[75]N. Gomes, F. Zhang, N. F. Berthusen, C.-Z. Wang, K.-M. Ho, P. P. Orth, and Y. Yao, "Efficient step-merged quantum imaginary time evolution algorithm for quantum chemistry", J. Chem. Theory Comput. **16**, 6256–6266 (2020).

[76]N. Gomes, A. Mukherjee, F. Zhang, T. Iadecola, C.-Z. Wang, K.-M. Ho, P. P. Orth, and Y.-X. Yao, "Adaptive variational quantum imaginary time evolution approach for ground state preparation", Adv. Quantum Technol. **4**, 2100114 (2021).

[77]T. Tsuchimochi, Y. Ryo, S. L. Ten-no, and K. Sasasako, "Improved algorithms of quantum imaginary time evolution for ground and excited states of molecular systems", J. Chem. Theory Comput. **19**, 503–513 (2023).

[78]J. M. Martyn, Z. M. Rossi, A. K. Tan, and I. L. Chuang, "Grand unification of quantum algorithms", PRX Quantum **2**, 040203 (2021).

[79]G. H. Low and I. L. Chuang, "Optimal hamiltonian simulation by quantum signal processing", Phys. Rev. Lett. **118**, 010501 (2017).

[80]S. Gribling, I. Kerenidis, and D. Szilágyi, "Improving quantum linear system solvers via a gradient descent perspective", arXiV preprint (2021), arXiv:2109.04248 [quant-ph].

[81]T. L. Silva, M. M. Taddei, S. Carrazza, and L. Aolita, "Fragmented imaginary-time evolution for early-stage quantum signal processors", Scientific Reports **13**, 18258 (2023).

[82]G. H. Low and I. L. Chuang, "Hamiltonian Simulation by Qubitization", Quantum **3**, 163 (2019).

[83]D. Camps, L. Lin, R. Van Beeumen, and C. Yang, "Explicit quantum circuits for block encodings of certain sparse matrices", SIAM J. Matrix Anal. Appl. **45**, 801–827 (2024).

[84]D. Camps and R. Van Beeumen, "FABLE: Fast Approximate Quantum Circuits for Block-Encodings", Proceedings - IEEE International Conference on Quantum Computing and Engineering, QCE, 104–113 (2022).

[85]G. H. Low, T. J. Yoder, and I. L. Chuang, "Methodology of resonant equiangular composite quantum gates", Phys. Rev. X **6**, 041067 (2016).

[86]Y. Dong, X. Meng, K. B. Whaley, and L. Lin, "Efficient phase-factor evaluation in quantum signal processing", Phys. Rev. A **103**, 042419 (2021).

[87]A. M. Childs and N. Wiebe, "Hamiltonian simulation using linear combinations of unitary operations", Quantum Info. Comput. **12**, 901–924 (2012).

[88]A. M. Childs, R. Kothari, and R. D. Somma, "Quantum Algorithm for Systems of Linear Equations with Exponentially Improved Dependence on Precision", SIAM Journal on Computing **46**, 1920–1950 (2017).

[89]Y. Liu, S. Arunachalam, and K. Temme, "A rigorous and robust quantum speed-up in supervised machine learning", Nature Physics **17**, 1013–1017 (2021).

[90]Y. Cao, J. Romero, J. P. Olson, M. Degroote, P. D. Johnson, M. Kieferová, I. D. Kivlichan, T. Menke, B. Peropadre, N. P. Sawaya, S. Sim, L. Veis, and A. Aspuru-Guzik, "Quantum Chemistry in the Age of Quantum Computing", Chemical Reviews **119**, 10856–10915 (2019).

[91]F. Arute, K. Arya, R. Babbush, D. Bacon, J. C. Bardin, R. Barends, R. Biswas, S. Boixo, F. G. Brandao, D. A. Buell, B. Burkett, Y. Chen, Z. Chen, B. Chiaro, R. Collins, W. Courtney, A. Dunsworth, E. Farhi, B. Foxen, A. Fowler, C. Gidney, M. Giustina, R. Graff, K. Guerin, S. Habegger, M. P. Harrigan, M. J. Hartmann, A. Ho, M. Hoffmann, T. Huang, T. S. Humble, S. V. Isakov, E. Jeffrey, Z. Jiang, D. Kafri, K. Kechedzhi, J. Kelly, P. V. Klimov, S. Knysh, A. Korotkov, F. Kostritsa, D. Landhuis, M. Lindmark, E. Lucero, D. Lyakh, S. Mandrà, J. R. McClean, M. McEwen, A. Megrant, X. Mi, K. Michielsen, M. Mohseni, J. Mutus, O. Naaman, M. Neeley, C. Neill, M. Y. Niu, E. Ostby, A. Petukhov, J. C. Platt, C. Quintana, E. G. Rieffel, P. Roushan, N. C. Rubin, D. Sank, K. J. Satzinger, V. Smelyanskiy, K. J. Sung, M. D. Trevithick, A. Vainsencher, B. Villalonga, T. White, Z. J. Yao, P. Yeh, A. Zalcman, H. Neven, and J. M. Martinis, "Quantum supremacy using a programmable superconducting processor", Nature **574**, 505–510 (2019).

[92]L. Egan, D. M. Debroy, C. Noel, A. Risinger, D. Zhu, D. Biswas, M. Newman, M. Li, K. R. Brown, M. Cetina, and C. Monroe, "Fault-tolerant control of an error-corrected qubit", Nature **598**, 281–286 (2021).

[93]P. Jurcevic, A. Javadi-Abhari, L. S. Bishop, I. Lauer, D. F. Bogorin, M. Brink, L. Capelluto, O. Günlük, T. Itoko, N. Kanazawa, A. Kandala, G. A. Keefe, K. Krsulich, W. Landers, E. P. Lewandowski, D. T. McClure, G. Nannicini, A. Narasgond, H. M. Nayfeh, E. Pritchett, M. B. Rothwell, S. Srinivasan, N. Sundaresan, C. Wang, K. X. Wei, C. J. Wood, J. B. Yau, E. J. Zhang, O. E. Dial, J. M. Chow, and J. M. Gambetta, "Demonstration of quantum volume 64 on a superconducting quantum computing system", Quantum Science and Technology **6**, 025020 (2021).

[94]M. S. Gordon, D. G. Fedorov, S. R. Pruitt, and L. V. Slipchenko, "Fragmentation Methods: A Route to Accurate Calculations on Large Systems", Chemical Reviews **112**, 632–672 (2011).

[95]K. M. Nakanishi, K. Mitarai, and K. Fujii, "Subspace-search variational quantum eigensolver for excited states", Physical Review Research **1**, 033062 (2019).

[96]I. G. Ryabinkin, S. N. Genin, and A. F. Izmaylov, "Constrained Variational Quantum Eigensolver: Quantum Computer Search Engine in the Fock Space", Journal of Chemical Theory and Computation **15**, 249–255 (2018).

[97]N. Nakatani and G. K. L. Chan, "Efficient tree tensor network states (TTNS) for quantum chemistry: Generalizations of the density matrix renormalization group algorithm", The Journal of Chemical Physics **138**, 134113 (2013).

[98]E. Abbasi, S. F. Aval, A. Akbarzadeh, M. Milani, H. T. Nasrabadi, S. W. Joo, Y. Hanifehpour, K. Nejati-Koshki, and R. Pashaei-Asl, "Dendrimers: synthesis, applications, and properties", Nanoscale Research Letters **9**, 247 (2014).

[99]Q. Sun, T. C. Berkelbach, N. S. Blunt, G. H. Booth, S. Guo, Z. Li, J. Liu, J. D. McClain, E. R. Sayfutyarova, S. Sharma, S. Wouters, and G. K. L. Chan, "PySCF: the Python-based simulations of chemistry framework", Wiley Interdisciplinary Reviews: Computational Molecular Science **8**, e1340 (2018).

[100]J. R. McClean, N. C. Rubin, K. J. Sung, I. D. Kivlichan, X. Bonet-Monroig, Y. Cao, C. Dai, E. S. Fried, C. Gidney, B. Gimby, P. Gokhale, T. Haner, T. Hardikar, V. Havlíček, O. Higgott, C. Huang, J. Izaac, Z. Jiang, X. Liu, S. Mcardle, M. Neeley, T. O'Brien, B. O'Gorman, I. Ozfidan, M. D. Radin, J. Romero, N. P. Sawaya, B. Senjean, K. Setia, S. Sim, D. S. Steiger, M. Steudtner, Q. Sun, W. Sun, D. Wang, F. Zhang, and R. Babbush, "OpenFermion: the electronic structure package for quantum computers", Quantum Science and Technology **5**, 034014 (2020).

[101]Y. Suzuki, Y. Kawase, Y. Masumura, Y. Hiraga, M. Nakadai, J. Chen, K. M. Nakanishi, K. Mitarai, R. Imai, S. Tamiya, T. Yamamoto, T. Yan, T. Kawakubo, Y. O. Nakagawa, Y. Ibe, Y. Zhang, H. Yamashita, H. Yoshimura, A. Hayashi, and K. Fujii, "Qulacs: a fast and versatile quantum circuit simulator for research purpose", Quantum **5**, 559 (2021).

[102]P. Virtanen, R. Gommers, T. E. Oliphant, M. Haberland, T. Reddy, D. Cournapeau, E. Burovski, P. Peterson, W. Weckesser, J. Bright, S. J. van der Walt, M. Brett, J. Wilson, K. J. Millman, N. Mayorov, A. R. J. Nelson, E. Jones, R. Kern, E. Larson, C. J. Carey, İ. Polat, Y. Feng, E. W. Moore, J. VanderPlas, D. Laxalde, J. Perktold, R. Cimrman, I. Henriksen, E. A. Quintero, C. R. Harris, A. M. Archibald, A. H. Ribeiro, F. Pedregosa, P. van Mulbregt, and SciPy 1.0 Contributors, "SciPy 1.0: Fundamental Algorithms for Scientific Computing in Python", Nature Methods **17**, 261–272 (2020).

[103]M. J. Frisch, G. W. Trucks, H. B. Schlegel, G. E. Scuseria, M. A. Robb, J. R. Cheeseman, G. Scalmani, V. Barone, G. A. Petersson, H. Nakatsuji, X. Li, M. Caricato, A. V. Marenich, J. Bloino, B. G. Janesko, R. Gomperts, B. Mennucci, H. P. Hratchian, J. V. Ortiz, A. F. Izmaylov, J. L. Sonnenberg, D. Williams-Young, F. Ding, F. Lipparini, F. Egidi, J. Goings, B. Peng, A. Petrone, T. Henderson, D. Ranasinghe, V. G. Zakrzewski, J. Gao, N. Rega, G. Zheng, W. Liang, M. Hada, M. Ehara, K. Toyota, R. Fukuda, J. Hasegawa, M. Ishida, T. Nakajima, Y. Honda, O. Kitao, H. Nakai, T. Vreven, K. Throssell, J. A. Montgomery Jr., J. E. Peralta, F. Ogliaro, M. J. Bearpark, J. J. Heyd, E. N. Brothers, K. N. Kudin, V. N. Staroverov, T. A. Keith, R. Kobayashi, J. Normand, K. Raghavachari, A. P. Rendell, J. C. Burant, S. S. Iyengar, J. Tomasi, M. Cossi, J. M. Millam, M. Klene, C. Adamo, R. Cammi, J. W. Ochterski, R. L. Martin, K. Morokuma, O. Farkas, J. B. Foresman, and D. J. Fox, *Gaussian˜16 Revision A.03*, Gaussian Inc. Wallingford CT, 2016.

[104]E. R. Sayfutyarova and S. Hammes-Schiffer, "Constructing Molecular π-Orbital Active Spaces for Multireference Calculations of Conjugated Systems", Journal of Chemical Theory and Computation **15**, 1679–1689 (2019).

[105]F. Aquilante, T. Bondo Pedersen, A. Sánchez De Merás, and H. Koch, "Fast noniterative orbital localization for large molecules", The Journal of Chemical Physics **125**, 174101 (2006).

[106]R. Babbush, J. R. McClean, M. Newman, C. Gidney, S. Boixo, and H. Neven, "Focus beyond quadratic speedups for error-corrected quantum advantage", PRX Quantum **2**, 010103 (2021).

[107]J. J. Goings, A. White, J. Lee, C. S. Tautermann, M. Degroote, C. Gidney, T. Shiozaki, R. Babbush, and N. C. Rubin, "Reliably assessing the electronic structure of cytochrome p450 on today's classical computers and tomorrow's quantum computers", Proc. Natl. Acad. Sci. **119**, e2203533119 (2022).

[108]C. J. Stein and M. Reiher, "Automated selection of active orbital spaces", J. Chem. Theory Comput. **12**, 1760–1771 (2016).

[109]E. R. Sayfutyarova, Q. Sun, G. K.-L. Chan, and G. Knizia, "Automated construction of molecular active spaces from atomic valence orbitals", J. Chem. Theory Comput. **13**, 4063–4078 (2017).

[110]J. J. Bao, S. S. Dong, L. Gagliardi, and D. G. Truhlar, "Automatic selection of an active space for calculating electronic excitation spectra by MS-CASPT2 or MC-PDFT", J. Chem. Theory Comput. **14**, 2017–2025 (2018).

[111]W. Jeong, S. J. Stoneburner, D. King, R. Li, A. Walker, R. Lindh, and L. Gagliardi, "Automation of active space selection for multireference methods via machine learning on chemical bond dissociation", J. Chem. Theory Comput. **16**, 2389–2399 (2020).

[112]D. S. King and L. Gagliardi, "A ranked-orbital approach to select active spaces for high-throughput multireference computation", J. Chem. Theory Comput. **17**, 2817–2831 (2021).

[113]D. S. King, M. R. Hermes, D. G. Truhlar, and L. Gagliardi, "Large-scale benchmarking of multireference vertical-excitation calculations via automated active-space selection", J. Chem. Theory Comput. **18**, 6065–6076 (2022).

[114]B. W. Kaufold, N. Chintala, P. Pandeya, and S. S. Dong, "Automated active space selection with dipole moments", J. Chem. Theory Comput. **19**, 2469–2483 (2023).

[115]D. I. Lyakh, M. Musiał, V. F. Lotrich, and R. J. Bartlett, "Multireference nature of chemistry: the coupled-cluster view", Chem. Rev. **112**, 182–243 (2012).

[116]T. Yanai, Y. Kurashige, W. Mizukami, J. Chalupský, T. N. Lan, and M. Saitow, "Density matrix renormalization group for ab initio calculations and associated dynamic correlation methods: a review of theory and applications", Int. J. Quantum Chem. **115**, 283–299 (2015).

[117]B. O. Roos, R. Lindh, P. Malmqvist, V. Veryazov, and P. O. Widmark, *Multiconfigurational Quantum Chemistry* (Wiley Blackwell, Aug. 2016), pp. 1–224.

[118]S. Pathak, L. Lang, and F. Neese, "A dynamic correlation dressed complete active space method: Theory, implementation, and preliminary applications", J. Chem. Phys. **147**, 234109 (2017).

[119]J. W. Park, R. Al-Saadon, M. K. Macleod, T. Shiozaki, and B. Vlaisavljevich, "Multireference electron correlation methods: journeys along potential energy surfaces", Chem. Rev. **120**, 5878–5909 (2020).

[120]A. Khedkar and M. Roemelt, "Modern multireference methods and their application in transition metal chemistry", Phys. Chem. Chem. Phys. **23**, 17097–17112 (2021).

[121]D. Casanova, "Restricted active space configuration interaction methods for strong correlation: recent developments", Wiley Interdiscip. Rev.: Comput. Mol. Sci. **12**, e1561 (2022).

[122]J. F. Gonthier, M. D. Radin, C. Buda, E. J. Doskocil, C. M. Abuan, and J. Romero, "Measurements as a roadblock to near-term practical quantum advantage in chemistry: resource analysis", Phys. Rev. Res. **4**, 033154 (2022).

[123]J. Tilly, P. V. Sriluckshmy, A. Patel, E. Fontana, I. Rungger, E. Grant, R. Anderson, J. Tennyson, and G. H. Booth, "Reduced density matrix sampling: self-consistent embedding and multiscale electronic structure on current generation quantum computers", Phys. Rev. Res. **3**, 033230 (2021).

[124]N. Takemori, Y. Teranishi, W. Mizukami, and N. Yoshioka, *Balancing error budget for fermionic k-rdm estimation*, 2023, arXiv:2312.17452 [quant-ph].

[125]F. M. Faulstich, M. Máté, A. Laestadius, M. A. Csirik, L. Veis, A. Antalik, J. Brabec, R. Schneider, J. Pittner, S. Kvaal, and Ö. Legeza, "Numerical and theoretical aspects of the dmrg-tcc method exemplified by the nitrogen dimer", J. Chem. Theory Comput. **15**, 2206–2220 (2019).

[126]E. Vitale, A. Alavi, and D. Kats, "Fciqmc-tailored distinguishable cluster approach", J. Chem. Theory Comput. **16**, 5621–5634 (2020).

[127]E. Vitale, G. Li Manni, A. Alavi, and D. Kats, "Fciqmc-tailored distinguishable cluster approach: open-shell systems", J. Chem. Theory Comput. **18**, 3427–3437 (2022).

[128]T. M. Henderson, I. W. Bulik, T. Stein, and G. E. Scuseria, "Seniority-based coupled cluster theory", J. Chem. Phys. **141**, 244104 (2014).

[129]K. Boguslawski and P. W. Ayers, "Linearized coupled cluster correction on the antisymmetric product of 1-reference orbital geminals", J. Chem. Theory Comput. **11**, 5252–5261 (2015).

[130]A. Leszczyk, M. Máté, Ö. Legeza, and K. Boguslawski, "Assessing the accuracy of tailored coupled cluster methods corrected by electronic wave functions of polynomial cost", J. Chem. Theory Comput. **18**, 96–117 (2022).

[131] A. Nowak, Ö. Legeza, and K. Boguslawski, "Orbital entanglement and correlation from pCCD-tailored coupled cluster wave functions", J. Chem. Phys. **154**, 084111 (2021).

[132] G. Peris, J. Planelles, and J. Paldus, "Single-reference ccsd approach employing three-and four-body cas scf corrections: a preliminary study of a simple model", Int. J. Quantum Chem. **62**, 137–151 (1997).

[133] X. Li, G. Peris, J. Planelles, F. Rajadall, and J. Paldus, "Externally corrected singles and doubles coupled cluster methods for open-shell systems", J. Chem. Phys. **107**, 90–98 (1997).

[134] G. Peris, F. Rajadell, X. Li, J. Planelles, and J. Paldus, "Externally corrected singles and doubles coupled cluster methods for open-shell systems. ii. applications to the low lying doublet states of oh, nh2, ch3 and cn radicals", Mol. Phys. **94**, 235–248 (1998).

[135] L. Z. Stolarczyk, "Complete active space coupled-cluster method. extension of single-reference coupled-cluster method using the casscf wavefunction", Chem. Phys. Lett. **217**, 1–6 (1994).

[136] E. Xu and S. Li, "The externally corrected coupled cluster approach with four- and five-body clusters from the CASSCF wave function", J. Chem. Phys. **142**, 094119 (2015).

[137] J. E. Deustua, I. Magoulas, J. Shen, and P. Piecuch, "Communication: Approaching exact quantum chemistry by cluster analysis of full configuration interaction quantum Monte Carlo wave functions", J. Chem. Phys. **149**, 151101 (2018).

[138] I. Magoulas, K. Gururangan, P. Piecuch, J. E. Deustua, and J. Shen, "Is externally corrected coupled cluster always better than the underlying truncated configuration interaction?", J. Chem. Theory Comput. **17**, 4006–4027 (2021).

[139] S. Lee, H. Zhai, S. Sharma, C. J. Umrigar, and G. K.-L. Chan, "Externally corrected ccsd with renormalized perturbative triples (r-ecccsd(t)) and the density matrix renormalization group and selected configuration interaction external sources", J. Chem. Theory Comput. **17**, 3414–3425 (2021).

[140] J. Lang, A. Antalík, L. Veis, J. Brandejs, J. Brabec, Ö. Legeza, and J. Pittner, "Near-linear scaling in dmrg-based tailored coupled clusters: an implementation of dlpno-tccsd and dlpno-tccsd(t)", J. Chem. Theory Comput. **16**, 3028–3040 (2020).

[141] R. Izsák, C. Riplinger, N. S. Blunt, B. de Souza, N. Holzmann, O. Crawford, J. Camps, F. Neese, and P. Schopf, "Quantum computing in pharma: a multilayer embedding approach for near future applications", J. Comput. Chem. **44**, 406–421 (2023).

[142] *Chemqulacs*, `https://wmizukami.github.io/chemqulacs/`, 2023.

[143]Q. Sun, X. Zhang, S. Banerjee, P. Bao, M. Barbry, N. S. Blunt, N. A. Bogdanov, G. H. Booth, J. Chen, Z.-H. Cui, J. J. Eriksen, Y. Gao, S. Guo, J. Hermann, M. R. Hermes, K. Koh, P. Koval, S. Lehtola, Z. Li, J. Liu, N. Mardirossian, J. D. McClain, M. Motta, B. Mussard, H. Q. Pham, A. Pulkin, W. Purwanto, P. J. Robinson, E. Ronca, E. R. Sayfutyarova, M. Scheurer, H. F. Schurkus, J. E. T. Smith, C. Sun, S.-N. Sun, S. Upadhyay, L. K. Wagner, X. Wang, A. White, J. D. Whitfield, M. J. Williamson, S. Wouters, J. Yang, J. M. Yu, T. Zhu, T. C. Berkelbach, S. Sharma, A. Y. Sokolov, and G. K.-L. Chan, "Recent developments in the PySCF program package", J. Chem. Phys. **153**, 024109 (2020).

[144]F. Neese, "Software update: the orca program system—version 5.0", Wiley Interdiscip. Rev.: Comput. Mol. Sci. **12**, e1606 (2022).

[145]M. Scheurer, G.-L. R. Anselmetti, O. Oumarou, C. Gogolin, and N. C. Rubin, "Tailored and externally corrected coupled cluster with quantum inputs", J. Chem. Theory Comput., 10.1021/acs.jctc.4c00037 (2024).

[146]E. Ventura, S. A. Do Monte, M. Dallos, and H. Lischka, "Cope rearrangement of 1,5-hexadiene: full geometry optimizations using analytic mr-cisd and mr-aqcc gradient methods", J. Phys. Chem. A **107**, 1175–1180 (2003).

[147]R. Shepard, H. Lischka, P. G. Szalay, T. Kovar, and M. Ernzerhof, "A general multireference configuration interaction gradient program", J. Chem. Phys. **96**, 2085–2098 (1992).

[148]V. N. Staroverov and E. R. Davidson, "The cope rearrangement in theoretical retrospect", J. Mol. Struct.: THEOCHEM **573**, 81–89 (2001).

[149]W. von E. Doering, V. Toscano, and G. Beasley, "Kinetics of the cope rearrangement of 1,1-dideuteriohexa-1,5-diene", Tetrahedron **27**, 5299–5306 (1971).

[150]K. Kanno, M. Kohda, R. Imai, S. Koh, K. Mitarai, W. Mizukami, and Y. O. Nakagawa, *Quantum-selected configuration interaction: classical diagonalization of hamiltonians in subspaces selected by quantum computers*, 2023, arXiv:2302.11320 [quant-ph].

[151]Y. O. Nakagawa, M. Kamoshita, W. Mizukami, S. Sudo, and Y.-y. Ohnishi, *Adapt-qsci: adaptive construction of input state for quantum-selected configuration interaction*, 2023, arXiv:2311.01105 [quant-ph].

[152]K. Liao, L. Ding, and C. Schilling, *Unveiling intrinsic many-body complexity by compressing single-body triviality*, 2024, arXiv:2402.16841 [quant-ph].

[153]R. Feldmann, M. Mörchen, J. Lang, M. Lesiuk, and M. Reiher, *complete active space iterative coupled cluster theory*, 2024, arXiv:2404.06070 [physics.chem-ph].

[154]A. Zhao, N. C. Rubin, and A. Miyake, "Fermionic partial tomography via classical shadows", Phys. Rev. Lett. **127**, 110504 (2021).

[155]C. Riplinger, B. Sandhoefer, A. Hansen, and F. Neese, "Natural triple excitations in local coupled cluster calculations with pair natural orbitals", J. Chem. Phys **139**, 134101 (2013).

[156]T. Gruber, K. Liao, T. Tsatsoulis, F. Hummel, and A. Grüneis, "Applying the coupled-cluster ansatz to solids and surfaces in the thermodynamic limit", Phys. Rev. X **8**, 021043 (2018).

[157]I. Y. Zhang and A. Grüneis, "Coupled cluster theory in materials science", Front. Mater. **6**, 10.3389/fmats.2019.00123 (2019).

[158]J. S. Smith, B. T. Nebgen, R. Zubatyuk, N. Lubbers, C. Devereux, K. Barros, S. Tretiak, O. Isayev, and A. E. Roitberg, "Approaching coupled cluster accuracy with a general-purpose neural network potential through transfer learning", Nat. Commun. **10**, 2903 (2019).

[159]D. M. Wilkins, A. Grisafi, Y. Yang, K. U. Lao, R. A. DiStasio Jr, and M. Ceriotti, "Accurate molecular polarizabilities with coupled cluster theory and machine learning", Proc. Natl. Acad. Sci. U.S.A. **116**, 3401–3406 (2019).

[160]K. Sorathia, D. Frantzov, and D. P. Tew, "Improved cps and cbs extrapolation of pno-ccsd (t) energies: the mobh35 and isol24 data sets", J. Chem. Theory Comput. **20**, 2740–2750 (2024).

[161]A. Gu, A. Lowe, P. A. Dub, P. J. Coles, and A. Arrasmith, *Adaptive shot allocation for fast convergence in variational quantum algorithms*, 2021, arXiv:2108.10434 [quant-ph].

[162]J. I. Cirac, D. Pérez-García, N. Schuch, and F. Verstraete, "Matrix product states and projected entangled pair states: concepts, symmetries, theorems", Rev. Mod. Phys. **93**, 045003 (2021).

[163]H.-Y. Huang, R. Kueng, and J. Preskill, "Predicting many properties of a quantum system from very few measurements", Nat. Phys. **16**, 1050–1057 (2020).

[164]F. A. Evangelista, G. K.-L. Chan, and G. E. Scuseria, "Exact parameterization of fermionic wave functions via unitary coupled cluster theory", J. Chem. Phys. **151**, 244112 (2019).

[165]A. G. Taube and R. J. Bartlett, "New perspectives on unitary coupled-cluster theory", Int. J. Quantum Chem. **106**, 3393–3401 (2006).

[166]V. Bergholm, J. Izaac, M. Schuld, C. Gogolin, S. Ahmed, V. Ajith, M. S. Alam, G. Alonso-Linaje, B. AkashNarayanan, A. Asadi, J. M. Arrazola, U. Azad, S. Banning, C. Blank, T. R. Bromley, B. A. Cordier, J. Ceroni, A. Delgado, O. D. Matteo, A. Dusko, T. Garg, D. Guala, A. Hayes, R. Hill, A. Ijaz, T. Isacsson, D. Ittah, S. Jahangiri, P. Jain, E. Jiang, A. Khandelwal, K. Kottmann, R. A. Lang, C. Lee, T. Loke, A. Lowe, K. McKiernan, J. J. Meyer, J. A. Montañez-Barrera, R. Moyard, Z. Niu, L. J. O'Riordan, S. Oud, A. Panigrahi, C.-Y. Park, D. Polatajko, N. Quesada, C. Roberts, N. Sá, I. Schoch, B. Shi, S. Shu, S. Sim, A. Singh, I. Strandberg, J. Soni, A. Száva, S. Thabet, R. A. Vargas-Hernández, T. Vincent, N. Vitucci, M. Weber, D. Wierichs, R. Wiersema, M. Willmann, V. Wong, S. Zhang, and N. Killoran, *Pennylane: automatic differentiation of hybrid quantum-classical computations*, 2022, arXiv:1811.04968 [quant-ph].

[167]R. Chao, D. Ding, A. Gilyen, C. Huang, and M. Szegedy, *Finding angles for quantum signal processing with machine precision*, 2020, arXiv:2003.02831 [quant-ph].

[168]J. Haah, "Product Decomposition of Periodic Functions in Quantum Signal Processing", Quantum **3**, 190 (2019).

[169]R. H. Byrd, P. Lu, J. Nocedal, and C. Zhu, "A limited memory algorithm for bound constrained optimization", SISC **16**, 1190–1208 (1995).

[170]P. K. Barkoutsos, J. F. Gonthier, I. Sokolov, N. Moll, G. Salis, A. Fuhrer, M. Ganzhorn, D. J. Egger, M. Troyer, A. Mezzacapo, S. Filipp, and I. Tavernelli, "Quantum algorithms for electronic structure calculations: particle-hole hamiltonian and optimized wave-function expansions", Phys. Rev. A **98**, 022322 (2018).

[171]N. Hatano and M. Suzuki, "Finding exponential product formulas of higher orders", in *Quantum annealing and other optimization methods*, edited by A. Das and B. K. Chakrabarti (Springer Berlin Heidelberg, Berlin, Heidelberg, 2005), pp. 37–68.

[172]D. W. Berry, G. Ahokas, R. Cleve, and B. C. Sanders, "Efficient quantum algorithms for simulating sparse hamiltonians", Commun. Math. Phys. **270**, 359–371 (2007).

[173]S. Hakkaku, Y. Tashima, K. Mitarai, W. Mizukami, and K. Fujii, "Quantifying fermionic nonlinearity of quantum circuits", Phys. Rev. Res. **4**, 043100 (2022).

[174]L. Erhart, Y. Yoshida, V. Khinevich, and W. Mizukami, "Coupled cluster method tailored with quantum computing", Phys. Rev. Res. **6**, 023230 (2024).

Appendix

In Tabs. 6.1, 6.2 and 6.3, we show the geometry of the molecules used in the Chapter 3. The distances are given in angstrom.

	X	Y	Z
H	0.000000	0.000000	0.000000
H	-1.732051	-0.000000	-1.000000
H	-1.848076	-0.866025	-2.799038
H	-3.348076	0.866025	-0.200962
H	0.000000	0.000000	2.000000
H	-1.500000	-0.866025	3.000000
H	1.500000	0.866025	3.000000
H	1.732051	0.000000	-1.000000
H	3.348076	-0.866025	-0.200962
H	1.848076	0.866025	-2.799038

Table 6.1: XYZ-coordinate of the 10 hydrogen molecule with stretching factor 1.

	X	Y	Z
H	0.000000	0.000000	0.000000
H	-1.732050	-0.000000	-1.000000
H	-1.848080	-0.866030	-2.799040
H	-3.348080	0.866030	-0.200960
H	-3.464100	-0.000000	-2.000000
H	0.000000	0.000000	2.000000
H	-1.500000	-0.866030	3.000000
H	1.500000	0.866030	3.000000
H	0.000000	0.000000	4.000000
H	1.732050	0.000000	-1.000000
H	3.348080	-0.866030	-0.200960
H	1.848080	0.866030	-2.799040
H	3.464100	0.000000	-2.000000

Table 6.2: XYZ-coordinate of the 13 hydrogen molecule with stretching factor 1.

Table 6.3: XYZ-coordinate of the retinal molecule.

	X	Y	Z
O	-8.60015	1.48468	0.81071
C	4.39241	-0.77397	0.51552
C	5.77904	-0.08948	0.48761
C	5.70665	1.40739	0.77579
C	3.33060	0.08350	-0.21654
C	4.86219	2.08607	-0.30026
C	3.57180	1.35840	-0.61706
C	3.94256	-1.00034	1.97865
C	4.55288	-2.15570	-0.16272
C	2.03748	-0.58705	-0.44366
C	2.62992	2.18732	-1.45862
C	0.81416	-0.05758	-0.20524
C	-0.46332	-0.72138	-0.41518
C	-0.46117	-2.12317	-0.97276
C	-1.60447	-0.03909	-0.09459
C	-2.96328	-0.48737	-0.21634
C	-4.03235	0.27778	0.13513
C	-5.42820	-0.10540	0.04014
C	-5.75579	-1.47964	-0.49730
C	-6.37349	0.79473	0.44081
C	-7.82162	0.62021	0.43151
H	6.22690	-0.23284	-0.50558
H	6.43820	-0.59735	1.20232
H	6.71075	1.84544	0.80511
H	5.26112	1.58181	1.76272
H	5.44638	2.18475	-1.22944
H	4.61898	3.11698	-0.00678
H	4.64289	-1.66413	2.49891
H	3.88921	-0.05950	2.53474
H	2.94956	-1.45875	2.01686
H	5.40574	-2.68341	0.27827
H	3.67656	-2.79604	-0.02741
H	4.74164	-2.05316	-1.23676
H	2.08553	-1.61942	-0.78134
H	2.14548	2.97367	-0.86405
H	1.84672	1.59622	-1.93374
H	3.19801	2.70547	-2.24209
H	0.75642	0.95116	0.19869
H	-1.46418	-2.53053	-1.09921
H	0.09232	-2.80140	-0.31283
H	0.03720	-2.15163	-1.94837
H	-1.48044	0.96851	0.30163
H	-3.13972	-1.48470	-0.60830
H	-3.84165	1.27584	0.52734
H	-5.29038	-2.25362	0.12287
H	-5.35887	-1.59806	-1.51154
H	-6.82567	-1.67873	-0.53230
H	-6.05111	1.76391	0.81603
H	-8.21260	-0.34930	0.05918

Number of shot dependency of QC-CBT-TCC for LiH

In Figures 6.1 (a) and 6.1 (b) the results for LiH show a behavior similar to that of H_2O and N_2 in that increasing the number of measurements reduces the corrected energy distribution. This behavior can be explained by the higher accuracy and decreased uncertainty in determining the coefficients of a state on a quantum computer. Consequently, the obtained CBT state is more consistent, and therefore, the expected energy can be determined with a higher degree of confidence.

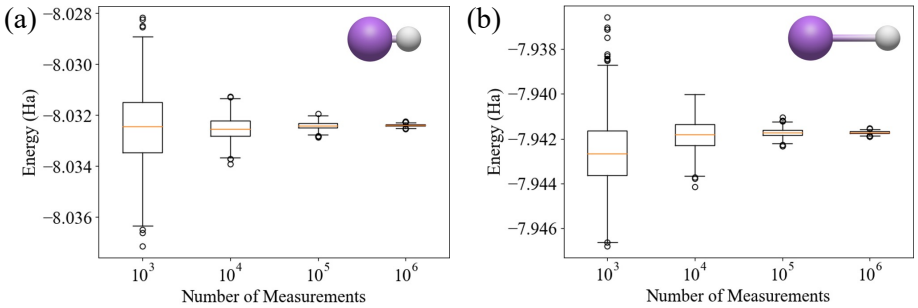

Figure 6.1: Energy insecurity of QC-CBT-TCC(c) for LiH with a different number of measurements for CBT. N_{sample}, N_U, and N_V were all measured in the specified quantities in the figure as the X-axis values. CBT was performed 1000 times for each setting to obtain an estimate for the statistical errors. The box indicates the range from the first to the third quartile called the inter-quartile range (IQR), with the median drawn in the middle. The box contains 50% of the data. Whiskers are the lines extending 1.5 times the IQR from the first and third quantiles. Data points that exceed the whiskers are considered outliers (fliers) and are represented as single dots. (a) Number of measurements dependency at an equilibrium distance of 3.016 Bohr. (b) Number of measurements dependency at 6.032 Bohr, twice the equilibrium distance.

Acknowledgments

First and foremost, I would like to express my immense gratitude to Prof. Keisuke Fujii, Prof. Wataru Mizukami, and Prof. Kosuke Mitarai for their continued support during my Ph.D. Their advice helped me become the researcher I am today. Despite their busy schedules, they work tirelessly to give me and other students the perfect environment for our research. Especially, I would like to thank Prof. Wataru Mizukami, for his guidance in the field of quantum chemistry. His insight and comments helped me develop the methods I could present today.

I would also like to thank Dr. Yuichiro Yoshida for his help, comments, and discussions, which were immensely helpful in my research work.

I am thankful for the helpful comments from Prof. Yasutaka Kitagawa, Prof. Takashi Yamamoto, Prof. Wataru Mizukami, Prof. Kosuke Mitarai, and Prof. Keisuke Fujii while reviewing my thesis.

Also I would like to thank all of my fellow lab mates for many discussions in and outside of the laboratory, making my research life immensely enjoyable.

Finally, I thank my beloved family for always being a strong pillar of support.

List of Publications

Publications

1. L. Erhart, K. Mitarai, W. Mizukami, K. Fujii, "Constructing Local Bases for a Deep Variational Quantum Eigensolver for Molecular Systems", Phys. Rev. Applied **18**, 064051 (2022).

2. L. Erhart, Y. Yoshida, V. Khinevich, W. Mizukami, "Coupled cluster method tailored with quantum computing", Phys. Rev. Research **6**, 023230 (2024).

3. L. Erhart, Y. Yoshida, V. Khinevich, W. Mizukami, "Chebyshev Approximated Variational Coupled Cluster for Quantum Computing", arXiv:2406.07364.